https://doi.org/10.5194/tc-2019-120
Preprint. Discussion started: 17 June 2019

The Cryosphere Discussions
Open Access
EGU

Satellite Passive Microwave Sea-Ice Concentration Data Set Intercomparison: Closed Ice and Ship-Based Observations

Stefan Kern[1], Thomas Lavergne[2], Dirk Notz[3], Leif Toudal Pedersen[4], Rasmus Tage Tonboe[5], Roberto Saldo[4], and Atle Macdonald Sørensen[2]

[1]Integrated Climate Data Center (ICDC), Center for Earth System Research and Sustainability (CEN), University of Hamburg, Hamburg, Germany
[2]Research and Development Department, Norwegian Meteorological Institute, Oslo, Norway
[3]Max-Planck Institute for Meteorology, Hamburg, Germany
[4]Danish Technical University, Lyngby, Denmark
[5]Danish Meteorological Institute, Copenhagen, Denmark

Correspondence to: Stefan Kern (stefan.kern@uni-hamburg.de)

Abstract. Accurate sea-ice concentration (SIC) data are a pre-requisite to reliably monitor the polar sea-ice covers. Over the last four decades, many algorithms have been developed to retrieve the SIC from satellite microwave radiometry, some of them applied to generate long-term data products. We report on results of a systematic inter-comparison of ten global SIC data products at 12.5 to 50.0 km grid resolution for both the Arctic and the Antarctic. The products are compared with each other with respect to differences in SIC, sea-ice area (SIA), and sea-ice extent (SIE), and they are compared against a global winter-time near-100% reference SIC data set for closed pack ice conditions and against global year-round ship-based visual observations of the sea-ice cover. We can group the products based on the observed inter-product consistency and differences of the inter-comparison results. Group I consists of data sets using the self-optimizing EUMETSAT-OSISAF – ESA-CCI algorithms. Group II includes data using the NASA-Team 2 and Comiso-Bootstrap algorithms, and the NOAA-NSIDC sea-ice concentration climate data record (CDR). The standard NASA-Team and the ARTIST Sea Ice (ASI) algorithms are put into a separate group III because of their often quite diverse results. Within group I and II evaluation results and intra-product differences are mostly very similar. For instance, among group I products, SIA agrees within ±100 000 km² in both hemispheres during maximum and minimum sea-ice cover. Among group II products, satellite- minus ship-based SIC differences agree within ±0.7%. Standing out with large negative differences to other products and evaluation data is the standard NASA-Team algorithm, in both hemispheres. The three CDRs of group I (SICCI-25km, SICCI-50km, and OSI-450) are biased low compared to the 100% reference SIC with biases of -0.4% to -1.0% (Arctic) and -0.3% to -1.1% (Antarctic). Products of group II appear to be mostly biased high in the Arctic by between +1.0% and +3.5%, while their biases in the Antarctic only range from -0.2% to +0.9%. The standard deviation is smaller in the Arctic for the quoted group I products: 1.9% to 2.9% and Antarctic: 2.5% to 3.1%, than for group II products: Arctic: 3.6% to 5.0%, Antarctic: 4.5% to 5.4%. Products of group I exhibit larger overall satellite- minus ship-based SIC differences than group II in both hemispheres. However, compared to group II, group I products' standard deviations are smaller, correlations higher and evaluation results are less sensitive to seasonal changes. We discuss the impact of truncating the SIC distribution, as naturally retrieved by the algorithms around the 100% sea-ice concentration end. We show that evaluation studies of such truncated SIC products can result in misleading statistics and favour data sets that systematically overestimate SIC. We describe a method to re-construct the un-truncated distribution of SIC before the evaluation is performed. On the basis of this evaluation, we open a discussion about the overestimation of SIC in data products, with far-reaching consequences for, e.g., surface heat-flux estimations in winter. We also document inconsistencies in the behaviour of the weather filters used in products of group II, and suggest advancing studies about the influence of these weather filters on SIA and SIE time-series and their trends.

https://doi.org/10.5194/tc-2019-120
Preprint. Discussion started: 17 June 2019

1 Introduction

For more than 40 years, the fraction of the polar oceans covered with sea ice, or sea-ice concentration, has been monitored by means of satellite microwave radiometry. This enabled a better understanding of ocean–sea-ice–atmosphere interactions in the polar regions where observations with other means than satellites are challenging due to remoteness, harsh environment and limited daylight. Based on the long-term satellite record, a substantial negative trend in the Arctic sea-ice area and extent has been found (e.g. Meier et al., 2014; Comiso et al., 2012, 2017a). In the Antarctic, sea-ice area and extent are highly variable with a period of positive trend (Turner et al., 2013; Comiso et al., 2017b) and sea-ice extent maxima (Reid et al., 2015) being followed recently by record minima (Schlosser et al., 2018; Turner et al., 2017; Stuecker et al., 2017).

In this contribution, we evaluate a number of satellite estimates of spatially and temporally resolved sea-ice concentration from which sea-ice area and extent are derived. Such detailed evaluation allows one to better estimate the uncertainties of these products, knowledge of which is required for all their applications. These applications range from estimates of the future evolution of the Arctic sea-ice cover, whose confidence is directly affected by observational uncertainty of sea-ice concentration (e.g., Niederdrenk and Notz, 2018), and short-term forecasts for ship routing (e.g., Wayand et al., 2019; Melia et al., 2017) to detailed climate-model evaluation (e.g., Ivanova et al., 2017).

The sea-ice concentration, from which sea-ice area and extent are derived, is computed from satellite observations of the microwave brightness temperature (TB), which is a measure of the Earth-leaving thermal microwave radiation received by the satellite sensor. A number of different satellite sensors has been in place for sea-ice monitoring, summarized in Table 1 (see also Lavergne et al., 2019, Table 2). With these sensors the polar regions are covered almost completely daily since October 1978 (every other day with SMMR before July 1987).

A considerable number of different algorithms to compute the sea-ice concentration from microwave satellite TB measurements has been developed during the past decades. All exploit the fact that under typical viewing angles (50-55 degrees) the difference in microwave brightness temperature between open water and sea ice is sufficiently large to estimate sea-ice concentration. Whether or not a given algorithm is accepted by the scientific community as an algorithm to compute a climate data record (CDR) depends among other things on the length of the available satellite raw data, spatial and temporal resolution, quantification of uncertainties, noise reduction and mitigation of artificial trends (e.g., Tonboe et al., 2016; Lavergne et al., 2019).

Several inter-comparison studies were carried out to assess the quality of the sea-ice concentration obtained with different algorithms (e.g., Andersen et al., 2007; Ivanova et al., 2014, 2015; Beitsch et al., 2015; Comiso et al., 2017a). Two different kinds of such inter-comparisons exist. One kind deals with an inter-comparison of sea-ice cover products of a certain number of algorithms without incorporating independent information of the sea-ice cover. Such inter-comparisons provide very valuable information about inter-product consistencies in, e.g. the overall sea-ice concentration distribution, and in sea-ice area and extent time series and trends. They also reveal differences, for instance, with respect to the representation of the seasonal cycle or with respect to regional differences between sea-ice concentration estimates. Inter-comparisons of this kind are, e.g., Ivanova et al. (2014) and Comiso et al. (2017a). These studies, however, do not provide information about the absolute accuracy of a sea-ice concentration product. The other kind of algorithm inter-comparison studies deals with the comparison of the satellite sea-ice concentration with independent data. These can be ship-based observations, or sea-ice concentration estimates derived from independent satellite observations, for instance, in the optical frequency range or with active microwave sensors such as Synthetic Aperture Radar (SAR). Inter-comparisons of this second kind seldom involve more than one to two algorithms (e.g., Wiebe et al., 2009; Meier, 2005; Comiso et al., 1997; Comiso and Steffen, 2001; Markus and Dokken, 2002; Kern et al., 2003; Cavalieri et al., 2010; Spreen et al., 2008). Exceptions to this are Andersen et al. (2007), who compared seven different algorithms with ship-based sea-ice cover observations and SAR imagery for the Arctic, and Beitsch et al. (2015), who compared six different algorithms with ship-based sea-ice cover observations in the Antarctic.

https://doi.org/10.5194/tc-2019-120
Preprint. Discussion started: 17 June 2019

84 This paper is the first of a series of papers in which we are going to present and discuss results of a systematic evaluation
85 of ten sea-ice concentration products (see Sect. 2). We want to provide users and algorithm developers with new information
86 about the accuracy and precision of this suite of products, some of which are widely used in the climate research community,
87 in less than a handful of papers, and in a form allowing a comparison of product skills at a glance. In this contribution, we
88 present the sea-ice concentration products used. We focus on differences in sea-ice concentration, area and extent, on inter-
89 comparisons with winter-time near-100% reference sea-ice concentrations, and with a large suite of ship-based manual visual
90 observations of the sea-ice conditions. The second contribution is going to focus on Arctic summer conditions, presenting and
91 discussing results of an inter-comparison with sea-ice parameters derived from MODerate resolution Imaging
92 Spectroradiometer (MODIS) satellite observations. The third contribution is going to focus on presenting and discussing results
93 of an inter-comparison with sea-ice concentrations computed from Landsat satellite visible imagery.
94 In the following Sect. 2, we introduce the sea-ice concentration data sets and ancillary data used as input. It further
95 describes the preparation of the ancillary data and inter-comparison steps. Section 3 illustrates how the sea-ice concentration
96 products compare with each other in terms of multi-annual monthly average sea-ice concentration as well as sea-ice area and
97 extent. In Sect. 4 and Sect. 5, we show the results of the inter-comparison against a near-100% reference data set and against
98 ship-based sea-ice observations, respectively. Section 6 covers a discussion, an outlook, and conclusions.

99 2 Data & Methodologies

100 2.1 Sea-ice concentration data sets

101 For this study, we consider 10 different sea-ice concentration products (Table 2, with more details in Appendices A to
102 F). There are many more algorithms and products available than we are using here, see e.g. Ivanova et al. (2015). The main
103 criteria for our choice of algorithms and products are 1) length of the product time series, 2) grid resolution, 3) accessibility
104 and continuation. We avoid products with less than ten years coverage and/or with a considerably finer grid resolution than 25
105 km. After Table 2 we comment on several specific issues that are important for the correct interpretation of sea-ice
106 concentration products, namely the grid resolution, the land spill-over correction, the weather / open water filter, and the sea-
107 ice concentration distributions around 0% and 100%.
108

109 2.1.1 Grid resolution

110 Given grid resolutions apply to every grid cell for OSI-450 and SICCI-12km, SICCI-25km, and SICCI-50km since
111 their EASE grid has equal area of all grid cells (App. A). For all other products (App. B through F), the grid resolution is true
112 at 70 degrees latitude (see also Peng et al., 2013). For the computation of sea-ice area and extent (Sect. 3), we take this
113 difference in grid-cell area into account and use the respective files of the grid-cell areas provided by NSIDC
114 (ftp://sidads.colorado.edu/pub/DATASETS/brightness-temperatures/polar-stereo/tools/geo-coord/grid, last access date:
115 26/9/2018).
116

117 2.1.2 Land spill-over correction

118 The difference in brightness temperatures observed over open water (low) and land (high) combined with the size of
119 the field-of-view of several kilometres to a few tens of kilometres can cause spurious sea-ice concentrations to appear along
120 coasts (e.g., Lavergne et al., 2019). Various methods to reduce this so-called land spill-over effect are applied in all products
121 (Cavalieri et al., 1999; Cho et al., 1996; Maass and Kaleschke, 2010). For ASI-SSMI (App. B), reduction of land spill-over
122 effects is carried out for both the ASI algorithm as well as the NASA-Team algorithm product used for open water. For NOAA-
123 CDR (App. F), the reduction of land spill-over effects is applied separately to both input data sets before merging (Meier and
124 Windnagel, 2018). In this paper, we do not further correct potential differences between the ten products caused by this effect.

https://doi.org/10.5194/tc-2019-120
Preprint. Discussion started: 17 June 2019


The Cryosphere Discussions
Open Access
EGU

125

126 **2.1.3 Weather / open water filter**

127 The two standard weather filters based on brightness temperature gradient ratios at 19 GHz, 22 GHz, and 37 GHz,
128 which mitigate noise due to atmospheric moisture and wind-induced roughening of the ocean surface (Cavalieri et al., 1995,
129 1999) are applied in the products NT1-SSMI and NT2-AMSRE. In the products CBT-SSMI and CBT-AMSRE, spurious sea-
130 ice concentrations caused by weather effects are filtered using the same frequencies as mentioned above but applying a
131 bootstrap technique (Comiso and Nishio, 2008). For NOAA-CDR (App. F), the above-mentioned weather filters are applied
132 before the merging (Meier and Windnagel, 2018). In the two NASA GSFC (App. C, D) sea-ice concentration products, i.e.
133 NT1-SSMI, version 1, and CBT-SSMI, version 3, weather effects are reduced by screening of input brightness temperatures,
134 application of the above-mentioned weather filters, and some additional manual correction (Meier and Windnagel, 2018; Peng
135 et al., 2013, https://nsidc.org/data/g02202/versions/3, https://nsidc.org/data/nsidc-0051, and https://nsidc.org/data/nsidc-
136 0079). In the ASI-SSMI product no specific weather filter is applied to the ASI algorithm itself. However, ASI algorithm sea-
137 ice concentrations are set to 0% where NASA-Team algorithm sea-ice concentration values are < 30% (see App. B). Because
138 the above-mentioned two weather filters are applied to the NASA-Team sea-ice concentration, the ASI-SSMI product
139 implicitly contains a weather filter as well (Ezraty et al., 2007). Note that the 5-day median filter used for the ASI-SSMI
140 product used here (Kern et al., 2010) not only removes remaining spurious sea ice over open ocean but also reduces weather-
141 induced elevated sea-ice concentrations along the ice edge. In the EUMETSAT-OSISAF – ESA-CCI products a dynamic open
142 water filter is applied. It roots on the quoted standard weather filters but takes into account changes in filter efficiency due to
143 changes in the frequencies between the different sensors, for instance between SMMR and SSM/I. Also, it does not use the
144 channels close to 22 GHz. Still, that filter uses a global sea-ice concentration cut-off at about 10% SIC (Lavergne et al., 2019).
145 Finally, all ten products apply a monthly varying climatological sea-ice cover mask to erase spurious sea ice at low latitudes.

146 We investigate the temporal consistency of the weather filters by computing time-series of the monthly mean 5%
147 percentile of sea-ice concentrations of the range]0.0% to 30.0%], i.e. excluding the grid cells set by the open water filter to
148 exactly 0.0%. We look at two aspects. First, it is desirable that these time-series are mostly stable across the time-period
149 covered by a given data record, indicating that the weather filter cuts the sea-ice edge evenly across inter-annual variability
150 and changes of frequencies. Second, it is also desirable that the weather filter cuts "well below" the 15% SIC value so that it
151 does not interfere with the computation of sea-ice area (SIA) and extent (SIE) that use this threshold to define the sea-ice edge
152 (e.g., Gloersen et al., 1992). We choose the 5% percentile (and not a minimum value) to obtain less noisy time-series. We plot
153 examples of these time-series for all ten products in Fig. 1 and Fig. 2 for the Arctic and Antarctic, respectively. For the Arctic
154 we use March (Fig. 1 a) and September (Fig. 1 g); for the Antarctic September (Fig. 2 a) and February (Fig. 2 g). In addition
155 to the time-series, we also plot the cumulative distribution of the daily sea-ice concentrations of the range]0.0% to 30.0%] for
156 the respective month for the year 2004 as an example for CBT-SSMI, OSI-450, NT1-SSMI, ASI-SSMI, and NT2-AMSRE.

157 We confirm the finding from Lavergne et al. (2019, their Fig. 9), with little inter-annual variation of the monthly
158 mean percentile sea-ice concentration over time particularly for OSI-450 and SICCI-25km. Changes as caused, e.g., due to a
159 switch in sensor remain below 1%. On average, the 5% percentile sea-ice concentration is < 12%, which ensures that the
160 enhanced open water filter applied in these two products barely influences computation of SIA and SIE. For CBT-AMSRE,
161 CBT-SSMI and NOAA-CDR, these monthly mean 5% percentile sea-ice concentrations are considerably larger and sometimes
162 exceed 15%. Additionally, the time-series for CBT-SSMI and NOAA-CDR reveal larger inter-annual variations than OSI-450,
163 inter-sensor transitions (e.g. in 1987-1988 changing from SMMR to SSM/I, Fig. 1 g), and in 2007-2008 changing from SSM/I
164 to SSMIS, Fig. 1 a) leading to trends in the percentile time-series. The time-series for NT1-SSMI, ASI-SSMI, and NT2-
165 AMSRE, in contrast, have very low (partly ~1%) monthly mean 5% percentile sea-ice concentration values with little or no
166 inter-annual variation.

https://doi.org/10.5194/tc-2019-120
Preprint. Discussion started: 17 June 2019

167 In the plots of the sample daily cumulative fraction for year 2004, CBT-SSMI and OSI-450 reveal a hockey-stick
168 shaped cumulative distribution with no sea-ice concentrations below ~10% and ~8%, respectively (Fig. 1 b, c, h and i; Fig. 2
169 b, c, h and i). This agrees with the application of the open water filter presented in Lavergne et al. (2019). NT1-SSMI and
170 NT2-AMSRE, in contrast, reveal a substantial amount of near-0% sea-ice concentrations (Fig. 1 d, f, j and l; Fig. 2 d, f, j and
171 l). This suggests that while a weather filter is applied (according to the documentations) there are still concentrations near 0%
172 left. We checked this by looking at the respective daily sea-ice concentration maps. Both products reveal a considerable number
173 of grid cells with < 5% sea-ice concentration along the ice edge. Note that the fact that except the EUMETSAT-OSISAF –
174 ESA-CCI products all products provide integer sea-ice concentration values, paired with this large number of near-0% sea-ice
175 concentration values for, e.g. NT2-AMSRE, results in a no-show of this product in the time series in plots a) and g) of Fig. 1
176 and Fig. 2. We take the information from these two figures into account when discussing the results presented in Sect. 3.
177
178 **2.1.4 Distribution around 0% and 100%**
179 A considerable fraction of this paper focuses on the evaluation near 100% sea-ice concentration. While the
180 EUMETSAT-OSISAF – ESA-CCI products allow using the naturally retrieved sea-ice concentration on either side of 100%
181 the others do not; in those other products sea-ice concentrations are truncated at 0% and 100%. Figure 3 illustrates the sea-ice
182 concentration distribution at the locations of the near-100% sea-ice concentration reference data set (see Sect. 2.2) for SICCI-
183 25km, SICCI-50km and NOAA-CDR for the Arctic (plots a) to c)) and the Antarctic (plots d) to f)).
184 We use a Gaussian fit to simulate the true distribution of the sea-ice concentration retrieval around 100%. This is done
185 by finding that Gaussian curve which provides the lowest root-mean-squared difference (RMSD) to the sea-ice concentration
186 distribution for values ≤ 99%, i.e., basically the left hand side of the histograms shown in Fig. 3. For the fitting process, we
187 also take into account the fraction of sea-ice concentrations ≤ 99% relative to the entire count of valid sea-ice concentrations:
188 F_{99}. The difference between original F_{99} and F_{99} resulting from the Gaussian fit, ΔF_{99}, has to be < 0.1. We allow a maximum
189 RMSD value of 0.0125. We first binned SICCI-25km and SICCI-50km sea-ice concentration values to integer values to
190 comply with the other products. Figure 3 a, b and d, e) illustrate that the fits (red) agree well with the originally retrieved
191 SICCI-25km and SICCI-50km sea-ice concentrations (blue) with modal values slightly below 100%. Figure 3 c, f) illustrate
192 how well the Gaussian fit matches the original sea-ice concentration distribution for sea-ice concentrations ≤ 99% for NOAA-
193 CDR as an example. Here the modal sea-ice concentrations of the Gaussian fit are larger than 100%: 103.5% for NH (Fig. 3
194 c) and 100.9% for SH (Fig. 3 f). In addition, the Gaussian curve is broader than for SICCI-25km and SICCI-50km, resulting
195 in larger values for the standard deviation. We also note that F_{99} is ~0.6 and ~0.5 for SICCI-25km and SICCI-50km,
196 respectively, but only ~0.2 and ~0.4 for NOAA-CDR. We take the information from Fig. 3 into account when interpreting the
197 results presented in Sect. 4 and Sect. 5.

198 **2.2 The near-100% sea-ice concentration reference data set**

199 For the evaluation of the ten products at 100% sea-ice concentration (see Sect. 4), we use the Round Robin Data Package
200 version 2 (RRDP2) near-100% reference sea-ice concentration data set developed within the ESA Sea_Ice_cci and EU-SPICES
201 projects (Pedersen et al., 2019). In short, for this reference data set, areas of ~100% sea-ice concentration are found by
202 identifying areas of interest (AOI) of approximately 100 km x 100 km size with net convergence in the ice drift pattern on two
203 consecutive 1-day periods. Information about convergence is derived from the PolarView / MyOcean / CMEMS ice drift data
204 set derived from Envisat ASAR, RADARSAT-2 SAR and Sentinel-1 SAR imagery. By choosing AOIs in high-concentration
205 regions, near 100% sea-ice concentration can be assured (e.g., Kwok, 2002; Andersen et al., 2007) in winter. Each AOI contains
206 up to hundred 10 km x 10 km cells for which the SAR ice drift is computed. The number of cells depends on SAR image
207 coverage. Convergence in the ice drift pattern results in a decrease in the total area of these cells. A cell is included in the
208 dataset of ~100% sea-ice concentration if the area reduction between day 1 and day 2 is between 0% and 2% and if more than

https://doi.org/10.5194/tc-2019-120
Preprint. Discussion started: 17 June 2019

40% of the AOI contains cells with such an area reduction. The RRDP2 near-100% sea-ice concentration reference data set contains the AOI centre geographic latitude and longitude, time, total sea-ice concentration (100%) and AOI average area reduction due to net ice convergence. It is available for years 2007 through 2015 for both hemispheres.

We only use AOIs for winter months, i.e., November through March (Arctic) and May through September (Antarctic). By doing so we ensure that small-scale openings, which may remain in an area of high ice concentration and net ice convergence, are frozen and thus sea-ice concentrations are close to 100%. We use only AOIs for which the average area reduction between day 1 and day 2 is between 0.4 and 1.5%.

We co-locate the sea-ice concentrations of the ten products with the selected AOI grid cells by computing the minimum distance between AOI grid cell centre and grid cell centre of the respective sea-ice concentration product. For this step, we convert the geographic coordinates of all data sets into cartesian coordinates taking into account the different projections. Figure 4 illustrates the spatial distribution of selected AOIs for both hemispheres for two different years by showing the co-located OSI-450 sea-ice concentration. We give an example for a typical good distribution (Fig. 4 a, c) and for a typical poor distribution (Fig. 4 b, d). The RRDP2 near-100% sea-ice concentration reference data set contains basically no AOIs in the Eastern Antarctic because of the lack of sufficiently frequent SAR image acquisitions required for the ice drift product used to generate this RRDP2 data set.

We evaluate the products at their native grid resolution without applying any spatial averaging. For each product, we compute the mean difference "product minus 100%" and its standard deviation as well as the cumulative distribution function of the differences.

2.3 Ship-based visual sea-ice cover observations

According to the Antarctic Sea Ice Processes & Climate (ASPeCt) protocol http://www.aspect.aq (Worby and Allison, 1999; Worby and Dirita, 1999, see also Worby et al., 2008), ship-based observations of the sea-ice conditions shall be carried out every hour, at least every second hour, during daylight conditions while the ship is traversing the sea ice. Observations shall be carried out from the ship's bridge for an area of about one kilometre around the ship and shall report ice conditions as follows: total ice concentration, type of openings, and concentration, thickness, ridge fraction and height, and snow depth and type for up to three ice types. Such a protocol was not implemented in the Arctic in the same rigorous way as in the Antarctic. Nevertheless, ship-based visual observations were carried out as well during numerous cruises into the Arctic Ocean and its peripheral seas, using a slightly different protocol, established in the late 2000s. The need for a slightly different protocol can be explained by various forms of melt on Arctic sea ice, which are largely lacking for Antarctic sea ice. All ship-based visual observations used here result from manual, non-automated observations.

For our evaluation of the ten products with respect to ship-based visual observations of the sea-ice conditions (see Sect. 5), we use about 15 000 individual observations. About ~7000 of these were carried out in the Antarctic under the framework of the ASPeCt protocol. A substantial fraction of the Antarctic observations (until 2005) is available via http://www.aspect.aq (Worby et al., 2008). The more recent observations were collected from various sources (e.g. PANGAEA, ACE-CRC, AWI, see also Beitsch et al., 2015), merged with the existing ASPeCt data and standardized. Standardization means that the resulting ascii format data file containing all observations uses similar formats for all variables and missing data. The data are also manually quality checked for outliers. For the comparison presented in this manuscript, we use all ASPeCt observations from the period June 2002 through December 2015. This data set is available via http://icdc.cen.uni.hamburg.de/1/daten/cryosphere/seaiceparameters-shipobs, last access date: 28/3/2019.

In the Arctic, ship-based sea-ice observations have been collected under the IceWatch/ASSIST (Arctic Ship-based Sea-Ice Standardization) initiative and are available via http://icewatch.gina.alaska.edu. The majority of the data used in this manuscript for the Arctic is taken from that portal. Additional sources for ship-based sea-ice observations are again PANGAEA (for Polarstern cruises before IceWatch/ASSIST), the Arctic Data Center of the NSF: https://arcticdata.io/catalog/#data, and

https://doi.org/10.5194/tc-2019-120
Preprint. Discussion started: 17 June 2019

the data archive of the Bering Sea Ecosystem Study (BEST): https://www.eol.ucar.edu/projects/best/ice.shtml. In total ~8000 observations are available for the Arctic. We prepare these data in the same way as the ASPeCt observations for the Antarctic and use all observations from the period June 2002 through December 2015. This data set is available via http://icdc.cen.uni.hamburg.de/1/daten/cryosphere/seaiceparameters-shipobs, last access date: 28/3/2019.

Figure 5 summarizes the locations of the ship-based observations used in this manuscript, separately for the Arctic (Fig. 5 a, b) and the Antarctic (Fig. 5 c, d). In both hemispheres, just comparably small regions contain such observations. Figure 5 a, c) illustrates that some regions are visited during several years while others just once or twice during the 13-year period considered. The seasonal distribution (Fig. 5 b, d) illustrates that the more central (Arctic) or southern (Antarctic) regions were only visited during summer months due to harsh winter conditions paired with lack of daylight in these regions.

We co-locate the sea-ice concentrations of the ten products with the selected ship-based observations by computing the minimum distance between geographic location of the ship-based observation and the grid cell centre of the respective sea-ice concentration product. For this step, we convert the geographic coordinates of all data sets into cartesian coordinates taking into account the different projections of the sea-ice concentration products. After the co-location, we average over all ship-based and all satellite-based sea-ice concentration values, including reports of open water, i.e. 0% concentration, of one day following the approach of Beitsch et al. (2015). This results in a comparison of along ship-track daily average sea-ice conditions. Data pairs with less than three ship-based observations per day are discarded. The results of the comparison between ship-based and satellite-based sea-ice concentration are solely based on these daily average sea-ice concentrations. Note that all satellite-based data are used at their native grid resolution.

The ship-based and satellite-based sea-ice concentration data sets are compared by means of histograms, scatterplots and linear regression analysis and statistics separately for summer data, winter data, and data of the entire year. Summer comprises months May through September for the Arctic and months November through March for the Antarctic; winter comprises the respective remaining months. For the histograms, sea-ice concentrations are put into bins 0 … 5%, 5% … 15%, 15% … 25%, … , 85% … 95%, 95% … 100%. By doing so we get an impression about the distribution of both sea-ice concentration data sets at the precision of the ship-based observations, which is ~10%. In the scatterplots, we compare the daily average sea-ice concentrations and additionally compute averages of the satellite-based sea-ice concentration for each of the above-mentioned bins applied to the ship-based data and vice versa. We compute the overall average sea-ice concentration difference and its standard deviation, and perform a linear regression analysis based on the daily average and the binned data. All these results are presented in Sect. 5.

3 Inter-comparison of sea-ice area and extent

We follow Ivanova et al. (2014) and begin our inter-comparison with time-series of the sea-ice area (SIA) and sea-ice extent (SIE) derived from monthly mean sea-ice concentration. The monthly mean sea-ice concentration is derived for every product at the native grid and grid resolution. SIE is computed by summing over the grid-cell area of grid cells with > 15% sea-ice concentration. SIA is computed by summing over the ice-covered portion of the grid-cell area of grid cells with > 15% sea-ice concentration. By using this threshold, we follow Gloersen et al. (1992) and numerous SIA and SIE inter-comparison studies. We compare SIA and SIE time-series for the entire period for which we have data from the respective products at the time of the analysis. We exclude sea-ice concentrations estimated for lakes and other inland waters. We fill the circular area with missing data around the pole caused by the satellite orbit inclination and swath width with a constant sea-ice concentration value of 98%; this applies to the Arctic and only to the products at polar-stereographic projection. This area is interpolated spatially in the four EUMETSAT-OSISAF – ESA-CCI products already. Note that we use the fully filtered and truncated versions of these products, i.e. the variables, which are the main entry point to this product files. The two most relevant filters applied are the open-water filter, and a statistical land spill-over removal filter (Lavergne et al., 2019). In addition, these filtered

https://doi.org/10.5194/tc-2019-120
Preprint. Discussion started: 17 June 2019

sea-ice concentrations are truncated to values between 0% and 100%, even though the retrieval naturally provides a sea-ice concentration distribution around these two values (see Fig. 3 and Lavergne et al. (2019)). Without this truncation the SIA of the EUMETSAT-OSISAF – ESA-CCI products increases slightly, while the SIE does not change because the number of grid cells covered with > 15% sea ice is not influenced by the truncation (not shown). In Fig. 6, we present the SIA and SIE time series of months March and September for the Arctic; in Fig. 8 we show the SIA and SIE extent time series of months February and September for the Antarctic. The months chosen reflect the time of the typical minimum and maximum SIA and SIE.

We complement these SIA and SIE time series with maps of the multi-annual average sea-ice concentration difference for selected months in the Arctic (Fig. 7) and Antarctic (Fig. 9 and Fig. 10) for the AMSR-E measurement period: June 2002 to September 2011. We choose this period to be able to compare all ten products for a similarly long time-period. For these maps, we first re-grid the monthly mean sea-ice concentrations of all products, except SICCI-50km, onto the EASE grid version 2.0 with 50 km grid resolution using bilinear interpolation. Then we compute the multi-annual average sea-ice concentration for each month from which we subsequently calculate an ensemble mean (see map k) in Fig. 7 and Fig. 9 and 10) and the difference product minus ensemble mean (all other maps in Fig. 7 and Fig. 9 and 10).

Finally, we summarize differences between the mean sea-ice concentrations of all products and differences between the mean SIA and SIE values of all products in Fig. 11 and in Appendix G, Fig. G1 through Fig. G6. Similarly to the sea-ice concentration maps mentioned above, we re-grid the monthly mean sea-ice concentration onto the EASE grid version 2.0 with 50 km grid resolution using bilinear interpolation and apply a common land mask (the one of SICCI-50km) to all products. The differences between SIA and SIE values shown in Fig. 11 are computed from these gridded 50 km resolution, common land mask products.

3.1 Arctic sea-ice area and extent

The SIA and SIE time-series shown in Fig. 6 for the Arctic reveal a very similar overall development for the products extending back into the 1980ties and 1990ties. This applies to: i) the overall negative trend in both quantities; ii) the inter-annual variability as, for instance, during 1991-1997 and around 2007 and 2012 for the September SIA and SIE (Fig. 6 b, d), or in 2011 for the relative minimum in March SIA and SIE (Fig. 6 a, c); iii) to the ranking between the products. NOAA-CDR and CBT-SSMI provide largest SIA and SIE for both March and September, exceeding the next largest one, OSI-450, by ~600 000 km² (SIA) and ~200 000 km² (SIE). NT1-SSMI provides lowest SIA and SIE for September, while for March we find SIA and SIE from ASI-SSMI to be even lower. It is obvious that differences between products are smaller for SIE than for SIA as was shown also by Ivanova et al., (2014).

For the AMSR-E period, when SIA and SIE of all ten products are available, the inter-annual variation is similar for all ten products. We find that the products not discussed in the previous paragraph, i.e. the ESA-CCI products, CBT-AMSRE and NT2-AMSRE, fall into the ranges of SIA and SIE given by the other products. An exception to this is SICCI-50km, providing clearly the lowest SIE of all products in March (Fig. 6 c). We will discuss this finding in the context of Fig. 7.

3.2 Arctic sea-ice distribution differences

For March, the difference between the sea-ice concentration of an individual product and the ensemble mean of all ten products (Fig. 7) remains within ±5% over most of the Arctic Ocean, except for ASI-SSMI (Fig. 7 d) and SICCI-12km (Fig. 7 f). While the former exhibits less sea ice than the ensemble mean over almost the entire Arctic Ocean, the latter exhibits less sea ice particularly north of Greenland and the Canadian Arctic Archipelago with differences < -5%. The largest differences between individual products and the ensemble mean are located in the peripheral seas, i.e. Sea of Okthosk, Bering Sea, Baffin Bay, Labrador Sea, Irminger Sea, Greenland and Barents Seas. CBT-SSMI, NOAA-CDR, CBT-AMSRE and NT2-AMSRE (Fig. 7 b, c, i, j) show more sea ice than the ensemble mean – especially in the Irminger Sea (the two SSM/I products), the

https://doi.org/10.5194/tc-2019-120
Preprint. Discussion started: 17 June 2019

Labrador Sea (the two AMSR-E products), and Sea of Okthosk and Bering Sea (all four products); differences can exceed 20%. Note the similarity in the distribution of differences for CBT-SSMI and NOAA-CDR (Fig. 7 b, c). NT1-SSMI (Fig. 7 a) shows less sea ice than the ensemble mean with differences of < -10% or even < -15% in all peripheral seas. Differences of OSI-450 or SICCI-25km and the ensemble mean are within ±5% overall (Fig. 8 e, g). SICCI-50km shows ~2% more sea ice than the ensemble mean for most of the sea-ice cover. However, we find areas of considerably less sea ice than the ensemble mean, i.e. differences ≤ -20%, along some of the coastlines, e.g., in the Labrador Sea, the Irminger Sea or the coastlines in the Pechora and Barents Seas (Fig. 7 h). A careful check of these areas in daily and monthly mean maps of the SICCI-50km sea-ice concentration reveals that in regions of a relatively narrow sea-ice cover stretching along coastlines, the combination of land spill-over filter and open water filter can result in an unwanted complete removal of SICCI-50km product grid cells with ice. We are confident that this explains the particularly low SICCI-50km SIA and SIE shown in Fig. 6 a) and c) in Arctic SIE for March.

Figure 11 a) agrees with the results shown in Fig. 7. For March, small, i.e. < 1%, overall sea-ice concentration differences are found within three groups of products: I) EUMETSAT-OSISAF – ESA-CCI, II) NT2-AMSRE, CBT-AMSRE, CBT-SSMI, and NOAA-CDR, and III) ASI-SSMI and NT1-SSMI. Note we assign the two products of group III to a separate group only for simplicity; they often differ considerably. Group III exhibits less sea ice than the other groups: ~2% compared to group I and ~5% compared to group II. For September (Fig. 11 b), we find small overall sea-ice concentration differences within groups I and II of < 2% but not within group III; here differences exceed 10% between ASI-SSMI and NT1-SSMI. Of the ten products, NT1-SSMI exhibits the smallest overall mean September sea-ice concentration, which is 7-8% below the products of group I, and more than 10% below the products of group II. Group II September sea-ice concentrations exceed those of group I by 5-8%. We refer to App. G for the respective results for the other months.

3.3 Antarctic sea-ice area and extent

The SIA and SIE time-series shown in Fig. 8 for the Antarctic reveal a similar overall development for products extending back into the 1980ties and 1990ties. This applies to i): the overall positive trend until 2015 in both quantities; ii) the inter-annual variability, for instance, during 2000-2003 for the February SIA and SIE (Fig. 8 b, d), or in 2008 for the relative minimum in September SIA and SIE (Fig. 8 a, c); iii) the ranking between products. NOAA-CDR and CBT-SSMI provide largest SIA while NT1-SSMI provides smallest SIA, being ~1.8 million km² and 300 000 km² below the SIA of NOAA-CDR and CBT-SSMI for September and February, respectively. OSI-450 and ASI-SSMI SIA mostly fall into the range given by the other products. OSI-450 and CBT-SSMI provide largest SIE, exceeding the smallest SIE: NT1-SSMI by ~500 000 km² and ~300 000 km² in September and February, respectively (Fig. 8 c, d). Inter-product differences are larger for SIA than SIE for September but not for February.

For the AMSR-E period, the inter-annual variation is similar for all ten products. For September, SIA and SIE of the ESA-CCI products mostly fall between ASI-SSMI and OSI-450 (Fig. 8 a, c). For February (Fig. 8 b, d), SICCI-50km provides smallest overall SIA and SIE while the SICCI-12km and SICCI-25km products agree closely with OSI-450. In contrast to the Arctic (compare Fig. 6), NT2-AMSRE clearly provides largest SIA for both September and February, exceeding the second largest SIA: CBT-AMSRE for September and ASI-SSMI for February by ~ 500 000 km² (Fig. 8 a, b). NT2-AMSRE provides largest SIE for February as well (Fig. 8 d).

3.4 Antarctic sea-ice distribution differences

In September (Fig. 9), most products show more sea ice than the ensemble mean over high-concentration ice and less sea ice along the marginal ice zone. Exceptions are NT1-SSMI, ASI-SSMI, and NT2-AMSRE / CBT-AMSRE. NT1-SSMI (Fig. 9 a) exhibits less sea ice than the ensemble mean almost everywhere with differences even < -20%. ASI-SSMI (Fig. 9 d) exhibits a difference distribution reversed compared to most other products, exhibiting less sea ice than the ensemble mean

https://doi.org/10.5194/tc-2019-120
Preprint. Discussion started: 17 June 2019


The Cryosphere Discussions
Open Access
EGU

374 over high-concentration ice and more sea ice along the marginal ice zone. CBT-AMSRE and especially NT2-AMSRE (Fig. 9
375 i, j) show more sea ice than the ensemble mean in most regions – except the marginal ice zone in the Pacific ocean; differences
376 exceed 15% for NT2-AMSRE in the northern Weddell Sea.
377 Figure 11 g) agrees with these findings. NT1-SSMI and NT2-AMSRE stand out by providing the smallest and the largest
378 September mean sea-ice concentration, respectively. The overall mean NT1-SSMI September sea-ice concentration is smaller
379 than EUMETSAT-OSISAF – ESA-CCI (group I, compare Sect. 3.2) by 7-9%, and group II (CBT-SSMI, NOAA-CDR, CBT-
380 AMSRE, and NT2-AMSRE) by 9-14%; 14% is for NT2-AMSRE. The overall mean NT2-AMSRE September sea-ice
381 concentration exceeds those from group I by 5-6%, and the other products within group II by 3-4%. Between the EUMETSAT-
382 OSISAF – ESA-CCI products (group I), sea-ice concentration differences are within ±1.1%, consistent to the Arctic where
383 these differences are within ±0.7% (Fig. 11 a).
384 In January (Fig. 10), the few, comparably small, high-concentration areas exhibit sea-ice concentration differences mostly
385 below ±5%. Over the lower concentration areas, i.e. mainly in the Weddell and Ross Seas, most products show less sea ice
386 than the ensemble mean but differences are small, staying between 0 and -6%. Exceptions to this are NT1-SSMI, ASI-SSMI,
387 and NT2-AMSRE. NT1-SSMI shows even less sea ice (Fig. 10 a), differences reach -10%. ASI-SSMI (Fig. 10 d) and NT2-
388 AMSRE (Fig. 10 j) show more sea ice than the ensemble mean; differences are < 6% for ASI-SSMI but exceed 10% for NT2-
389 AMSRE. Important to note is the fringe of large, ~ -10%, negative differences along most of the Antarctic coast for SICCI-
390 50km (Fig. 10 h). Careful check of these regions in the daily and monthly SICCI-50km sea-ice concentration maps reveals
391 that as in the Arctic, the combined application of land-spill over filter and open water filter can result in the unwanted removal
392 of grid cells with ice (compare Fig. 7 h) and discussion of it). We are therefore confident that the comparably small February
393 SICCI-50km SIA and SIE values (Fig. 8 b, d) are, like in the Arctic, caused by a too aggressive filtering.
394 The sea-ice concentration differences shown in Fig. 11 j) confirm the observations from Fig. 10. As for September
395 (compare Fig. 11 g), NT2-AMSRE stands out as the product with a substantially larger mean sea-ice concentration than all
396 other products in February; differences range from 6.5% for ASI-SSMI to 12% for NT1-SSMI. Compared to September, NT1-
397 SSMI stands out less in February. Sea-ice concentration differences within group II (excluding NT2-AMSRE) are smaller for
398 CBT-AMSRE but larger for the other two products. Differences within group I are as small as for September, i.e. within
399 ±1.1%, but not for SICCI-50km (as can be expected from Fig. 10 h). Note that we show February (Fig. 11 j) instead of January
400 (Fig. 10) to be consistent with the SIA and SIE differences shown in Figure 11 k), l) and refer the reader to Fig. G2 a, b) in
401 App. G for comparison of the sea-ice concentration difference matrices of months January and February.

402 **4 Comparison with near-100% SIC reference data set**

403 In this section, we present the results of the evaluation of the ten products at 100% sea-ice concentration using the data
404 described in Sect. 2.2. We note that this is an extension of the analysis shown in Lavergne et al. (2019), where the non-truncated
405 SICCI-25km, SICCI-50km and OSI-450 sea-ice concentrations were used, i.e. including the natural geophysical retrieval noise
406 with a certain fraction of the sea-ice concentration values above 100% (see Sect. 2.1.4). Here, in contrast, we need to focus on
407 the truncated products, i.e. those constrained to the sea-ice concentration range 0% … 100%, because none of the other products
408 provide access to the non-truncated sea-ice concentration values.
409 We note upfront that caution should be exercised when reporting and interpreting evaluation statistics like bias (mean
410 value minus 100%) or root mean square error, near the 100% end of truncated sea-ice concentration products. This applies to
411 the results presented in this section but also to Sect. 5. First, the bias of truncated products will necessarily be negative or zero
412 (mean value lower than or equal to 100%), even though the bias of the product was exactly 0% before truncation. Second,
413 products whose non-truncated distribution is biased high (modal value larger than 100%) will seemingly achieve better
414 evaluation statistics after truncation, because of the accumulation of values > 100% being folded to exactly 100%. Both bias

https://doi.org/10.5194/tc-2019-120
Preprint. Discussion started: 17 June 2019

and RMSE of these products are smaller than those of products that do not overestimate at 100% sea-ice concentration. The larger the fraction of truncated values, the better the statistics. This is also illustrated in Fig. 3, where we infer the distribution of non-truncated values (red) from the distributions of truncated products (black). The values that accumulate at the 100% bin in the truncated product are in majority from the above 100% range of the non-truncated distribution (note the value of F_{99} in Fig. 3), and improve the evaluation statistics (bias and RMSE). In fact, under the hypothesis that the distribution of the retrieved sea-ice concentration is mostly Gaussian around the modal value before truncation, products with overestimation of the non-truncated distribution can be recognized by their abnormal (with respect to a Gaussian model) accumulation of values exactly at 100%. In the following, we thus start our analysis of the comparison against the near-100% sea-ice concentration reference data with a description of the observed distribution of values, using frequency histograms. We then report bias and RMSE values of the truncated and non-truncated sea-ice concentrations, using Gaussian fits (Sect. 2.1.4).

For more discussion and quantification of the error distribution of sea-ice concentration products and algorithms before truncation around 100% (and around 0%), see Ivanova et al. (2015).

4.1 Arctic

The distribution of the sea-ice concentration near 100% is shown for the Arctic for each product in Fig. 12 a) in form of the cumulative fraction of the deviation (bias) from 100% as a colour coded vertical bar. As expected the cumulative fraction increases towards 100% for all products. Distributions within the pair: SICCI-25km and OSI-450 as well as the pair: CBT-SSMI and CBT-AMSRE are quite similar, as expected; distributions of SICCI-12km and ASI-SSMI are similar particularly at the uppermost five to six bins. Apart from these similarities, considerable differences between the products are evident. EUMETSAT-OSISAF – ESA-CCI products exhibit a cumulative fraction between ~0.5 (SICCI-50km) and ~0.7 (SICCI-12km) in the last bin but one, i.e. in bin -1.5% … -0.5%. Both CBT products, NT1-SSMI and NOAA-CDR exhibit a substantially lower cumulative fraction for this bin: ~0.2 (NOAA-CDR, see also F_{99} in Fig. 3 c) to ~0.4 (NT1-SSMI). The distributions for these products look like as if one has taken the distribution of, for instance, OSI-450 but deleted the fractions of (at least) bins -1.5% … -0.5% and -2.5% … -1.5% if not also -3.5% … -2.5%; the distributions look incomplete. ASI-SSMI and NT2-AMSRE exhibit a cumulative fraction of ~0.8 in the last but one bin. However, while the cumulative fraction increases slowly towards a value of 0.8 for ASI-SSMI, for NT2-AMSRE it increases abruptly from < 0.1 in bin -2.5% … -1.5% to ~0.8. This behaviour is completely different to all other products and confirms the results of Ivanova et al (2015). They aimed to compare the precision of existing sea-ice concentration algorithms at 100% by means of computing the standard deviation of the sea-ice concentration at 100%. They were, however, unable to obtain standard deviations with a comparable statistics because of large positive biases for the, e.g., NT2 and ASI algorithms and because of the truncation of sea-ice concentrations at 100%. Only by constructing a reference sea-ice concentration of 75%, Ivanova et al. (2015) were able to carry out a comparison of the sea-ice concentration standard deviation based on non-truncated sea-ice concentrations.

These cumulative distributions suggest that an inter-comparison of the mean difference and its standard deviation should be carried out by means of the Gaussian fit proposed in Subsection 2.1.4 and Fig. 3. Consequently, the mean sea-ice concentrations of the ten products shown by the black symbols in Fig. 13 a) for the Arctic near-100% reference sea-ice concentration locations are the modal values of the Gaussian fits and the error bars denote one standard deviation of this fit around the modal value. The blue symbols and error bars denote the respective mean and one standard deviation computed from the non-truncated EUMETSAT-OSISAF – ESA-CCI sea-ice concentration products. All values shown here are summarized together with the results obtained from the truncated sea-ice concentration products in Table 3.

Figure 13 a) confirms our hypothesis that those products where the cumulative distributions seem to be incomplete (Fig. 12 a), i.e. the two CBT products, NT1-SSMI and NOAA-CDR, are likely to over-estimate the actual sea-ice concentration. These products reveal a modal sea-ice concentration > 100% according to the Gaussian fit applied; the over-estimation is particularly high for NOAA-CDR with a modal sea-ice concentration of ~103% (see also Table 3). Of the EUMETSAT-

https://doi.org/10.5194/tc-2019-120
Preprint. Discussion started: 17 June 2019

OSISAF – ESA-CCI products SICCI-50km (99.5%), OSI-450 (99.0%), SICCI-25km and SICCI-12km, in this order, exhibit modal sea-ice concentrations that are slightly below and closest to the near-100% reference. Figure 13 a) illustrates that the Gaussian fit almost perfectly matches the actually observed non-truncated sea-ice concentration for SICCI-50km also in terms of the standard deviation (compare blue and black symbols in Fig. 13 a) and Table 3). The match is less good for OSI-450 and SICCI-25km, where the mean observed sea-ice concentration falls below the fitted one by ~1%.

In addition, Fig. 13 a) and Table 3 confirm our hypothesis that the two CBT products, NT1-SSMI and NOAA-CDR, are likely to exhibit a standard deviation that is lowered considerably by truncating sea-ice concentrations to a maximum of 100%. All four products exhibit a standard deviation around the modal sea-ice concentration from the Gaussian fit of 4-5%, while the standard deviation computed from the truncated SICs is < 2% for the two CBT products and NOAA-CDR (Table 3). For EUMETSAT-OSISAF – ESA-CCI products the standard deviation of the non-truncated sea-ice concentration exceeds that of the truncated one systematically, as expected, by 0.4-0.6% (Table 3). Under the assumption that the standard deviation of the Gaussian fit is a better measure of the spread in sea-ice concentrations near (but below) 100%, we state that SICCI-50km, OSI-450, and SICCI-25km allow a precision of ~2%, ~3%, and ~3%, respectively, while products such as NOAA-CDR or the CBT products allow a precision of ~5% and ~3.5%, respectively. We also confirm the findings of Lavergne et al. (2019) that the EUMETSAT-OSISAF - ESA-CCI products are slightly – but significantly – biased low.

For ASI-SSMI and NT2-AMSRE, the application of a Gaussian fit is potentially not justified given the way sea-ice concentrations are retrieved. ASI-SSMI is non-linear near 100% (Kaleschke et al., 2001) while no statement about the functional relationship of the input satellite data and the retrieved sea-ice concentrations can be made for NT2-AMSRE (Markus and Cavalieri, 2000; Brucker et al., 2014). Our analysis, however, results in a reasonable Gaussian fit for ASI-SSMI in terms of RMSD of the fitted histogram (0.0062) as well as values for F_{99}: 0.806 and ΔF_{99} (0.001) (see App. H, Fig. H1 a). We are confident therefore that the values taken from the fit and shown in Fig. 13 a) and Table 3 can be used. In contrast, the NT2-AMSRE sea-ice concentration distribution does not allow reasonable application of a Gaussian fit (see App. H, Fig H1 j) and the respective values shown in Fig. 13 a) and Table 3 (and also Fig. 13 b) and Table 4) have to be interpreted carefully. Note that the standard deviation of 1.7% provided in Table 3 for the Gaussian fit of NT2-AMSRE is actually a weighted mean RMSD obtained from an evaluation of NT2-AMSRE sea-ice concentration data against satellite Landsat and air-borne optical imagery (Cavalieri et al., 2006). The respective standard deviation of 3.2% provided in Table 4 is a weighted mean RMSD obtained from an evaluation of NT2-AMSRE sea-ice concentration data against satellite MODIS optical imagery (Cavalieri et al., 2010).

Finally, we remark that the results of this comparison are based on data from winter months (see Sect. 2.2). But also during winter temperatures can get close to 0°C which might influence the brightness temperatures used to compute the sea-ice concentration and which also questions the assumption of prevailing freezing conditions applied in the generation of the near-100% reference sea-ice concentration data set. By using the co-located air temperature from ERA-Interim reanalysis data included in the RRDP2 data set (Pedersen et al., 2019), we repeated our analysis for cases with air temperatures below -10°C. We find that biases between satellite and reference sea-ice concentrations change by less than 0.1% for all products except NT1-SSMI for which we find a reduction in the bias by 0.3-0.4% when constraining the analysis to cold cases. The same finding applies to the Antarctic (see Sect. 4.2) where the reduction in the bias for NT1-SSMI is even higher: 0.6-0.7%.

4.2 Antarctic

The cumulative fraction of the deviation (bias) from 100% for the Antarctic sea-ice concentration of the ten products is shown in Fig. 12 b). While we again observe considerable differences between the products, we find more similarities between products than for the Arctic. Common to all products that show a gradual increase of the cumulative fraction, i.e. all products except NT2-AMSRE and ASI-SSMI, is a step change in the cumulative fraction between the last but one bin (-1.5% … -0.5%) and the last bin around 0%. This step change is least pronounced for NT1-SSMI and most pronounced for NOAA-

https://doi.org/10.5194/tc-2019-120
Preprint. Discussion started: 17 June 2019

CDR exhibiting cumulative fractions of ~0.8 and ~0.4, respectively, at the last but one bin (see also F_{99} value in Fig. 3 f). Step changes seem slightly larger for the two CBT products with a cumulative fraction: 0.4-0.5 compared to the EUMETSAT-OSISAF – ESA-CCI products with cumulative fractions of 0.5-0.6 (see also F_{99} values in Fig. 3 d), e)). Again, as expected, CBT-SSMI and CBT-AMSRE are very similar as are SICCI-25km, OSI-450 and, this time also, SICCI-12km (compare with Fig. 12 a). The cumulative distribution of ASI-SSMI sea-ice concentration biases seems to level off before the last bins which is also confirmed by a F_{99} value of the Gaussian fit of 0.93 (see App. H, Fig. H2 a), indicating that 93% of the ASI-SSMI sea-ice concentrations at the near-100% reference sea-ice concentration locations are below 99.5%. Similar to the Arctic, the distribution for NT2-AMSRE is extremely narrow; only the last two bins are occupied with the last but one bin exhibiting a cumulative fraction of ~0.25, suggesting that 75% of the NT2-AMSRE sea-ice concentrations at the near-100% reference sea-ice concentration locations are above 99.5%. This behaviour is, like in the Arctic, completely different to all other products and echo the findings of Ivanova et al. (2015), see also our discussion in Sect. 4.1.

Figure 13 b) and Table 4 illustrate that, when using the Gaussian fit as a measure, all products except ASI-SSMI, NT1-SSMI and NT2-AMSRE provide a modal sea-ice concentration which deviates by less than ~1% from 100%. While the two CBT products and NOAA-CDR tend to have a modal sea-ice concentration > 100%, all EUMETSAT-OSISAF – ESA-CCI products have modal sea-ice concentrations < 100%. NT1-SSMI and ASI-SSMI both under-estimate the near-100% reference sea-ice concentration by ~5%. We find that the modal sea-ice concentration obtained with the Gaussian fit agrees within 0.5% to the actually measured mean sea-ice concentration derived from the non-truncated values of the EUMETSAT-OSISAF – ESA-CCI products (compare black and blue symbols in Fig. 13 b). In addition, the respective standard deviations match better in the Antarctic than the Arctic (compare black and blue bars Fig. 13 a) and b) as well as Table 3 and 4). Like in the Arctic, using the non-truncated EUMETSAT-OSISAF – ESA-CCI products results in a systematically larger standard deviation, as expected, by 0.5 to 1.0% (Table 4), than obtained with the truncated products. We can confirm the notion from Sect. 4.1 that application of the Gaussian fit results in a larger standard deviation for the two CBT products and NOAA-CDR. Using the truncated products results in a standard deviation between 2.0% and 2.5% while the Gaussian fit suggests standard deviations of ~4.5% for CBT-SSMI and NOAA-CDR and ~5.5% for CBT-AMSRE. Therefore, again under the assumption that the standard deviations obtained from the Gaussian fit of the sea-ice concentration distribution at the near-100% reference sea-ice concentration locations is a reasonable measure for the spread of the concentration values, we find highest precision for SICCI-50km, SICCI-25km, and OSI-450 with standard deviations of 2.5%, 3.0% and 3.0%, respectively. For CBT-SSMI, NOAA-CDR, and CBT-AMSRE we find a lower precision with standard deviations of ~4.5%, 4.5%, and 5.5%, respectively. Similarly but to a lesser extent than in the Arctic, the EUMETSAT-OSISAF – ESA-CCI products are slightly biased low with respect to the validation data set.

5 Comparison with ship-based visual sea-ice cover observations

In this section, we present the results of the evaluation of the ten products at intermediate sea-ice concentrations by means of an inter-comparison to the visual ship-based observations described in Sect. 2.3. Like in Sect. 4 we show the results separately for the Arctic (Sect. 5.1) and the Antarctic (Sect. 5.2).

Upfront we note the limitations of the manual ship-based visual sea-ice cover observations used here. They were collected by a myriad of different observers with different levels of experience for this task. For an untrained observer it is relatively straightforward to estimate the total sea-ice concentration for closed ice conditions, i.e. > 80%, or very open ice conditions, i.e. < 30%. It is more difficult, however, to estimate whether sea ice covers, e.g. 40% or 50% of the 1 km radius area around the ship. Therefore, we can expect a reduced accuracy for ship-observations of the intermediate sea-ice concentration range from ~30% to ~ 80%. At the same time, this is possibly the sea-ice concentration range where the different spatial scales of the two kind of observations compared here have the largest impact on the results. In addition, ship observations were collected

https://doi.org/10.5194/tc-2019-120
Preprint. Discussion started: 17 June 2019

under different weather and daylight conditions as well as during different ship speeds. The first two points influence the visibility and change the visual appearance of sea ice and openings, and can result in a larger spread of an observed sea-ice concentration value around the actual value. Different weather conditions also have an influence on the size of the area actually observed around the ship that is difficult to quantify. This observation area is supposed to be of one kilometre radius but it can be assumed that it is smaller in case of poor visibility than it is in case of clear-sky, good visibility conditions; visibility is not regularly reported along with the ice observations. A single observation of the sea-ice conditions takes a certain period of time. The duration of this period is a function of the experience of the observer. The observation area around the ships' track represented by a single observation is hence a function of the ships' speed and of the experience of the observer. As long as ice conditions do not change for a few kilometres this does not matter but in highly heterogeneous ice conditions, this can be important. Therefore, there is a variable representativity of the observed sea-ice conditions around the ships' track.

A systematic investigation that allows quantification of the uncertainty in ship-based sea-ice observations has not been carried out yet and is beyond our scope. Even though we do not use single ship-based observations but follow Beitsch et al. (2015) and average over all ship-based sea-ice observations along the ships' track of one day, discarding days with less than three observations (see Sect. 2.3), we cannot exclude that some of these daily average observations are biased because of the reasons discussed above.

5.1 Arctic

The first question to answer is how the two sorts of observational data (ship and satellite) are distributed over the sea-ice concentration range from 0% to 100%. This is illustrated in Fig. 14 in the form of histograms showing the number of sea-ice concentration data falling into bins as described in Sect. 2.3. We find relatively few observations, in total less than 60 daily average along-track mean sea-ice concentration values, for bins < 55% sea-ice concentration. This applies to both ship and satellite observations, with the exception of NT1-SSMI (Fig. 14 a) with ~130 sea-ice concentration values in these lower concentration bins. Between 40 and 60 ship observations fall into each of the bins centred at 60% to 80%. The majority of the ship observations fall into the two bins with highest sea-ice concentrations: 110 into bin 85-95% and 125 into bin 95-100%. The products NT1-SSMI, OSI-450, SICCI-25km, and SICCI-50km (Fig. 14 a, e, g and h) exhibit the largest number of observations in bin 85-95%. All other products exhibit the largest number of observations in bin 95-100% (Fig. 14 b, c, d, f, i and j). Differences in the occupation of the two high-concentration bins are large for, e.g., NT2-AMSRE (Fig. 14 i): 95 and CBT-SSMI (Fig. 14 b): 130 while for EUMETSAT-OSISAF – ESA-CCI products and ASI-SSMI, values distribute relatively evenly into the two high-concentration bins.

Overall, for the Arctic, all ten products compare reasonably well to the ship-based observations (Fig. 15). However, the daily average along-track mean sea-ice concentrations scatter substantially around the diagonal. At high concentrations (> ~80%), EUMETSAT-OSISAF – ESA-CCI and ASI-SSMI products (Fig. 15 d to h) exhibit the most symmetric distributions around the diagonal. NT1-SSMI (Fig. 15 a) has an asymmetric distribution with a considerable fraction of satellite sea-ice concentrations even < 60%. Both other AMSRE products: CBT and NT2 (Fig. 15 i, j), and the two remaining SSM/I products: CBT-SSMI and NOAA-CDR (Fig. 15 b, c), show an asymmetric distribution with more high satellite- than high ship-based sea-ice concentrations. For most products, substantially more data pairs are situated below the diagonal, suggesting that satellite- are smaller than ship-based sea-ice concentrations. This is illustrated by a negative overall bias and regression lines located below the 1-to-1 fit line for six of the ten products (see Table 5). CBT-AMSRE, NT2-AMSRE, CBT-SSMI, and NOAA-CDR provide the smallest absolute overall bias of < 1%, but while CBT-SSMI and NOAA-CDR are the two products with slopes of the linear regression being closest to 1: 0.994 and 0.998, respectively, CBT-AMSRE and NT2-AMSRE are the two products with such slopes deviating most from 1: 1.063 and 1.061, respectively. The three ESA-CCI products provide – together with CBT-AMSRE – the highest squared linear correlation: 0.775 (SICCI-50km) to 0.784 (SICCI-12km).

https://doi.org/10.5194/tc-2019-120
Preprint. Discussion started: 17 June 2019

In Fig. 15, several of the products exhibit points along the y=0% sea-ice concentration line, i.e. conditions where sea-ice cover is reported by the ship-based estimate while the satellite estimates exactly 0%. This applies most to CBT-SSMI, NOAA-CDR, ASI-SSMI, and CBT-AMSRE (Fig 15 b, c, d and j). These points with zero daily mean sea-ice concentration are very likely the result of the weather filters applied (Sect. 2.1.3), which besides removing false sea ice caused by atmospheric effects, also removes true sea ice (Ivanova et al., 2015; Lavergne et al., 2019). The combination of explicit atmospheric correction and dynamic tuning of the weather filter in the EUMETSAT-OSISAF – ESA-CCI products seems to reduce the occurrence of such cases (Fig. 15 e, f and g) notably. Also NT1-SSMI (Fig. 15 a) and NT2-AMSRE (Fig. 15 i) exhibit a comparably small number of satellite sea-ice concentration at exactly 0% at non-zero ship-based concentrations. These observations agree well with the results shown in Fig. 1 – except for ASI-SSMI.

Now we briefly compare the results obtained for the entire year with those obtained separately for winter or summer months (see Fig. 5 for differences in location). For winter (highest correlation is obtained for SICCI-50km: $R^2 = 0.606$) for all products, R^2 is lower while for summer (highest correlation is obtained for SICCI-12km: $R^2 = 0.784$) R^2 is a little higher than for the entire year. For winter, this can be explained by fewer observations in general and by substantially less sea-ice concentration values at lower concentrations; most observations during winter are > 75%. The bias changes mostly by less than 1% between summer, winter and the entire year. ASI-SSMI provides the by far largest change in bias between winter and summer: 4.9%, while OSI-450 stands out with an inter-seasonal bias change of only ~0.1% (Table 5). Almost all products provide a lower standard deviation (SDEV) for winter than summer, except SICCI-12km and ASI-SSMI. For winter, CBT-SSMI has the smallest SDEV: 10.9% while NOAA-CDR, SICCI-25km and SICCI-50km are slightly higher: ~11.7%. For summer, EUMETSAT-OSISAF – ESA-CCI products provide the smallest SDEV: 11.7% to 12.9%. Again, OSI-450 stands out with an inter-seasonal SDEV change of only ~0.1%, followed by SICCI-25km and CBT-AMSRE with a value of 0.5%; CBT-SSMI provides the largest such change: 3.6%.

Binning the sea-ice concentrations of one data set, e.g. ship observations, into 10% wide bins and computing the mean sea-ice concentration of the other data set, e.g. here satellite observations, results in the red symbols in Fig. 15; doing the same but exchanging ship- and satellite observations in the blue symbols in Fig. 15. The motivation for such a step comes from the notion in Sect. 2.3 that the average accuracy of the ship-based sea-ice concentration observations is 10%. From these binned values and associated regression lines we find: 1) Ship-based observations in the range 50% to 80% are under-estimated by the satellite-based ones, particularly by the EUMETSAT-OSISAF – ESA-CCI products as illustrated in Fig. 15 e to h): a mean satellite sea-ice concentration of 55% compares to a ship-based sea-ice concentration of 70%. The only product where this is even worse is NT1-SSMI (Fig. 15 a). 2) Red regression line slopes of ESA-CCI products are closer to 1 than the black ones. For most of the other products – except CBT-SSMI and NOAA-CDR – red regression line slopes deviate more from 1 than the black ones.

5.2 Antarctic

In the Antarctic, we have a larger relative fraction of ship observations at lower concentrations <50%: ~ 90 values. Between 25 and 55 values fall into bins 60% to 80%. Bin 85% to 95% is the bin with the highest count of ship observations: ~100 while bin 95% to 100% contains ~70 ship observations. We find a similar distribution over the different sea-ice concentration bins for all ESA-CCI products (Fig. 16 f, g and h), ASI-SSMI (Fig. 16 d) and OSI-450 (Fig. 16 e). All these products share a maximum count in bin 85% to 95% and agree with the ship observations count of most other bins within 10 counts. An exception is bin 45% to 55% with considerably more ship than satellite observations. All other products either have the highest count in bin 95% to 100%, especially NT2-AMSRE (Fig. 16 i), or have a similarly large count for bin 85% to 95% and bin 75% to 85%: ~80, but a count almost as low as 10 for bin 95% to 100% (NT1-SSMI, Fig. 16 a). We note that all products have larger counts at sea-ice concentrations < 25% than the ship observations.

https://doi.org/10.5194/tc-2019-120
Preprint. Discussion started: 17 June 2019

622 The scatterplots of the daily average along-track mean sea-ice concentrations for the Antarctic (Fig. 17) reveal, for
623 sea-ice concentrations > ~80%, mostly symmetric distributions for seven of the ten products; only CBT-AMSRE, and
624 particularly NT1-SSMI and NT2-AMSRE have asymmetric distributions here (Fig 17 j, and a, i). Like in the Arctic, NT1-
625 SSMI has considerably more low than high sea-ice concentration values (compare Fig. 15 a). NT2-AMSRE exhibits almost
626 no data points below the 1-to-1 fit line at > ~80% with data pairs concentrated at 100% satellite sea-ice concentration. While
627 the sea-ice concentrations distribute symmetric around the 1-to-1 line for most products until about 50%, there is a considerable
628 drop in the count of data values above the 1-to-1 line at lower concentrations and the distribution becomes asymmetric. This
629 agrees with Fig. 16 showing a general lack of ship-based sea-ice concentrations < ~ 20%. Not surprisingly we find the lowest
630 overall biases (see Table 6) for those products that exhibit more satellite- than ship-based high sea-ice concentrations and, at
631 the same time, less satellite- than ship-based low sea-ice concentrations, i.e. CBT-SSMI, CBT-AMSRE and NOAA-CDR with
632 biases between -1.4% and -2.3%. We find the largest bias for NT1-SSMI: -11.0%. NT2-AMSRE is the only product with a
633 considerable positive bias: +4.5%. NT1-SSMI, ASI-SSMI, and OSI-450 all provide slopes of the linear regression close to 1:
634 0.993, 0.993, and 1.010, respectively. Slopes for CBT-SSMI, NOAA-CDR and CBT-AMSRE increasingly deviate from 1:
635 1.057, 1.082, and 1.126, respectively. The highest overall linear correlation is obtained for SICCI-12km, followed by CBT-
636 AMSRE and the other EUMETSAT-OSISAF – ESA-CCI products. These provide the lowest SDEV values ranging between
637 13.4% and 14.0% (Table 6), followed by NT1-SSMI and CBT-AMSRE with 14.8%. As is the case in the Arctic, all products
638 but the EUMETSAT-OSISAF – ESA-CCI ones exhibit data pairs along the y=0% axis, associated with removal of true sea-
639 ice concentration by a weather filter.
640 A comparison between the results of the entire year with those obtained separately for winter and summer (see Fig. 5
641 for difference in locations) reveals differences to the Arctic. For winter (highest correlation is obtained for SICCI-12km and
642 SICCI-25km: $R^2 = 0.771$) R^2 increases for most products compared to the entire year while for summer all products exhibit a
643 smaller R^2 value (highest correlation is obtained for SICCI-12km: $R^2 = 0.698$). For all products, except ASI-SSMI and NT1-
644 SSMI, biases are smaller in winter than summer by mostly < 2%. NT2-AMRE is the only product with a positive bias in both
645 seasons. The largest inter-seasonal bias change is obtained for CBT-AMSRE: 2.7% and SICCI-25km: 2.9%, respectively, the
646 smallest for CBT-SSMI: 0.4%. For all products, the SDEV is smaller by 3-5% compared to the entire year in winter while for
647 summer, SDEV values are larger by 2-3%. Inter-seasonal SDEV changes are hence considerably larger than for the Arctic
648 with smallest values of 4.9% and 5.1% for NT1-SSMI and OSI-450, respectively, and largest value of 9.3% for NT2-AMSRE
649 (compare Tables 5 and 6).
650 Binning the sea-ice concentrations like described in Sect. 5.1 (red symbols in Fig. 17) leads to the following main
651 observations. 1) All products – except NT1-SSMI and NT2-AMSRE – have the best agreement with ship-based observations
652 in the sea-ice concentration range 60% to 80%. 2) All products under-estimate ship-based sea-ice concentrations for
653 concentrations < ~50%. 3) The negative bias of ~10% observed for NT1-SSMI applies to the entire sea-ice concentration
654 range. 4) NT2-AMSRE is the only product over-estimating ship-based sea-ice concentrations considerably; this over-
655 estimation reaches 10% for the range 60% to 80%. Regression lines based on these binned data (red lines in Fig. 17) have a
656 similar or slightly steeper slope than those based on the un-binned data (black lines). Applying the binning to the satellite sea-
657 ice concentration (blue symbols in Fig. 17) results in a distribution of the data pairs which without exception – as for the Arctic
658 – yields substantially steeper regression lines, underpinning the over-estimation of the ship-based observations particularly at
659 low concentrations.

https://doi.org/10.5194/tc-2019-120
Preprint. Discussion started: 17 June 2019

6 Discussion, Outlook and Conclusions

6.1 Discussion

In this paper, we assessed the quality of sea-ice concentration of the EUMETSAT-OSISAF – ESA-CCI products against other sea-ice concentration products and independent data sets. These data sets are: 1) A near-100% reference sea-ice concentration data set based on the analysis of regions with convergent sea-ice motion in high-concentration sea ice during winter based on SAR imagery (Sect. 2.2 and Sect. 4), and 2) quality-controlled compilations of about 15 000 individual visual ship-based observations of the sea-ice cover (Sect. 2.3 and Sect. 5). The first part of the assessment we carried out without additional data by showing and discussing time-series of sea-ice area (SIA) and extent (SIE) as well as difference between the sea-ice concentrations of all ten products (Sect. 3).

6.1.1 Observed differences in sea-ice area and extent

Time series of SIA and SIE have since long been used to derive conclusions about the past development of the sea-ice cover and to even extrapolate its future development. In order to do so, such time series need to be sufficiently long, consistent and accurate. A long, consistent time-series is typically obtained using a fundamental climate data record of brightness temperatures as input for the retrieval, as is done, e.g., for group I product OSI-450, to ensure that inter-sensor differences are as small as possible. Our paper suggests that additional steps might be required, for instance, dynamic retrieval of tie points and dynamic adaptation of weather filters (see Sect. 6.1.2) to reach the goal of a long-term consistent sea-ice concentration data set to be used to compute long-term consistent time-series of SIA and SIE.

Recently, Meier and Steward (2019) suggested a method to obtain an estimate of SIE and sea-ice index accuracy, which they found to be ~50 000 km² under certain circumstances for the Arctic. They also pointed out, however, that there is a clear bias (or spread) of 500 000 km² to 1 million km² between SIE estimates from different products. Therefore, as long as one does not know which product provides the best representation of the actual sea-ice cover, one is left with a relatively precise estimate of the SIE, which might likely be biased by an amount an order of magnitude larger. Considerable spreads between products are also visible in our Fig 6 and Fig. 8, especially for SIA, which we think is the parameter suited better to describe state and variability of the polar sea-ice covers. Notz (2014) found that the SIE and its trend provide a limited metric for the performance of numerical models. Petty et al. (2018) suggested that predictions of the September Arctic sea-ice minimum in area and extent would benefit from giving more weight to SIA. Niederdrenk and Notz (2018) concluded that observational uncertainty is the main source of uncertainty for estimating at which level of global warming the Arctic will lose its summer sea-ice cover. In the light of these findings, we suggest putting emphasis on discussing inter-product biases in SIE and especially SIA is warranted in the context of this paper about sea-ice concentration product evaluation.

The inter-annual variability of the ten products' SIA and SIE is very similar (Fig. 6 and Fig. 8) while differences in sea-ice concentration between the products can be substantial (Fig. 7, Fig. 9 through Fig. 11). Extensive filtering of potential coastal artifacts in the sea-ice concentration can cause a particularly large difference in SIA and SIE between SICCI-50km, and the three other EUMETSAT-OSISAF – ESA-CCI products (see Fig. 7 and Fig. 10). A difference in SIA can often be explained with a difference in sea-ice concentration retrieved by a particularly algorithm. A difference in SIE is, however, independent of the actual sea-ice concentration as long as it is above 15%. The observed differences in SIE (Fig. 6 c, d) and Fig. 8 c, d) therefore potentially result from different sea-ice concentrations in the marginal ice zone / along the ice edge, from differences in correction of the land spill-over effect (coastal correction henceforth), from differences in the weather filter, or from differences in the land-cover fraction.

In the matrices showing the differences between SIA and SIE for all ten products for the AMSR-E period (Fig. 11, middle and right column), the influence of the different land cover fractions has been mitigated. We first discuss the Arctic. For SIA, EUMETSAT-OSISAF – ESA-CCI (group I) products agree with each other within ~ ±100 000 km² in March and

https://doi.org/10.5194/tc-2019-120
Preprint. Discussion started: 17 June 2019

September (Fig. 11 b, e). This is an important result taking into account that within this group data of different satellite sensors are used (SICCI-2: AMSR-E; OSI-450: SSM/I, SSMIS). The same applies to group II, i.e. CBT-SSMI, NOAA-CDR, CBT-AMSRE, and NT2-AMSRE in September but not in March, when within group II SIA based on SSM/I-SSMIS data agrees to SIA based on AMSR-E data only within ~ ±300 000 km². In March, NT1-SSMI and ASI-SSMI (group III) stand out with a ~400 000 km² to ~800 000 km² smaller SIA than all other products. In September, only NT1-SSMI stands out with SIA differences to all other products similar to those in March. For SIE, the majority of all products agrees with each other within ~ ±200 000 km² (~ 4-5% of mean SIE) in September (Fig. 11 f); larger differences only occur between NT1-SSMI and OSI-450, CBT-SSMI or NOAA-CDR. In March, OSI-450, SICCI-12km, SICCI-25km, CBT-SSMI and NOAA-CDR exceed three to five of the other products by ≥ ~ 300 000 km², and only half of the products agree with each other within ~ ±200 000 km² (Fig. 11 c).

In the Antarctic (Fig. 11 h, i, k and l), EUMETSAT-OSISAF – ESA-CCI (group I) SIA values agree with each other within ~ ±200 000 km² in September and February (Fig. 11 h, i). For September (Fig. 11 h), NT1-SSMI and NT2-AMSRE stand out. NT1-SSMI SIA is smaller than all other products by between ~1.4 million km² (ASI-SSMI) and ~2.8 million km² (NT2-AMSRE). This confirms the documented under-estimation of Antarctic sea-ice concentration by the NASA-Team algorithm during that time of the year (e.g., Comiso et al., 1997). In contrast, NT2-AMSRE SIA is larger than all other products by ~0.6 million km² (CBT-AMSRE) and ~2.8 million km² (NT1-SSMI). CBT-AMSRE SIA is larger than all other products (except NT2-AMSRE) while ASI-SSMI SIA is smaller than all other products (except NT2-AMSRE). For February (Fig. 11 k) inter-product SIA differences are overall small except for NT2-AMSRE, which exceeds all other products by ~300 000 km² (~15%) or more. For SIE, inter-product differences are much smaller than for SIA in September (Fig. 11 i) and comparable to those for SIA in February (Fig. 11 l). Most products agree with each other within ±200 000 km² in September and within ±300 000 km² in February. For September, we find largest differences for NT1-SSMI being by between 300 000 km² and 700 000 km² smaller than all other products, and for OSI-450 being larger than most other products by ~200 000 km². Note that, in contrast to SIA, NT2-AMSRE SIE differences are much smaller and compare to, e.g., CBT-AMSRE. In February, NT2-AMSRE SIE is larger than six other products by 300 000 km² (10%) or more, while SICCI-50km SIE is smaller than six other products by 300 000 km² or more. For SICCI-50km, we can attribute this smaller SIE in February to the already mentioned too aggressive filtering (see discussion of Fig. 7 and Fig. 10).

For Fig. 6 through Fig. 11 we used the truncated sea-ice concentration values as far as it concerns the EUMETSAT-OSISAF – ESA-CCI products. Repeating these computations with the non-truncated values, e.g. for September and March, does not change the results with respect to SIE because only the 15% sea-ice concentration threshold counts which is not changed by this action. With respect to SIA we find an increase by ~50 000 km² in the respective winter months and almost no impact for the summer months.

6.1.2 The role of weather filters

In Fig. 1 and Fig. 2 we illustrated that the weather filters implemented in each of the ten products, have quite different behaviour, despite the fact they all use the same gradient ratios of brightness temperature frequency channels. The potential users should be aware of this. We confirm that the dynamic open water filters designed for the EUMETSAT-OSISAF - ESA-CCI products have a stable impact on the lower part of the sea-ice concentration, cutting through it at about 10% SIC. This is across the months, changes of sensors (and thus frequencies, calibration, etc…) and for both hemispheres. We refer to Lavergne et al. (2019) for discussions how this consistency could be improved further. The analysis sheds also light on how the other six products perform in terms of stability. We are here interested both in the temporal consistency of the weather filter effects (e.g. jumps across instruments, across months, across climate-induced trends) and the absolute level at which they cut through the sea-ice concentration distribution, especially with respect to the 15% threshold embedded in the SIE and SIA curves shown

https://doi.org/10.5194/tc-2019-120
Preprint. Discussion started: 17 June 2019

in Fig. 6 and Fig. 8. CBT-SSMI, NOAA-CDR, and CBT-AMSRE products all cut around 15%, sometimes below, sometimes above, but in general at higher sea-ice concentration than the EUMETSAT-OSISAF – ESA-CCI ones (Fig. 1 and Fig. 2).

CBT-SSMI exhibits jumps when transitioning from one sensor to the next, for example from 1987 to 1988 (SMMR to SSM/I) for both hemispheres in September (Fig. 1 g, Fig. 2 a) and in the Arctic in March (Fig. 1 a); see also NT1-SSMI in the Antarctic (Fig. 2 a). It is noteworthy that the 23.0 GHz channels of the SMMR instrument have been highly unstable since launch, and eventually ceased to function on 11 March 1985 (Njoku et al., 1998). Thus, the water-vapour part of the "classic" weather filter is un-reliable in the early decade of the satellite data record. This is solved in the OSI-450 product by relying on explicit atmospheric correction of the brightness temperatures using -among others- water vapour fields from atmosphere re-analysis (see Lavergne et al., 2019). This discontinuity seems to be apparent in the September Antarctic SIE (Fig. 7 c): OSI-450 and CBT-SSMI agree with each other for the SMMR period while after 1987 CBT-SSMI is below OSI-450 by ~ 150 000 km². This corresponds to the area of one quarter of all 25 km grid cells centred at 60°S, the approximate average location of the Antarctic September sea-ice edge. This change in SIE is concomitant with a jump in the weather-filter sea-ice concentration from 11% to 14% (Fig. 2 a).

The NOAA-CDR starts with SSM/I in 1987 and thus avoids the 1987/88 jump. However, compared to OSI-450 and SICCI-25km we find for NOAA-CDR: 1) The sea-ice concentration at which the weather filter applies varies seasonally. For instance, in the year 1996, the mean 5% percentile of sea-ice concentrations within the interval]0%, 30%] is 14% for March but 17% for September in the Arctic, and 16% for September but 18% for February in the Antarctic. OSI-450 cuts at 10%, SICCI-25km at 11% for these months, and in both hemispheres. 2) The inter-annual variation of the sea-ice concentration at which the filter applies is larger for NOAA-CDR than for OSI-450 and SICCI-25km. In addition, the curves for NOAA-CDR (and CBT-SSMI) in Fig. 1 a) (March) and Fig. 2 (September) exhibit a discontinuity in the transition from 2007 to 2008, which corresponds to when SSMIS (F17) is processed instead of SSM/I (F15). OSI-450 exhibits no discontinuity here. This discontinuity occurs in March (Arctic) and September (Antarctic), i.e. both at maximum sea-ice extent, and is concomitant with a shift between OSI-450 and NOAA-CDR SIE by 50 000 to 100 000 km² between 2007 and 2008 (not shown). Our conclusion from these observations is that because the weather-filters of this class of products cut the sea-ice concentration distribution within ±5% to the sea-ice concentration threshold of 15% typically applied to compute SIA and SIE, they might have an influence on the observed differences in SIA and SIE between the products.

It appears as if for the remaining three products: NT2-AMSRE, NT1-SSMI and ASI-SSMI, considerations of the kind discussed above do not apply. NT2-AMSRE and ASI-SSMI provide a weather-filter cut-off sea-ice concentration of ~1-2% according to our analysis (Fig. 1 and Fig. 2), well below 15%; little can be said about potential inconsistencies between SSM/I and SSMIS for ASI-SSMI and their impact for SIA or SIE estimates. NT1-SSMI exhibits a rather constant weather-filter cut-off sea-ice concentration of ~1% for the Arctic (Fig. 1) but shows much more variability of it for the Antarctic (Fig. 2). Weather-filter cut-off sea-ice concentrations are ~5% for the SMMR period, decrease to ~2% for the SSM/I period, and then jump to ~6% for the SSMIS period; note that Fig. 2 d) is from the year 2004 and hence from the SSM/I period. Since these inconsistencies are, however, well below 15% we do not expect any impact on our results as far as it concerns the overall mean sea-ice concentration, SIA and SIE.

In any case, Fig. 1 and Fig. 2 are a new illustration that data products can differ in many ways. Such time-series, adapted from Lavergne et al. (2019), are an effective tool for data-producers and users to assess the temporal consistency of sea-ice concentration data products.

6.1.3 The role of truncating sea-ice concentrations at 100%

In near-100% sea-ice concentration conditions, retrieval algorithms will naturally retrieve bell-shaped distribution of values, returning values both below and above 100% sea-ice concentration. However, the above-100% values are almost never accessible to the user, and thus generally not accessible for validation. Here, we used the availability of these "off-range"

https://doi.org/10.5194/tc-2019-120
Preprint. Discussion started: 17 June 2019

784 estimates in the four EUMETSAT-OSISAF - ESA-CCI products to demonstrate how the "off-range" distribution can
785 effectively be reconstructed a-posteriori from the products with truncated sea-ice concentration distributions (Fig. 3). This
786 Gaussian-fit methodology allows us to go deeper in the analysis of near-100% conditions. Indeed, if the analysis had been
787 limited to the truncated distributions only (shown in Fig. 12), algorithms that over-estimate sea-ice concentration (modal value
788 of the non-truncated distribution larger than 100%) would obtain better validation statistics (smaller bias and RMSE) than
789 products with no over-estimation (modal value of the non-truncated distribution exactly at 100%). The larger the over-
790 estimation, the better the statistics would be. Using the Gaussian fit, we unveil a possible over-estimation of several sea-ice
791 concentration products, including NT1-SSMI, CBT-SSMI, and NOAA-CDR in the Arctic, and NOAA-CDR (but only slightly)
792 in Antarctic sea-ice conditions. This Gaussian-fit methodology also confirms that the EUMETSAT-OSISAF - ESA-CCI
793 products are slightly low biased in the Arctic (as already documented by Lavergne et al., 2019). The worst of these biases we
794 find in the Arctic for SICCI-12km that was not openly distributed at the end of the ESA CCI Sea Ice Phase 2 project, partly
795 based on these results.
796 In Appendix H, we present the full set of Gaussian fits for all ten products for both Arctic and Antarctic in Fig. H1
797 and Fig. H2 (see also Fig. 3). Based on these additional results we can see that indeed the Gaussian fit matches the non-
798 truncated sea-ice concentration distribution of the EUMETSAT-OSISAF – ESA-CCI products quite well by the good
799 agreement in the shape of the distributions as well as the reasonably low RMSD of 0.0037 in six of the eight cases (0.0025 and
800 0.0050 otherwise). We can see also, however, that there are discrepancies and limitations. In the Arctic (App. H, Fig. H1) the
801 Gaussian fit under-estimates the probability in the left tail for SICCI-12km, SICCI-25km, and OSI-450; in the Antarctic we
802 observe such an under-estimation for SICCI-25km and OSI-450 (App. H, Fig. H2). At the same time, we find an over-
803 estimation in the right tail, i.e. > 100% for SICCI-12km and SICCI-25km in the Arctic and for SICCI-50km in the Antarctic.
804 Possible explanations for the quoted under-estimation could be: i) Sea-ice concentrations have actually been that low even at
805 the locations of the RRDP2 near-100% references sea-ice concentration data set. ii) The impact of tie points not matching with
806 the actually present snow / sea-ice surface conditions on the retrieved sea-ice concentration is not symmetric around 100%.
807 We also see that for SICCI-50km, our step to bin the sea-ice concentrations to integer values before the inter-comparison with
808 the other products, results in a distribution around 100%, which is almost too narrow to fit it properly.
809 For the other algorithms, in the Arctic, the Gaussian fit matches perfectly well for sea-ice concentrations ≤ 99% for
810 CBT-SSMI, NOAA-CDR, and CBT-AMSRE with RMSD values of 0.0017 and 0.0023 (this is even better than for the
811 EUMETSAT-OSISAF – ESA-CCI). The match is less good for NT1-SSMI and ASI-SSMI with RMSD values of 0.0050 and
812 0.0062 (App. H, Fig. H1); we discussed the latter already in the context of Fig. 3 and refer to Ivanova et al. (2015) who,
813 because of the non-linearity of this algorithm, were forced to construct an artificial evaluation data set. By comparing the
814 fraction under the red curve for sea-ice concentrations > 99% with the value for F_{99} of 0.806, we consider the Gaussian fit
815 applicable. This can be confirmed for the Antarctic (App. H, Fig. H2 a)). For the Antarctic, the match between observed sea-
816 ice concentrations ≤ 99% and Gaussian fit is less good than in the Arctic for, especially, CBT-SSMI and CBT-AMSRE; RMSD
817 values are comparably large: 0.0050 and 0.0058, respectively, and the sea-ice concentration distributions is considerably less
818 bell shaped than in the Arctic. It is beyond the scope of this study to further fine tune the Gaussian fit so that the match with
819 the observations improves. We note that the results with respect to Gaussian fits shown in Appendix H, Fig. H1 and Fig. H2
820 apply also to the longer RRDP2 near-100% reference sea-ice concentration data set of winters 2007 through 2015, which
821 contains considerable more data pairs.
822 Finally, the analysis of the validation at 100% conditions raises a critical question to be discussed in the future among
823 data producers and with the data users: "Given that sea-ice concentration products are used after a 100% sea-ice concentration
824 threshold is applied, is it better to have algorithms (slightly) overshoot the sea-ice concentration distribution or should data
825 producers aim at an unbiased non-truncated distribution?" To let algorithms overshoot will return fewer below-100% estimates
826 in the product files which might be positive for large areas of the inner sea-ice cover during winter, but will also automatically

https://doi.org/10.5194/tc-2019-120
Preprint. Discussion started: 17 June 2019

reduce the sensitivity of the product to actual small openings in the sea-ice, which are so important for the ocean/atmosphere heat exchange in cold winter conditions. To aim at an unbiased algorithm might help with a better sensitivity to small openings (but note the RMSE of non-truncated retrievals ranges between 2% and 5% for the various algorithms studied here), however, the product grid will have more below-100% estimates. Our analysis, supported by the Gaussian-fit method, helps introducing the question and opening the discussion, but does not bring the answer.

6.1.4 Observed differences to ship-based observations

The comparison to the ship-based observations presented in Sect. 5 is carried out using truncated EUMETSAT-OSISAF – ESA-CCI sea-ice concentration data. Using the non-truncated EUMETSAT-OSISAF – ESA-CCI products does not considerably change our findings. Differences between satellite- and ship-based sea-ice concentrations reduce by between 0 and 0.3% with a concomitant increase in the standard deviation of up to 0.2% (see Fig. 15 and Fig. 17, and Tables 5 and 6); this applies primarily to winter when the fraction of near ~100% sea-ice concentrations is large. While application of the Gaussian-fit method (see Sect. 2.1.4 and Sect. 6.1.3) seems not appropriate given the wide sea-ice concentration range considered in this inter-comparison, it is reasonable to assume that it would change the differences (standard deviations) found for all other products by up to a few tenth of a percent (some tenths of a percent). However, these changes would be small compared to the accuracy of the ship-based sea-ice concentrations (see Sect. 2.3 and beginning of Sect. 5).

According to the summaries given in Tables 5 and 6, we can divide the ten products into three groups. Group I contains the EUMETSAT-OSISAF – ESA-CCI products, group II contains CBT-SSMI, NOAA-CDR, NT2-AMSRE and CBT-AMSRE, and group III consists of ASI-SSMI and NT1-SSMI. Note that this division into groups is similar to the one introduced in the context of, e.g., Fig. 11. Products of group II provide the smallest overall difference to the ship-based observations: around 0% (Arctic) and around -2% (Antarctic). An exception is NT2-AMSRE, which provides considerably more ice than the ship-observations in the Antarctic: +4.5%. Products of group I provide differences around -7.5% (Arctic) and -3.5% (Antarctic); in both hemispheres the difference is largest for SICCI-25km. Groups I and II share similar average values for R^2 in the Arctic: 0.77 and 0.76 and in the Antarctic: 0.74 and 0.72, respectively. Standard deviations are a little smaller for group I than group II: 12.3% versus 13.2% (Arctic) and 13.7% versus 15.6% (Antarctic). NT1-SSMI provides by far the largest difference to ship-observations in both hemispheres, paired with generally lower correlation and higher standard deviation.

ASI-SSMI provides the smallest values for R^2 in both hemispheres. ASI-SSMI reveals a substantially improvement in the inter-comparison results between winter and summer in the Arctic: correlation increases, difference and standard deviation decrease. This could be attributed to the higher fraction of inter-mediate sea-ice concentrations during summer for which the comparably fine grid resolution of 12.5 km of the ASI-SSMI product could be of advantage. While an increase of the correlation between winter and summer is observed also for all other products, such a notable decrease in difference and standard deviation is not – except for SICCI-12km. This product is also provided at 12.5 km grid resolution but in contrast to ASI-SSMI combines brightness temperatures at two different frequencies and hence different native resolutions (see Table 2). Because in the Antarctic the sea-ice cover is more open also during winter it is plausible that such an improvement in inter-comparison results between winter and summer is lacking there.

Figure 14 through Fig. 17 reveal quite a high fraction of sea-ice concentrations in the range 95% to 100%. This might have biased the results. We therefore repeated our comparison by discarding all data pairs with daily mean sea-ice concentrations $\geq$ 95%. Main results (not shown) are an overall increase in the differences by about 2% and of the standard deviations by ~ 1% (group I) and 2-3% (group II) and a reduction of the correlation by ~0.08. This results in R^2 of 0.68 versus 0.63 (Arctic) and 0.67 versus 0.63 (Antarctic) for group I and II, respectively, and in standard deviations of 13.8% versus 16.3% (Arctic) and 14.9% versus 18.0% (Antarctic). While group I exhibits larger differences than group II, inter-comparison results are better for group I than group II otherwise.

https://doi.org/10.5194/tc-2019-120
Preprint. Discussion started: 17 June 2019

One of the innovations of the products of group I is the self-optimizing capability of the algorithms to adopt to seasonally changing sea-ice conditions, i.e. the transition between winter and summer. If ship-based sea-ice observations are as reliable in summer as they are in winter then a comparison of the differences and standard deviations obtained for winter and summer could reveal how well an algorithm deals with the seasonally changing sea-ice conditions. In the Arctic, SICCI-25km, SICCI-50km and OSI-450 stand out with winter-to-summer changes in the difference by 0.2%, 0.3% and 0.1%, respectively, compared to ~3.5% for products of group II. Results are more diverse for the standard deviation where products of group II exhibit winter-to-summer changes between 0.1% (CBT-SSMI) and 5.2% (CBT-AMSRE) while SICCI-25km, SICCI-50km and OSI-450 exhibit values of 2.8%, 2.6% and 2.6%, respectively. Largest winter-to-summer changes are provided by ASI-SSMI: 6.7% (difference) and 6.1% (standard deviation). In the Antarctic, smallest winter-to-summer differences are obtained for SICCI-12km and OSI-450: 0.2% and 0.4%, respectively, compared to ~2.5% for products of group II. These provide a winter-to-summer change in standard deviation of ~6.5% while SICCI-12km and OSI-450 exhibit smaller values of 3.7% and 4.2%. These results, which have been obtained by, again, discarding mean sea-ice concentrations ≥ 95%, suggest that EUMETSAT-OSISAF – ESA-CCI products compare with the ship-based sea-ice observations more consistently across seasons than the other products.

6.2 Outlook

The algorithms implemented in the EUMETSAT-OSISAF – ESA-CCI products are continuously under development, and several improvements are planned in the course of the next phase of the ESA-CCI sea ice project (so called CCI+), and the running phase of the EUMETSAT-OSISAF project. Some of the research and development items planned are directly triggered by the findings in this paper. In particular, CCI+ will focus on improving upon the SICCI-12km data record that combines the ~19 GHz and ~90 GHz channels of AMSR-E and AMSR2 missions. The version of SICCI-12km evaluated in this paper was not performing well enough (especially bias in NH) and has not been released. Algorithms using ~90 GHz channels will be studied in more depth during CCI+, since these channels have the potential to bring higher spatial resolution and thus bridging the gap towards the WMO GCOS requirements. Another relative weakness of the EUMETSAT-OSISAF - ESA-CCI data products seems to be the correction of the land spill-over contamination, which showed most in the SIE and SIA time-series for SICCI-50km. A dedicated effort to improve on this is starting in the context of the EUMETSAT-OSISAF project. Finally, the small (but significant) low bias of the OSI-450 and SICCI-25km at near-100% conditions will be addressed towards the next version of the EUMETSAT-OSISAF – ESA-CCI data products, scheduled for 2021. The sea-ice concentration uncertainty estimates will be analysed during the next phase of the ESA-CCI sea ice project (CCI+). In particular, an end-to-end uncertainty analysis will be done with the aim of identifying individual uncertainty contributions and for possibly splitting the SIC uncertainty budget into more components.

6.3 Conclusions

Recently, three new global sea-ice concentration (SIC) climate data records (CDRs) have been released. They are described in Lavergne et al. (2019). These so-called EUMETSAT-OSISAF – ESA-CCI products: SICCI-25km, SICCI-50km, and OSI-450, utilize a dynamic, self-optimizing hybrid sea-ice concentration algorithm, which is applied to satellite microwave brightness temperature measurements of the SMMR, SSM/I and SSMIS instruments (OSI-450) or the AMSR-E and AMSR2 instruments (SICCI-25km and SICCI-50km); see Table 1 for instruments and frequencies. Within this paper, these EUMETSAT-OSISAF – ESA-CCI products are evaluated by means of an inter-comparison to products of seven other sea-ice concentration algorithms (see Table 2 for acronyms and satellite sensors and frequencies used) and with independent sea-ice cover data. These independent sea-ice cover data are a global winter-time near-100% reference sea-ice concentration data set (Sect. 2.2) and a global year-round data set of ship-based visual observations of the sea-ice cover (Sect. 2.3). Because five of

https://doi.org/10.5194/tc-2019-120
Preprint. Discussion started: 17 June 2019

909 the products are based on AMSR-E data, our core evaluation period is the AMSR-E measurement period, i.e. June 2002
910 through September 2011.
911 We find a very good and consistent agreement in inter-annual variation of the monthly mean SIA and SIE for both
912 hemispheres for the overlap periods of the respective products. Unexpected low SIE of SICCI-50km during Arctic winter and
913 Antarctic summer we can explain by a too aggressive filtering of near-coastal and potentially weather-influenced grid cells
914 near coastlines, which removed a substantial number of grid cells with ice. When taking this issue into account, the
915 EUMETSAT-OSISAF – ESA-CCI products provide quite similar values for SIC, SIA and SIE for both hemispheres, during
916 times of both maximum and minimum sea-ice cover. Overall differences are < 1.0% for SIC, and < 100 000 km² (Arctic) and
917 < 200 000 km² (Antarctic) for both SIA and SIE. A similarly good agreement in SIC, SIA and SIE for both hemispheres is
918 observed for the product pair CBT-SSMI – NOAA-CDR (see Table 2), as expected (see Appendix F and Peng et al., 2013).
919 Between the remaining four products, i.e., ASI-SSMI, NT1-SSMI, CBT-AMSRE, and NT2-AMSRE (Table 2), and between
920 these and the above-quoted six products, we find considerably larger differences between SIC, SIA, and SIE – which vary
921 with algorithm, season, and hemisphere. Largest differences are found for NT1-SSMI: less sea ice than other products
922 particularly for summer in the Arctic and winter in the Antarctic, and NT2-AMSRE: more sea ice than other products in the
923 Antarctic. Lowest spread among all ten products is achieved for the Arctic SIE in September; here the maximum inter-product
924 difference is < 400 000 km², i.e. ~10% of the total Arctic September SIE. We therefore can confirm that it matters which
925 algorithm and/or product is used for monitoring the polar sea-ice cover as long one is interested in absolute values; similarity
926 of trends has been shown elsewhere (e.g. Ivanova et al., 2014; Comiso et al., 2017a).
927 Results quoted in the previous paragraph rely on computations applying the often-used 15% SIC threshold (e.g. Gloersen
928 et al., 1992). Our investigations suggest that it might be worth to start re-thinking about this threshold because, as we illustrate
929 in Fig. 1 and Fig. 2, the weather filters applied might fail to cut at a sea-ice concentration remaining constant across the different
930 satellite sensors used. While sea-ice concentrations from sensor A might be cut by the weather filter at 14% these might be cut
931 at 17% for a subsequent sensor B. As a result, less ice is left and the sea-ice extent computed from sea-ice concentration data
932 of sensor B is smaller than the one computed from sensor A. We found evidence for this in our results and remark that the
933 impact of these inconsistencies is likely to be particularly pronounced in the peripheral seas with a comparably large fraction
934 of the marginal ice zone, such as the Bering Sea or the Barents Sea. Note that the OSI-450 algorithm provides a particularly
935 stable weather-filter induced sea-ice concentration cut-off at ~ 10% across the sensors used.
936 Sea-ice concentrations are retrieved from satellite microwave brightness temperatures using a geophysical model, which
937 usually involves tie points. These are brightness temperatures, or parameters derived from these, which are typical for the
938 encountered surface types, which in the simplest of our cases are open water: 0% SIC and close pack ice: 100% SIC. Because
939 of the natural variability of those surface properties of 100% sea ice relevant for its microwave remote sensing, one fixed tie
940 point value for 100% sea ice, even if retrieved daily, can only be an average representation of these properties. In other words,
941 ten different kinds of 100% sea ice can cause ten different brightness temperatures. As a result, a retrieved sea-ice concentration
942 naturally varies *around* 100%. This means even though the actual sea-ice concentration is exactly 100% the retrieved one
943 could be, for example, 97% or 100% or 103%. The natural variability of the sea-ice surface properties suggests that the spread
944 of retrieved sea-ice concentrations around 100% follows a Gaussian distribution. All ten products examined here either truncate
945 sea-ice concentrations at 100%, i.e. fold retrieved values > 100% to exactly 100%, or do simply not allow retrieval of SIC >
946 100% (NT2-AMSRE). We develop a Gaussian-fit method to re-construct the full distribution of sea-ice concentrations around
947 100%. We demonstrate its performance on EUMETSAT-OSISAF – ESA-CCI products (as they provide, for the first time,
948 both the non-truncated and truncated values) and subsequently use it to re-construct non-truncated sea-ice concentration
949 distributions for the remaining six products (Fig. 3, and Appendix H, Fig. H1 and Fig. H2). Based on our results we conclude
950 that it is worthwhile to re-think the concept of truncation at 100% (but also at 0% SIC) and critically re-assess evaluation
951 results at the two ends of the sea-ice concentration distribution. Indeed, we argue that direct evaluation of truncated data sets

https://doi.org/10.5194/tc-2019-120
Preprint. Discussion started: 17 June 2019

give a misleading information on the accuracy of the sea-ice concentration data, and favour those data sets that overestimate sea-ice concentrations. Such overestimation has direct implications on the ability of a given sea-ice concentration data set to e.g. observe small openings in an otherwise complete sea-ice cover. We invite the sea-ice concentration data producers and users to take this into consideration and discuss the implications towards future versions of such data products.

Data availability. All sea-ice concentration products except SICCI-12km are publicly available from the sources provided in the respective sections of the supplementary material and the reference list. The SICCI-12km product is available upon request from T. Lavergne. The standardized ship-based observations are available from the Integrated Climate Data Center (ICDC): http://icdc.cen.uni-hamburg.de/1/daten/cryosphere/seaiceparameter-shipobs/. The RRDP2 data set is publicly available from the source specified in the reference list.

7 Appendices

7.1 Appendix A. The EUMETSAT-OSISAF – ESA-CCI algorithm suite

The four products OSI-450, SICCI-12km, SICCI-25km, and SICCI-50km have in common that they are based on a hybrid, self-tuning, self-optimizing sea-ice concentration algorithm (Lavergne et al., 2019). This algorithm is applied to brightness temperature (TB) observations of the SMMR, SSM/I and SSMIS instruments for OSI-450, providing a fully revised version of the OSI-409 CDR (Tonboe et al., 2016). This algorithm is applied to brightness temperatures measured by the AMSR-E and AMSR2 instruments for the SICCI CDRs. Apart from the input satellite data the processing chains are the same for these four products. The algorithm is a generalization of the Comiso Bootstrap frequency mode algorithm (App. C) and of the Bristol algorithm (Smith and Barret, 1994; Smith 1996) and is described in detail in Lavergne et al. (2019). Two algorithms that each combine three frequency channels (e.g. ~19 GHz at vertical polarization, and ~37 GHz at both horizontal and vertical polarizations) are respectively optimized to provide best accuracy in Open Water (the B_{OW} algorithm) and Consolidated Ice (the B_{CI} algorithm) conditions. The sea-ice concentrations obtained with each of the two optimized algorithms are merged linearly into a hybrid sea-ice concentration SIC_{hybrid} according to the general formula:

$$\begin{cases} w_{OW} = 1; \text{for } B_{OW} < 0.7 \\ w_{OW} = 0; \text{for } B_{OW} > 0.9 \\ w_{OW} = 1 - \frac{B_{OW} - 0.7}{0.2}; \text{for } B_{OW} \in [0.7; 0.9] \end{cases} ; \quad SIC_{hybrid} = w_{OW} \times B_{OW} + (1 - w_{OW}) \times B_{CI} , \tag{A1}$$

For sea-ice concentrations below 70%, SIC_{hybrid} relies completely on B_{OW} and for sea-ice concentrations above 90% it relies entirely on B_{IC}. The B_{OW} and B_{IC} algorithms can be regarded as a generalized version of the Comiso Bootstrap and Bristol algorithms, in that sense that they combine the three different brightness temperature channels used by the two algorithms in a 3-dimensional TB space, and optimize their data projection plane for best accuracy.

In this paper, we use the sea-ice concentration CDR derived from SMMR, SSM/I and SSMIS data: OSI-450 [https://doi.org/10.15770/EUM_SAF_OSI_0008], and two sea-ice concentration CDRs derived from AMSR-E and AMSR2 data: SICCI-25km [https://doi.org/10.5285/f17f146a31b14dfd960cde0874236ee5] and SICCI-50km [https://doi.org/10.5285/5f75fcb0c58740d99b07953797bc041e]. While SICCI-25km is based on brightness temperatures measured at ~19 GHz and ~37 GHz, similar to OSI-450, SICCI-50km is based on brightness temperatures measured at ~7 GHz and ~37 GHz. OSI-450 and SICCI-25km come at 25 km grid resolution while SICCI-50km has 50 km grid resolution. In addition, we use a fourth product, SICCI-12km, which is provided at 12.5 km grid resolution and is based on brightness temperatures measured by AMSR-E and AMSR2 at ~19 GHz and ~90 GHz. Here, we use a prototype of SICCI-12km, which was produced during the ESA CCI Sea Ice project, but was not released publicly (partly based on the results presented in this manuscript). All these data sets have daily temporal resolution and are provided on polar EASE grids version 2.0 (Brodzik et al. 2012, 2014).

https://doi.org/10.5194/tc-2019-120
Preprint. Discussion started: 17 June 2019

7.2 Appendix B. The ARTIST sea-ice (ASI) algorithm

The ARTIST Sea Ice (ASI) algorithm (Kaleschke et al., 2001; Spreen et al., 2008) is a modified hybrid of the Near 90 GHz algorithm (Svendsen et al., 1987) and the NASA Team algorithm (see App. D). Water and ice are distinguished at high resolution by the TB polarization difference (P) at ~90 GHz:

$$P = TB_{90}^{V} - TB_{90}^{H}$$

The basic equations for the ASI algorithm are based on the Near 90 GHz algorithm of Svendsen et al. (1987):

$$P = a \times (C \times \Delta\epsilon_{ice} \times T_{ice} + (1 - C) \times \Delta\epsilon_{water} \times T_{water}) \quad \text{(B1)}$$

with the atmospheric influence $a = (1.1 \times e^{-\tau} - 0.11) \times e^{-\tau}$

C is the total sea-ice concentration, T is the temperature, $\Delta\epsilon$ is the difference in surface emissivity between vertical and horizontal polarization for the ice or water surface fraction, and τ is the total atmospheric optical depth for Arctic conditions at this frequency and viewing conditions. For ice free (C = 0) and totally ice covered (C = 1) conditions, Eq. (B1) yields the tie-points for open water $P_{water} = a_{water} \times \Delta\epsilon_{water} \times T_{water}$ and sea ice $P_{ice} = a_{ice} \times \Delta\epsilon_{ice} \times T_{ice}$. Taylor expansions of Eq. (B1) around C=0 and C=1 lead to a pair of equations for P, in which the atmospheric influences a_{water} and a_{ice} can be substituted with the aid of the tie point equations – provided that the variation of the atmospheric influence is small over water or ice (see Spreen et al., 2008). After substitution one obtains

$$C = \left(\frac{P}{P_{water}} - 1\right) \times \left(\frac{\Delta\epsilon_{water} \times T_{water}}{\Delta\epsilon_{ice} \times T_{ice} - \Delta\epsilon_{water} \times T_{water}}\right) \text{ for C} \rightarrow 0 \quad \text{(B2)}$$

$$C = \frac{P}{P_{ice}} + \left(\frac{P}{P_{ice}} - 1\right) \times \left(\frac{\Delta\epsilon_{water} \times T_{water}}{\Delta\epsilon_{ice} \times T_{ice} - \Delta\epsilon_{water} \times T_{water}}\right) \text{ for C} \rightarrow 1 \quad \text{(B3)}$$

According to Svendsen et al. (1987) the ratio of the surface emissivity differences can be set to a constant value (-1.14). With this simplification and by assuming that the atmospheric influence inherent in P is a smooth function of the sea-ice concentration one can use a third order polynomial function to interpolate between the solutions of Eq. (B2) and Eq. (B3) to obtain sea-ice concentrations between 0 and 1 as a function of P:

$$C(P) = d_3 \times P^3 + d_2 \times P^2 + d_1 \times P + d_0 \quad \text{(B4)}$$

The coefficients d_i are derived with a linear equation system based on Eq. (B2) and Eq. (B3) and their first derivatives (Spreen et al., 2008).

The larger, compared to the lower frequencies used in most products (see Table 2), weather influence at ~90 GHz frequencies by atmospheric water content and surface wind speed can cause substantial over-estimation of the sea-ice concentration over open water and within the ice edge (Kern, 2004; Andersen et al., 2006). Over open water, the weather influence is reduced by combining sea-ice concentrations obtained with Eq. (B4) with NASA-Team algorithm (NTA, see also App. D) sea-ice concentrations following:

$$C = C_{ASI} \text{ for } C_{NTA} > 5\%;\ C = 0\% \text{ for } C_{NTA} \leq 5\% \quad \text{(B5)}$$

Hence, the ASI algorithm is a hybrid of the near-90GHz algorithm (Eq. (B1) through Eq. (B4)) and the NTA (Kaleschke et al., 2001; Ezraty et al., 2007; Girard-Ardhuin, personal communication, June 3 2019).

We use the ASI algorithm sea-ice concentration product provided via the Integrated Climate Data Center: https://icdc.cen.uni-hamburg.de [last access date: 27/2/2019]. This product is processed at the French Institute for Exploitation of the Sea (IFREMER) from SSM/I and SSMIS data, and provided via ICDC after application of a running 5-day-median filter, further reducing spurious weather-influence induced sea-ice concentration in the open water (Kern et al., 2010), on a polar-stereographic grid with 12.5 km grid resolution (at 70 degrees latitude). We abbreviate this data with ASI-SSMI.

https://doi.org/10.5194/tc-2019-120
Preprint. Discussion started: 17 June 2019


The Cryosphere Discussions
Open Access
EGU

7.3 Appendix C. The Comiso-Bootstrap algorithm

The Comiso-Bootstrap algorithm (Comiso, 1986; Comiso et al, 1997; Comiso et al., 2003; Comiso and Nishio, 2008) combines TB observations at either two different frequencies (frequency mode, 37 GHz and 19 GHz, vertical polarization) or at two different polarizations (polarization mode, 37GHz, vertical and horizontal polarization). It is rooted on the observation that brightness temperatures measured at these frequencies / polarizations over closed sea ice tend to cluster along a line (ice line) while those over open water tend to cluster around a single point in the respective two-dimensional brightness temperature space. The total sea-ice concentration is computed using

$$C = \frac{TB_f^V - TB_{f,OW}^V}{TB_{f,I}^P - TB_{f,OW}^V} \quad \text{(C1)}$$

with the brightness temperature measured at vertical polarization and frequency f = 37 GHz (polarization mode) or f = 19 GHz (frequency mode): TB_f^V, the open water tie point $TB_{f,OW}^V$ at vertical polarization and the same frequency as TB_f^V, and the intersection of the ice line with a line from the open water tie point through the observed brightness temperature: $TB_{f,I}^P = A \times \frac{B-W}{Q-A} + B$. Scalars A and B are functions of the ice tie points for first-year ice (FYI) and multiyear ice (MYI) at 37 GHz at vertical and horizontal polarization (polarization mode) or at 19 GHz and 37 GHz, both vertical polarization (frequency mode). Q and W are functions of the actually observed brightness temperature and the water tie point at the respective frequencies / polarizations. The two algorithms (frequency and polarization mode) are combined so that only the polarization mode is used in high concentration conditions and the frequency mode otherwise.

We use daily gridded sea-ice concentrations derived with the Comiso-Bootstrap (CBT) algorithm from SMMR, SSM/I and SSMIS instruments, as processed at NASA Goddard Space Flight Center (GSFC), and made available at https://nsidc.org/data/nsidc-0079. They are on a polar-stereographic grid with 25 km grid resolution (at 70 degrees latitude). We abbreviate this data with CBT-SSMI. For practical reasons, we access these GSFC CBT-SSMI fields from the NOAA sea-ice concentration CDR (App. F) files, where they are provided as additional data (Meier and Windnagel, 2018). The GSFC CBT-SSMI sea-ice concentration data set involves manual filtering, especially at the beginning of the record (SMMR period).

In addition, we use daily gridded sea-ice concentrations derived with this algorithm from AMSR-E data (Comiso et al., 2003; Comiso and Nishio, 2008) as provided by NSIDC (AE_SI25.003, Cavalieri et al., 2014, https://nsidc.org/data/ae_si25/versions/3, last access date: 26/4/2018) on the same polar-stereographic grid. The AMSR-E Comiso Bootstrap algorithm sea-ice concentration is referred with CBT-AMSRE throughout this paper. Note that the NSIDC product AE_SI25.003 does not contain CBT-AMSRE sea-ice concentrations itself. It contains the NT2 sea-ice concentration and the difference "Comiso Bootstrap minus NT2 sea-ice concentration". Therefore, we needed to compute the CBT-AMSRE sea-ice concentration by adding the NT2 sea-ice concentration to that difference.

7.4 Appendix D. The NASA-Team algorithm

The NASA-Team algorithm (Cavalieri et al., 1984, 1992, 1999) combines the large difference of the normalized brightness temperature polarization difference at 19 GHz, $PR = \frac{TB_{19}^V - TB_{19}^H}{TB_{19}^V + TB_{19}^H}$, between water and ice, with the observation, that the normalized brightness temperature frequency difference between 37 and 19 GHz at vertical polarization, $GR = \frac{TB_{37}^V - TB_{19}^V}{TB_{37}^V + TB_{19}^V}$, is negative for MYI and close to zero or slightly positive for FYI and open water. The total sea-ice concentration is derived as the sum of the fractions of MYI and FYI, which is constrained to a maximum of 1:

$$C_{FYI} = \frac{F_0 + F_1 \, x \, PR + F_2 \times GR + F_3 \times PR \times GR}{D}, \; C_{MYI} = \frac{M_0 + M_1 \, x \, PR + M_2 \, x \, GR + M_3 \, x \, PR \, x \, GR}{D},$$

$$\text{with } D = D_0 + D_1 \times PR + D_2 \times GR + D_3 \times PR \times GR \quad \text{(D1)}$$

Where coefficients F_i, M_i and D_i include the tie point information.

https://doi.org/10.5194/tc-2019-120
Preprint. Discussion started: 17 June 2019

We use daily gridded sea-ice concentrations derived with the NASA-Team (NT1) algorithm from SMMR, SSM/I and SSMIS instruments, as processed at NASA Goddard Space Flight Center (GSFC), and made available at https://nsidc.org/data/nsidc-0051. They are on a polar-stereographic grid with 25 km grid resolution (at 70 degrees latitude). We abbreviate this data with NT1-SSMI. For practical reasons, we access these GSFC NT1-SSMI fields from the NOAA sea-ice concentration CDR (App. F) files, where they are provided as additional data (Meier and Windnagel, 2018). The GSFC NT1-SSMI sea-ice concentration data set involves manual filtering, especially at the beginning of the record (SMMR period).

7.5 Appendix E. The enhanced NASA-Team algorithm (NT2)

Inter-comparison studies such as those of Comiso and Steffen (2001) and Comiso et al. (1997) led to the development of the enhanced NASA-Team algorithm (NT2) (Markus and Cavalieri, 2000; Comiso et al., 2003) to mitigate effects such as layering in snow on sea ice on the accuracy of the sea-ice concentrations obtained with the NT1. The NT2 is conceptually different from the other algorithms presented here. The three relevant parameters (see below) are modelled as a function of sea-ice concentration in steps of 1% for 12 different atmospheric states using a radiative transfer model. The sea-ice concentration resulting in the minimum cost function between modelled and observed values of these parameters is taken as the retrieved total sea-ice concentration. The three parameters used are selected such that the influence of layering in snow on sea ice is mitigated:

$$\Delta GR = \frac{TB_{90}^{H} - TB_{19}^{H}}{TB_{90}^{H} + TB_{19}^{H}} - \frac{TB_{90}^{V} - TB_{19}^{V}}{TB_{90}^{V} + TB_{19}^{V}}$$

$$PR_{19}^{rotated} = -\frac{TB_{37}^{V} - TB_{19}^{V}}{TB_{37}^{V} + TB_{19}^{V}} \times sin\,\theta_{19} + \frac{TB_{19}^{V} - TB_{19}^{H}}{TB_{19}^{V} + TB_{19}^{H}} \times cos\,\theta_{19}$$

$$PR_{90}^{rotated} = -\frac{TB_{37}^{V} - TB_{19}^{V}}{TB_{37}^{V} + TB_{19}^{V}} \times sin\,\theta_{90} + \frac{TB_{90}^{V} - TB_{90}^{H}}{TB_{90}^{V} + TB_{90}^{H}} \times cos\,\theta_{90} \quad \text{(E1)}$$

The rotation is done in the space given by PR_{19} and GR (see App. D) or by PR_{90} and GR for $PR_{19}^{rotated}$ and $PR_{90}^{rotated}$, respectively, at an angle Θ chosen such that the ice lines in the respective space are parallel to the GR axis.

We use daily gridded NT2 sea-ice concentrations derived from AMSR-E data as provided by NSIDC: AE_SI25.003 (Cavalieri et al., 2014, https://nsidc.org/data/ae_si25/versions/3, last access date: 26/4/2018) on polar-stereographic grid with 25 km grid resolution. We abbreviate this data with NT2-AMSRE.

7.6 Appendix F. The NOAA/NSIDC sea-ice concentration CDR

The NOAA/NSIDC sea-ice concentration CDR combines sea-ice concentrations computed with the NT1 algorithm (App. D) with those computed with the CBT algorithm (App. C), via

$$C = \max(C_{NT1}, C_{CBT}) \quad \text{(F1)}$$

within the ice edge. The ice edge is defined by the CBT sea-ice concentration of 10%. The generation and characteristics of the NOAA/NSIDC CDR as well as details about filters (see also Sect. 2.1) and about the statistical uncertainty estimate provided with the product are described in Peng et al. (2013) and Meier and Windnagel (2018). We use the daily gridded sea-ice concentration data of NOAA/NSIDC CDR version 3, named NOAA-CDR in this manuscript, provided by NSIDC on polar-stereographic grid with 25 km grid resolution (https://nsidc.org/data/g02202/versions/3, last access date: 7/2/2019).
It is important to note that the data sets NT1-SSMI (App. D) and CBT-SSMI (App. C), both from GSFC are not used as input in the NOAA/NSIDC CDR. Instead, sea-ice concentrations are computed at NSIDC using re-implementations of the two algorithms, which allow for a fully-automated and transparent processing as required for a CDR, and combined with Eq. (F1). One of the key difference between the NSIDC and GSFC versions is that the NSIDC ones do not involve manual editing, and start with SSM/I in July 1987.

https://doi.org/10.5194/tc-2019-120
Preprint. Discussion started: 17 June 2019

7.7 Appendix G. Matrices of sea-ice concentration, area, and extent differences

This subsection contains the full set of matrices of differences between all ten products of the overall hemispheric average monthly mean sea-ice concentration of the AMSR-E measurement period and of the respective overall monthly mean sea-ice area (SIA) and extent (SIE) in Fig. G1 through Fig. G6.

7.8 Appendix H. Gaussian fits for all ten products

This subsection contains the two sets of Gaussian fits obtained for the Arctic (Fig. H1) and Antarctic (Fig. H2) based on the methodology described in Sect. 2.1.4; see also Fig. 3). These are the fits obtained from data of the overlap period between the AMSR-E measurement period and the RRDP2 near-100% reference sea-ice concentration data set period, that is for winter of years 2007 through 2011.

Author contributions. SK led the writing in most sections, with contributions by TL (Sect. 2.1, Sect. 6.1, Sect. 6.2), LTP (Sect. 1, Sect. 2.1), DN (Sect. 1, Sect. 3), and RTT (Sect. 2.1, Sect. 6.2). AMS and TL contributed to concept and work of Sect. 2.1.3. TL contributed to concept and work of Sect. 2.1.4. RS and LTP produced and provided the RRDP2 data set and consulted its usage (Sect. 2.2). DN and TL contributed to concept and work as well as design of figures of Sect. 3. SK performed the data analysis and inter-comparison with contributions in the interpretation of the results from all co-authors.

Competing interests. The authors declare that they have no conflict of interest.

Acknowledgements. The work presented here was funded by EUMETSAT (through the 2nd Continuous Developments and Operation Phase of OSI SAF) and ESA (through the Climate Change Initiative Sea_Ice_cci project), and the German Research Foundation (DFG) Excellence Initiative CLISAP under Grant EXC 177/2. The publication itself is funded by the Deutsche Forschungsgemeinschaft (DFG, German Research Foundation) under Germany's Excellence Strategy – EXC 2037 'CLICCS – Climate, Climatic Change, and Society' – Project Number: 390683824, contribution to the Center for Earth System Research and Sustainability (CEN) of the University of Hamburg.

8 References

Andersen, S., Tonboe, R. T., Kern, S., and Schyberg, H.: Improved retrieval of sea ice total concentration from spaceborne passive microwave observations using Numerical Weather Prediction model fields: An intercomparison of nine algorithms, Rem. Sens. Environ., 104(4), 374-392, 2006.

Andersen, S., Pedersen, L. T., Heygster, G., Tonboe, R. T., and Kaleschke, L.: Intercomparison of passive microwave sea ice concentration retrievals over the high concentration Arctic sea ice, J. Geophys. Res., 112, C08004, https://doi.org/10.1029/2006JC003543, 2007.

Beitsch, A., Kern, S., and Kaleschke, L.: Comparison of SSM/I and AMSR-E sea ice concentrations with ASPeCt ship observations around Antarctica, IEEE Trans. Geosci. Rem. Sens., 53(4), 1985-1996, https://doi.org/10.1109/TGRS.2014.2351497, 2015.

Brodzik, M. J., Billingsley, B., Haran, T., Raup, B., and Savoie, M. H.: EASE-Grid 2.0: Incremental but Significant Improvements for Earth-Gridded Data Sets, ISPRS Int. Geo-Inf., 1(1), 32-45, https://doi.org/10.3390/ijgi1010032, http://www.mdpi.com/2220-9964/1/1/32., 2012.

Brodzik, M. J., Billingsley, B., Haran, T., Raup, B., and Savoie, M. H.: Correction: Brodzik, M. J. et al. EASE-Grid 2.0: Incremental but Significant Improvements for Earth-Gridded Data Sets, ISPRS Int. Geo-Inf., 1(1), 32-45, 2012. ISPRS Int. Geo-Inf., 3(3), 1154-1156, https://doi.org/10.3390/ijgi3031154, http://www.mdpi.com/2220-9964/3/3/1154, 2014.

Brucker, L., Cavalieri, D. J., Markus, T., and Ivanoff, A.: NASA Team 2 sea ice concentration algorithm retrieval uncertainty, IEEE Trans. Geosci. Rem. Sens., 52(11), 7336-7352, https://doi.org/10.1109/TGRS.2014.2311376, 2014.

https://doi.org/10.5194/tc-2019-120
Preprint. Discussion started: 17 June 2019

1145 Cavalieri D. J., Gloersen, P., and Campbell, W. J.: Determination of Sea Ice Parameters With the NIMBUS 7 SMMR, J.
1146 Geophys. Res., 89(D4), 5355-5369, 1984.
1147 Cavalieri, D. J., Crawford, J., Drinkwater, M., Emery, W. J., Eppler, D. T., Farmer, L. D., Goodberlet, M., Jentz, R., Milman,
1148 A., Morris, C., Onstott, R., Schweiger, A., Shuchman, R., Steffen, K., Swift, C. T., Wackerman, C., and Weaver, R. L.: NASA
1149 sea ice validation program for the DMSP SSM/I: final report. NASA Technical Memorandum 104559. National Aeronautics
1150 and Space Administration, Washington, D.C., 126 pp., 1992.
1151 Cavalieri, D. J., St. Germain, K. M., and Swift, C. T.: Reduction of weather effects in the calculation of sea ice concentration
1152 with the DMSP SSM/I, J. Glaciol., 41(139), 455-464, 1995.
1153 Cavalieri, D. J., Parkinson, C. L., Gloersen, P., Comiso, J. C., and Zwally, H. J.: Deriving long-term time series of sea ice
1154 cover from satellite passive-microwave multisensor data sets, J. Geophys. Res., 104(C7), 15803–15814,
1155 https://doi.org/10.1029/1999JC900081, 1999.
1156 Cavalieri, D. J., Markus, T., Hall, D. K., Gasiewski, A. J., Klein, M., and Ivanoff, A.: Assessment of EOS Aqua AMSR-E
1157 Arctic sea ice concentrations using Landsat-7 and airborne microwave imagery, IEEE Trans. Geosci. Rem. Sens., 44(11),
1158 3057-3069, https://doi.org/10.1109/TGRS.2006.878445, 2006.
1159 Cavalieri, D. J., Markus, T., Hall, D. K., Ivanoff, A., and Glick, E.: Assessment of AMSR-E Antarctic winter sea-ice
1160 concentrations using Aqua MODIS, IEEE Trans. Geosci. Rem. Sens., 48(9), 3331-3340,
1161 https://doi.org/10.1109/TGRS.2010.2046495, 2010.
1162 Cavalieri, D. J., Markus, T., and Comiso, J. C.: AMSR-E/Aqua daily L3 25km brightness temperature and sea ice concentration
1163 polar grids, version 3, Boulder, Colorado USA, NASA National Snow and Ice Data Center Distributed Arctive Archive Center,
1164 https://doi.org/10.5067/AMSR-E/AE_SI25.003, [date accessed: 2018-04-26], 2014.
1165 Cho, K., Sasaki, N., Shimoda, H., Sakata, T., and Nishio, F.: Evaluation and improvement of SSM/I sea ice concentration
1166 algorithms for the Sea of Okhotsk, J. Rem. Sens. of Japan, 16(2), 47-58, 1996.
1167 Comiso J. C.: Characteristics of arctic winter sea ice from satellite multispectral microwave observations, J. Geophys. Res.,
1168 91(C1), 975-994, 1986.
1169 Comiso, J. C.: Large Decadal Decline of the Arctic Multiyear Ice Cover. J. Climate, 25(4), 1176–1193,
1170 https://doi.org/10.1175/JCLI-D-11-00113.1, 2012.
1171 Comiso, J. C., and Nishio, F.: Trends in the sea ice cover using enhanced and compatible AMSR-E, SSM/I, and SMMR data, J.
1172 Geophys. Res., 113, C02S07, https://doi.org/10.1029/2007JC004257, 2008.
1173 Comiso, J. C., and Steffen, K.: Studies of Antarctic sea ice concentrations from satellite data and their applications, J. Geophys.
1174 Res., 106(C12), 31361-31385, 2001.
1175 Comiso, J. C., Cavalieri, D. J., Parkinson, C. L., and Gloersen, P.: Passive microwave algorithms for sea ice concentration: A
1176 comparison of two techniques, Rem. Sens. Environ., 60(3), 357-384, 1997.
1177 Comiso, J. C., Cavalieri, D. J., and Markus, T.: Sea ice concentration, ice temperature, and snow depth, using AMSR-E data,
1178 IEEE Trans. Geosci. Rem. Sens., 41(2), 243-252, https://doi.org/10.1109/TGRS.2002.808317, 2003.
1179 Comiso, J. C., Meier, W. N., and Gersten, R. A.: Variability and trends in the Arctic Sea ice cover: Results from different
1180 techniques, J. Geophys. Res. - Oceans, 122(8), 6883–6900, https://doi.org/10.1002/2017JC012768, 2017a.
1181 Comiso, J. C., Gersten, R. A., Stock, L.V., Turner, J., Perez, G. J., and Cho, K.: Positive trends in the Antarctic sea ice cover
1182 and associated changes in surface temperature, J. Climate, 30(6), 2251–2267, https://doi.org/10.1175/JCLI-D-16-0408.1,
1183 2017b.
1184 Ezraty, R., Girard-Ardhuin, F., Piollé, J.-F., Kaleschke, L., and Heygster, G.: Arctic and Antarctic sea ice concentration and
1185 Arctic sea ice drift estimated from special sensor microwave data – Users's Manual, Version 2.1, IFREMER, Brest, France,
1186 February 2007.

1187 Gloersen, P., Campbell, W., Cavalieri, D. J., Comiso, J. C., Parkinson, C. L., and Zwally, H. J.: Arctic and Antarctic sea ice,
1188 1978-1987: satellite passive-microwave observations and analysis, Scientific and technical information program, vol. NASA
1189 SP-511, National Aeronautics and Space Administration (NASA), Washington D.C., 1992.
1190 Ivanova, D. P., Gleckler, P. J., Taylor, K. E., Durack, P. J., and Marvel, K. D.: Moving beyond the total sea ice extent in
1191 gauging model biases. J. Clim., 29(24), 8965-8987, https://doi.org/10.1175/JCLI-D-16-0026.1, 2017.
1192 Ivanova, N., Johannessen, O. M., Pedersen, R. T., and Tonboe, R. T.: Retrieval of Arctic sea ice parameters by satellite passive
1193 microwave sensors: A comparison of eleven sea ice concentration algorithms, IEEE Trans. Geosci. Rem. Sens., 52(11), 7233-
1194 7246, https://doi.org/10.1109/TGRS.2014.2310136, 2014.
1195 Ivanova, N., Pedersen, L. T., Tonboe, R. T., Kern, S., Heygster, G., Lavergne, T., Sørensen, A., Saldo, R., Dybkjær, G.,
1196 Brucker, L., and Shokr, M.: Inter-comparison and evaluation of sea ice algorithms: towards further identification of challenges
1197 and optimal approach using passive microwave observations, The Cryosphere, 9, 1797-1817, https://doi.org/10.5194/tc-9-
1198 1797-2015, 2015.
1199 Kaleschke, L., Lüpkes, C., Vihma, T., Haarpaintner, J., Bochert, A., Hartmann, J., and Heygster, G.: SSM/I sea ice remote
1200 sensing for mesoscale ocean-atmosphere interaction analysis, Can. J. Rem. Sens., 27(5), 526-537, 2001.
1201 Kern, S.: A new method for medium-resolution sea ice analysis using weather-influence corrected Special Sensor
1202 Microwave/Imager 85 GHz data, Int. J. Rem. Sens., 25(21), 4555-4582, https://doi.org/10.1080/01431160410001698898,
1203 2004.
1204 Kern, S., Kaleschke, L., and Clausi, D. A.: A comparison of two 85-GHz SSM/I ice concentration algorithms with AVHRR
1205 and ERS-2 SAR imagery, IEEE Trans. Geosci. Rem. Sens., 41(10), 2294-2306, https://doi.org/10.1109/TGRS.2003.817181,
1206 2003.
1207 Kern, S., Kaleschke, L., and Spreen, G.: Climatology of the Nordic (Irminger, Greenland, Barents, Kara and White/Pechora)
1208 Seas ice cover based on 85 GHz satellite microwave radiometry: 1992-2008, Tellus, 62A(4), 411-434,
1209 https://doi.org/10.1111/j.1600-0870.2010.00457.x, 2010.
1210 Kwok, R.: Sea ice concentration estimates from satellite passive microwave radiometry and openings from SAR ice motion,
1211 Geophys. Res. Lett., 29(9), 1311, https://doi.org/10.1029/2002GL014787, 2002.
1212 Lavergne, T., Sørensen, A. M., Kern, S., Tonboe, R., Notz, D., Aaboe, S., Bell, L., Dybkjær, G., Eastwood, S., Gabarro, C.,
1213 Heygster, G., Killie M. A., Brandt Kreiner, M., Lavelle, J., Saldo, R., Sandven, S., and Pedersen, L. T.: Version 2 of the
1214 EUMETSAT OSI SAF and ESA CCI sea-ice concentration climate data records, The Cryosphere, 13(1), 49-78,
1215 https://doi.org/10.5194/tc-13-49-2019, 2019.
1216 Maass, N., and Kaleschke, L.: Improving passive microwave sea ice concentration algorithms for coastal areas: applications
1217 to the Baltic Sea, Tellus, 62A(4), 393-410, https://doi.org/10.1111/j.1600-0870.2010.00452.x, 2010.
1218 Markus, T., and Cavalieri, D. J.: An enhancement of the NASA Team sea ice algorithm, IEEE Trans. Geosci. Rem. Sens.,
1219 38(3), 1387-1398, 2000.
1220 Markus, T., and Dokken, S. T.: Evaluation of late summer passive microwave Arctic sea ice retrievals, IEEE Trans. Geosci.
1221 Rem. Sens., 40(2), 348-356, 2002.
1222 Meier, W. N.: Comparison of passive microwave ice concentration algorithm retrievals with AVHRR imagery in Arctic
1223 peripheral seas, IEEE Trans. Geosci. Rem. Sens., 43(6), 1324-1337, https://doi.org/10.1109/TGRS.2005.846151, 2005.
1224 Meier, W. N., and Steward, J. S.: Assessing uncertainties in sea ice extent climate indicators, Environ. Res. Lett., 14, 035005,
1225 https://doi.org/10.1088/1748-9326/aaf52c, 2019.
1226 Meier, W. N., and Windnagel, A.: Sea ice concentration – climate algorithm theoretical basis document, NOAA Climate Data
1227 Record Program CDRP-ATBD-0107 Rev. 7 (03/062018), available at https://www.ncdc.noaa.gov/cdr/oceanic/sea-ice-
1228 concentration, 2018.

1229 Meier, W. N., Hovelsrud, G. K., van Oort, B. E. H., Key, J. R., Kovacs, K. M., Michel, C., Haas, C., Granskog, M. A., Gerland,
1230 S., Perovich, D. K., Makshtas, A., and Reist, J. D.: Arctic sea ice in transformation: A review of recent observed changes and
1231 impacts on biology and human activity, Rev. Geophys., 51, 185-217, https://doi.org/10.1002/2013RG000431, 2014.
1232 Meier, W. N., Fetterer, F., Savoie, M., Mallory, S., Duerr, R., and Stroeve, J.: *NOAA/NSIDC Climate Data Record of Passive*
1233 *Microwave Sea Ice Concentration, Version 3*. Boulder, Colorado USA. NSIDC: National Snow and Ice Data
1234 Center, https://doi.org/10.7265/N59P2ZTG, [Date accessed: 2019-02-07], 2017.
1235 Melia, N., Haines, K., Hawkins, E., and Day, J. J.: Towards seasonal Arctic shipping route predictons, Environ. Res. Lett.,
1236 12(8), 084005, https://doi.org/10.1088/1748-9326/aa7a60, 2017.
1237 Niederdrenk, A. L., and Notz, D.: Arctic sea ice in a 1.5°C warmer world, Geophys. Res. Lett., 45(4), 1963-1971,
1238 https://doi.org/10.1002/2017GL076159, 2018.
1239 Notz, D.: Sea-ice extent and its trend provide limited metrics of model performance, The Cryosphere, 8(1), 229-243,
1240 https://doi.org/10.5194/tc-8-229-2014, 2014.
1241 Njoku, E. G., Rague, B., and Fleming, K.: The Nimbus-7 SMMR Pathfinder Brightness Temperature Data Set, Jet Propulsion
1242 Laboratory Publication, Pasadena, USA, 98-4, 1998.
1243 Pedersen, L. T., Saldo, R., Ivanova, N., Kern, S., Heygster, G., Tonboe, R. T., Huntemann, M., Ozsoy, B., Girard-Ardhuin, F.,
1244 and Kaleschke, L.: Reference dataset for sea ice concentration, https://doi.org/10.6084/m9.figshare.6626549.v6,
1245 https://figshare.com/articles/Reference_dataset_for_sea_ice_concentration/6626549, 2019.
1246 Peng, G., Meier, W. N., Scott, D., and Savoie, M.: A long-term and reproducible passive microwave sea ice concentration data
1247 record for climate studies and monitoring, Earth Syst. Sci. Data, 5, 311-318, https://doi.org/10.5194/essd-5-311-2013, 2013.
1248 Petty, A. A., Stroeve, J. C., Holland, P. R., Boisvert, L. N., Bliss, A. C., Kimura, N., and Meier, W. N.: The Arctic sea ice
1249 cover of 2016: a year of record-low highs and higher-than-expected lows, The Cryosphere, 12(2), 433-452,
1250 https://doi.org/10.5194/tc-12-433-2018, 2018.
1251 Reid, P., Stammerjohn, S., Massom, R., Scambos, T., and Lieser, J. L.: The record 2013 Southern Hemisphere sea-ice extent
1252 maximum, Ann. Glaciol., 56(69), 99-106, https://doi.org/10.3189/2015AoG69A892, 2015.
1253 Schlosser, E., Haumann, F. A., and Raphael, M. N.: Atmospheric influences on the anomalous 2016 Antarctic sea ice decay,
1254 The Cryosphere, 12(3), 1103-1119, https://doi.org/10.5194/tc-12-1103-2018, 2018.
1255 Smith, D. M.: Extraction of winter total sea ice concentration in the Greenland and Barents Seas from SSM/I data, Int. J. Rem.
1256 Sens., 17(13), 2625-2646, 1996.
1257 Smith D. M., and Barrett, E. C.: Satellite mapping and monitoring of sea ice, CB/RAE/9/2/4/2034/113/ARE, RSU, University
1258 of Bristol, Bristol, UK, 1994.
1259 Spreen, G., Kaleschke, L., and Heygster, G., Sea ice remote sensing using AMSR-E 89-GHz channels, J. Geophys. Res., 113,
1260 C02S03, https://doi.org/10.1029/2005JC003384, 2008.
1261 Svendsen, E., Mätzler, C., and Grenfell, T. C.: A model for retrieving total sea ice concentration from a spaceborne dual-
1262 polarized passive microwave instrument operating near 90 GHz, Int. J. Rem. Sens., 8(10), 1479-1487, 1987.
1263 Stuecker, M. F., Bitz, C. M., and Armour, K. C.: Conditions leading to the unprecedented low Antarctic sea ice extent during
1264 the 2016 austral spring season, Geophys. Res. Lett., 44, 9008-9019, https://doi.org/10.1002/2017GL074691, 2017.
1265 Tonboe, R. T., Eastwood, S., Lavergne, T., Sørensen, A. M., Rathmann, N., Dybkjær, G., Pedersen, L. T., Høyer, J. L., and
1266 Kern, S.: The EUMETSAT sea ice concentration climate data record, The Cryosphere, 10, 2275-2290,
1267 https://doi.org/10.5194/tc-10-2275-2016, 2016.
1268 Turner, J., Hosking, J. S., Phillips, T., and Marshall, G. J.: Temporal and spatial evolution of the Antarctic sea ice prior to the
1269 September 2012 record maximum extent, Geophys. Res. Lett., 40, 5894-5898, https://doi.org/10.1002/2013GL058371, 2013.
1270 Turner, J., Phillips, T., Marshall, G. J., Hosking, J. S., Pope, J. O., Bracegirdle, T. J., and Deb, P.: Unprecedented springtime
1271 retreat of Antarctic sea ice in 2016, Geophys. Res. Lett., 44, 6868-6875, https://doi.org/10.1002/2017GL073656, 2017.

https://doi.org/10.5194/tc-2019-120
Preprint. Discussion started: 17 June 2019

1272 Wayand, N. E., Bitz, C. M., and Blanchard-Wrigglesworth, E.: A year-round subseasonal-to-seasonal sea ice prediction portal,
1273 Geophys. Res. Lett., 46(6), 3298-3307, https://doi.org/10.1029/2018GL081656, 2019.
1274 Wiebe, H., Heygster, G., and Markus, T.: Comparison of the ASI ice concentration algorithm with Landsat-7 ETM+ and SAR
1275 imagery, IEEE Trans. Geosci. Rem. Sens., 47(9), 3008-3015, https://doi.org/10.1109/TGRS.2009.2026367, 2009.
1276 Worby, A. P., and Allison, I. A.: Ship-Based Technique for Observing Antarctic Sea Ice: Part I: Observational Techniques and
1277 Results, Research Report No. 14, Antarctic Cooperative Research Centre, Hobart, TAS, Australia, 1999.
1278 Worby, A. P., and Dirita, V.: A technique for making ship-based observations of Antarctic sea-ice thickness and characteristics
1279 - Part II: User Operating Manual, Research Report No. 14, Antarctic Cooperative Research Centre, Hobart, TAS, Australia,
1280 1999.
1281 Worby, A. P., Geiger, C. A., Paget, M. J., Van Woert, M. L., Ackley, S. F., and DeLiberty, T. L.: The thickness distribution
1282 of Antarctic sea ice. J. Geophys. Res., 2008, 113, https://doi.org/10.1029/2007JC004254, 2008.
1283
1284 **Tables**
1285
1286 **Table 1.** Overview of relevant multi-channel satellite microwave sensors.

sensor	relevant frequencies	operation periods
Scanning Multichannel Microwave Radiometer (SMMR)	6.6, 10.7, 18.0, 21.0, 37.0	1978-10-25 – 1987-08-20
Special Sensor Microwave/Imager (SSM/I)	19.4, 22.2, 37.0, 85.5	1987-07-09 – today
Special Sensor Microwave Imager and Sounder (SSMIS)	19.4, 22.2, 37.0, 91.7	2003-10-18 – today
Advanced Microwave Scanning Radiometer on EOS (AMSR-E)	6.9, 10.7, 18.7, 23.8, 36.5, 89.0	2002-05-05 – 2011-10-04
Advanced Microwave Scanning Radiometer 2 (AMSR2)	6.9, 7.3, 10.7, 18.7, 23.8, 36.5, 89.0	2012-05-18 – today

1287
1288 **Table 2.** Overview of the investigated sea-ice concentration products. Column "ID (Algorithm)" holds the identifier we use
1289 henceforth to refer to the data record, and which algorithm it uses. Column "Input data" refers to the input satellite data for the
1290 data set. Column "Open water filter" refers to whether weather-related spurious sea-ice concentrations in open water and low
1291 concentration areas are filtered. Weather filters do not remove weather related noise over areas with near 100% sea-ice
1292 concentration. Column "Atmospheric correction" refers to correcting the input TBs for a potential inherent weather influence
1293 using additional independent weather information. Column "Uncertainties" refers to provision of sea-ice concentration
1294 uncertainties, and "Period" is the time period for which we use the data set, given as StartYearStartMonth-EndYearEndMonth.
1295

ID (algorithm)	Input data & frequencies	Grid resolution & type	Open water filter	Atmospheric correction	Uncertainties	Period
OSI-450 (SICCI2)	SMMR, SSM/I, SSMIS 19.35 & 37.0 GHz	25 km x 25 km EASE2.0	Yes	Yes	Yes	197901-201512
SICCI-12km (SICCI2)	AMSR-E, AMSR2 18.7 & 89.0 GHz	12.5 km x 12.5 km EASE2.0	Yes	Yes	Yes	200205-201705
SICCI-25km (SICCI2)	AMSR-E, AMSR2 18.7 & 36.5 GHz	25 km x 25 km EASE2.0	Yes	Yes	Yes	200205-201705
SICCI-50km (SICCI2)	AMSR-E, AMSR2 6.9 & 36.5 GHz	50 km x 50 km EASE2.0	Yes	Yes	Yes	200205-201705
ASI-SSMI (ASI)	SSM/I, SSMIS 85.5 GHz	12.5 km x 12.5 km PolarStereo	Yes	No	No	199201-201812
CBT-AMSRE (Comiso-Bootstrap)	AMSR-E 18.7 & 36.5 GHz	25 km x 25 km PolarStereo	Yes	No	No	200205-201109
CBT-SSMI (Comiso-Bootstrap)	SMMR, SSM/I, SSMIS 19.35 & 37.0 GHz	25 km x 25 km PolarStereo	Yes	No	No	197810-201712
NT1-SSMI (NASA-Team)	SMMR, SSM/I, SSMIS 19.35 & 37.0 GHz	25 km x 25 km PolarStereo	No	No	No	197810-201712
NOAA-CDR (Comiso-Bootstrap & NASA-Team)	SSM/I, SSMIS 19.35 & 37.0 GHz	25 km x 25 km PolarStereo	Yes	No	Yes	198708-201712
NT2-AMSRE (NASA-Team-2)	AMSR-E 18.7, 36.5 & 89.0 GHz	25 km x 25 km PolarStereo	Yes	Yes	No	200205-201109

1296

https://doi.org/10.5194/tc-2019-120
Preprint. Discussion started: 17 June 2019

Table 3. Inter-comparison results to near-100% SIC (RRDP2) for the Arctic (see Fig. 13 a). Rows "Gaussian": Mean difference of modal value of Gaussian fit to satellite SIC ≤ 99% (compare Fig. 3) minus near-100% reference SIC (RRDP2 SIC) ± one sigma of the Gaussian fit (see Fig. 13 a). Rows "'Non-truncated": Mean difference satellite SIC minus RRDP2 SIC ± one standard deviation of the difference for SICCI and OSI-450 products. Rows "Truncated": Mean difference of satellite SIC constrained to a maximum value of 100% minus RRDP2 SIC ± one standard deviation of the difference. All values in these rows are given in percent sea-ice concentration. Values in rows denoting the periods 2007-2015 and 2007-2011, contain the number of valid data pairs. See text for meaning of * in column "NT2-AMSRE".

NH	SICCI-12km	SICCI-25km	SICCI-50km	OSI-450	ASI-SSMI	NT1-SSMI	CBT-SSMI	NOAA-CDR	NT2-AMSRE	CBT-AMSRE
2007-2015	23262	23262	23262	23343	23343	23343	23343	23037	--	--
Gaussian	-2.4±5.2	-1.2±3.1	-0.5±1.9	-1.0±3.0	-4.1±3.6	+0.1±5.2	+1.4±4.5	+2.7±4.6	--	--
Non-truncated	-4.2±5.9	-2.2±3.7	-0.5±2.1	-1.9±3.6	--	--	--	--	--	--
Truncated	-4.8±5.2	-2.7±3.1	-1.1±1.5	-2.4±3.0	-4.5±3.5	-2.6±4.5	-1.1±1.9	-0.7±1.6	--	--
2007-2011	13351	13351	13351	13432	13432	13432	13432	13126	13344	13344
Gaussian	-2.4±5.0	-1.0±2.9	-0.4±1.9	-0.8±2.8	-3.7±3.7	+0.9±4.6	+1.3±3.6	+3.5±5.0	-0.7±1.7*	+1.0±3.9
Non-truncated	-4.2±5.4	-2.0±3.5	-0.6±2.0	-1.7±3.3	--	--	--	--	--	--
Truncated	-5.0±5.0	-2.8±3.1	-1.4±1.6	-2.2±2.7	-3.9±3.1	-1.9±3.7	-0.9±1.7	-0.6±1.4	-0.9±1.0	-1.1±1.8

Table 4. As Table 3 but for the Antarctic (see Fig. 13 b).

SH	SICCI-12km	SICCI-25km	SICCI-50km	OSI-450	ASI-SSMI	NT1-SSMI	CBT-SSMI	NOAA-CDR	NT2-AMSRE	CBT-AMSRE
2007-2015	6397	6397	6397	6449	6449	6449	6449	6430	--	--
Gaussian	-0.7±3.7	-1.1±3.0	-0.3±2.5	-1.1±3.1	-6.2±3.9	-5.1±5.9	+0.2±4.5	+0.8±4.4		
Non-truncated	-0.7±4.0	-1.4±4.0	-0.7±2.4	-1.5±3.8	--	--	--	--	--	--
Truncated	-1.9±2.9	-2.3±3.0	-1.3±1.7	-2.3±2.9	-6.5±4.0	-6.0±5.5	-1.7±2.4	-1.3±2.1	--	--
2007-2011	5896	5896	5896	5896	5896	5896	5896	5877	5896	5896
Gaussian	-0.6±4.2	-1.1±3.0	-0.3±2.5	-1.1±3.1	-5.6±4.0	-5.4±6.5	-0.2±4.6	+0.9±4.5	-0.2±3.2*	+0.2±5.4
Non-truncated	-0.7±3.9	-1.5±3.8	-0.8±2.4	-1.5±3.7	--	--	--	--	--	--
Truncated	-2.1±2.9	-2.6±3.1	-1.6±1.9	-2.2±2.8	-6.4±4.0	-5.8±5.5	-1.7±2.4	-1.3±2.1	-0.3±0.5	-1.8±2.5

Table 5. Summary of the statistics of the comparison between daily mean ship-based and satellite SIC data (see Fig. 15, black symbols) for – from top to bottom - the entire year, only winter and only summer. DIFF is the mean difference satellite minus ship-based SIC, SDEV is the respective standard deviation; R^2 is the squared linear correlation coefficient. All concentration values are given in percent.

All year	SICCI-12km	SICCI-25km	SICCI-50km	OSI-450	ASI-SSMI	NT1-SSMI	CBT-SSMI	NOAA-CDR	NT2-AMSRE	CBT-AMSRE
DIFF	-6.9	-7.8	-7.3	-7.3	-5.4	-13.8	+0.4	+0.6	-0.7	-0.7
SDEV	12.0	12.1	12.4	12.9	16.1	14.5	13.4	13.3	13.3	12.9
R^2	0.784	0.781	0.775	0.734	0.647	0.693	0.737	0.745	0.767	0.778
Winter										
DIFF	-7.4	-7.4	-6.2	-7.4	-8.6	-14.2	<|0.1|	-0.2	-0.3	-1.5
SDEV	12.6	11.8	11.8	12.8	17.4	13.8	10.9	11.6	11.5	12.6
R^2	0.558	0.594	0.606	0.591	0.429	0.507	0.595	0.587	0.595	0.551
Summer										
DIFF	-6.7	-8.0	-7.9	-7.3	-3.7	-13.6	+0.7	+0.9	-0.9	-0.3
SDEV	11.7	12.3	12.7	12.9	15.1	14.9	14.5	14.0	14.1	13.1
R^2	0.814	0.793	0.780	0.754	0.722	0.702	0.734	0.750	0.771	0.806

https://doi.org/10.5194/tc-2019-120
Preprint. Discussion started: 17 June 2019

1314 **Table 6.** As Table 5 but for the Antarctic (see Fig. 17, black symbols).

All year	SICCI-12km	SICCI-25km	SICCI-50km	OSI-450	ASI-SSMI	NT1-SSMI	CBT-SSMI	NOAA-CDR	NT2-AMSRE	CBT-AMSRE
DIFF	-3.0	-4.4	-3.1	-3.8	-3.3	-11.0	-1.8	-2.3	+4.5	-1.4
SDEV	13.4	13.8	14.0	13.7	15.7	14.8	15.2	15.5	16.9	14.8
R^2	0.763	0.745	0.737	0.733	0.671	0.698	0.711	0.716	0.679	0.755
Winter										
DIFF	-1.6	-2.7	-2.6	-3.2	-3.6	-11.6	-1.6	-2.0	+3.8	+0.2
SDEV	9.8	9.6	10.5	10.5	10.6	11.7	10.7	11.0	10.7	9.5
R^2	0.771	0.771	0.741	0.731	0.659	0.700	0.748	0.751	0.732	0.753
Summer										
DIFF	-3.9	-5.6	-3.4	-4.2	-3.1	-10.6	-2.0	-2.5	+5.0	-2.5
SDEV	15.3	16.1	16.0	15.6	18.4	16.6	17.7	17.9	20.0	17.4
R^2	0.698	0.666	0.675	0.667	0.614	0.640	0.643	0.651	0.621	0.693

1315
1316
1317
1318
1319
1320
1321
1322
1323
1324
1325
1326
1327
1328
1329
1330
1331
1332
1333
1334
1335
1336
1337
1338
1339
1340
1341
1342
1343
1344
1345
1346
1347
1348
1349
1350
1351
1352

https://doi.org/10.5194/tc-2019-120
Preprint. Discussion started: 17 June 2019

1353 **Figures**

1354

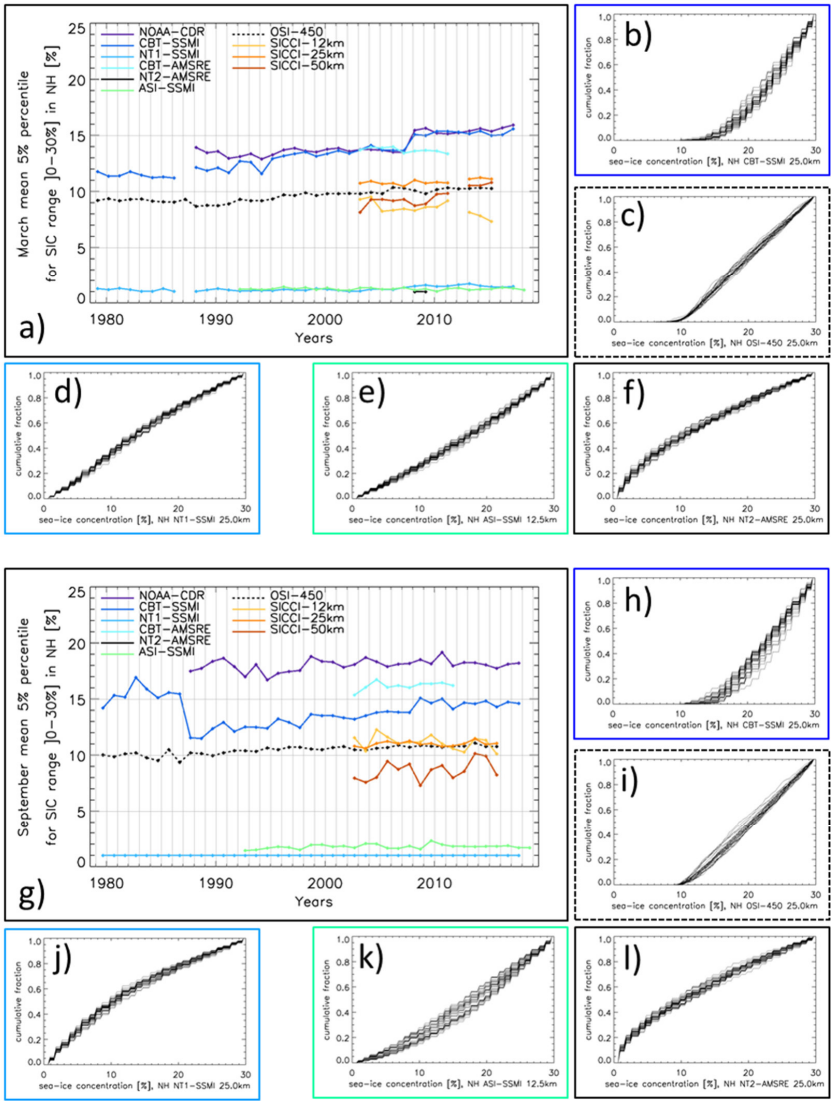

1355

1356

1357 **Figure 1.** Time series of the monthly mean 5%-percentile sea-ice concentration of the range]0.0% to 30.0%] for the Arctic for **(a)** March
1358 and **(g)** September for all ten products. **(b)** to **(f)** and **(h)** to **(l)** Daily cumulative sea-ice concentration distributions of five selected products
1359 for these two months, respectively, for a sample year: 2004. See Table 2 for the time periods with data from the respective products.

https://doi.org/10.5194/tc-2019-120
Preprint. Discussion started: 17 June 2019

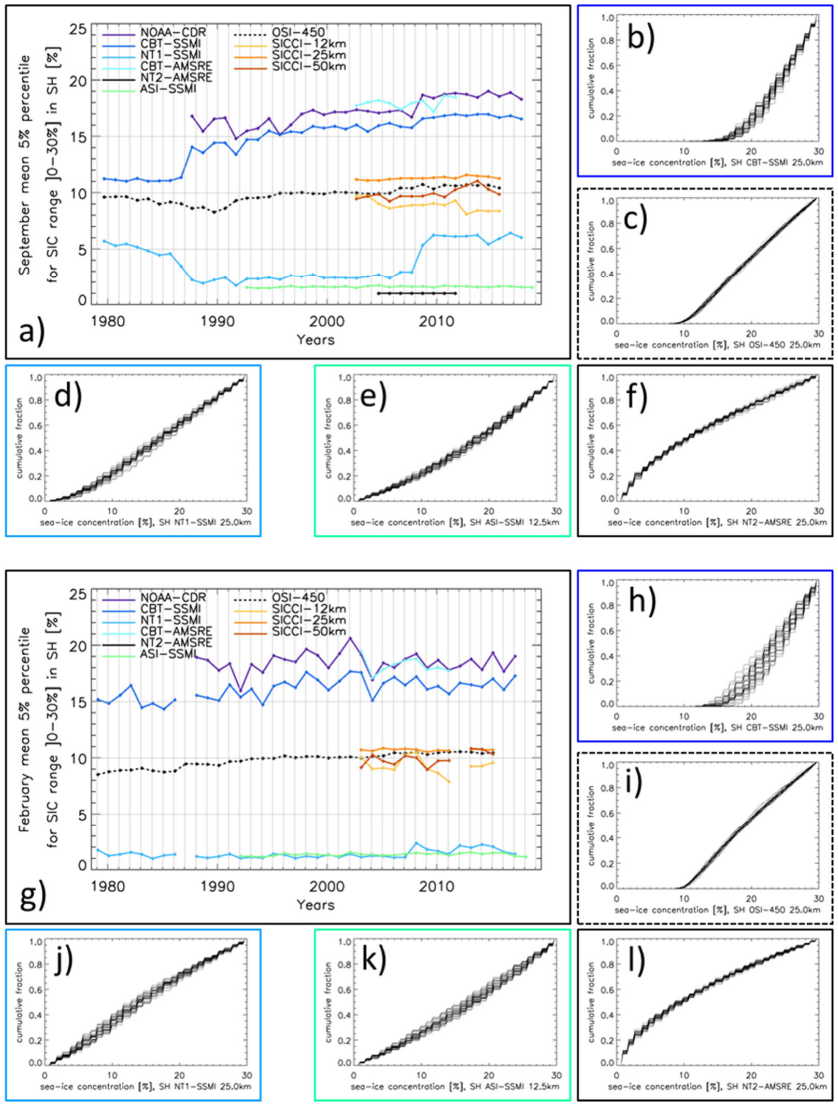

Figure 2. Time series of the monthly mean 5%-percentile sea-ice concentration of the range]0.0% to 30.0%] for the Antarctic for **(a)** September and **(g)** February for all ten products. **(b)** to **(f) and (h)** to **(l)** Daily cumulative sea-ice concentration distributions of five selected products for these two months, respectively, for a sample year: 2004. See Table 2 for the time periods with data from the respective products.

https://doi.org/10.5194/tc-2019-120
Preprint. Discussion started: 17 June 2019

The Cryosphere Discussions
Open Access
EGU

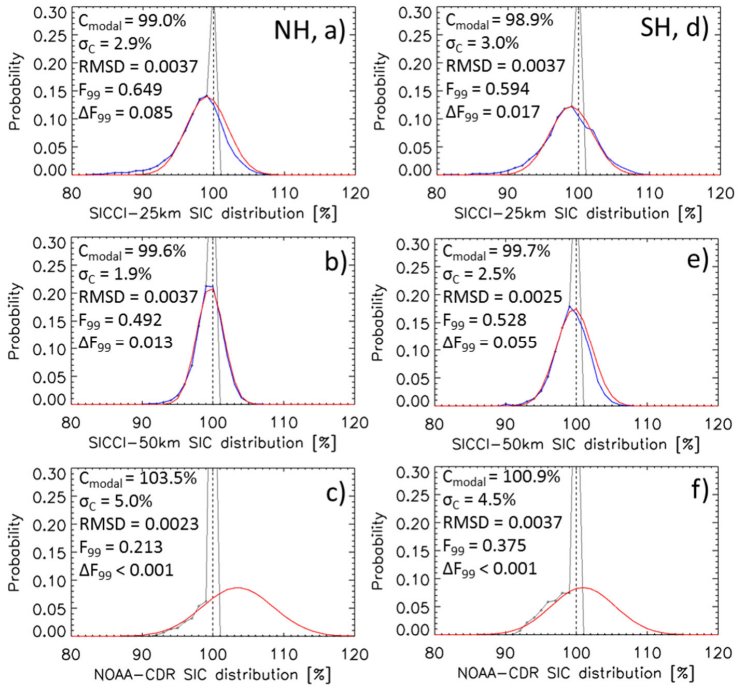

Figure 3. Examples of the sea-ice concentration distribution at near-100% reference sea-ice concentration locations. Black symbols and lines show values cut off at 100%; blue lines denote the original distribution (for SICCI-25km and SICCI-50km only); red lines denote the distribution resulting from the Gaussian fit to values of the distribution ≤ 99%. In each image the modal sea-ice concentration (= center of the Gaussian fit: C_{modal}), the standard deviation of the fit σ_C and fit parameters with respect to the fraction of the distribution ≤ 99% (F_{99}, ΔF_{99}, see text for more explanation) and the root-mean-squared difference (RMSD) between original and fitted probability are given. **(a)** to **(c)** Arctic, **(d)** to **(f)** Antarctic. See Appendix H for Fig. H1 and Fig. H2 containing plots of this kind for all ten products.

https://doi.org/10.5194/tc-2019-120
Preprint. Discussion started: 17 June 2019

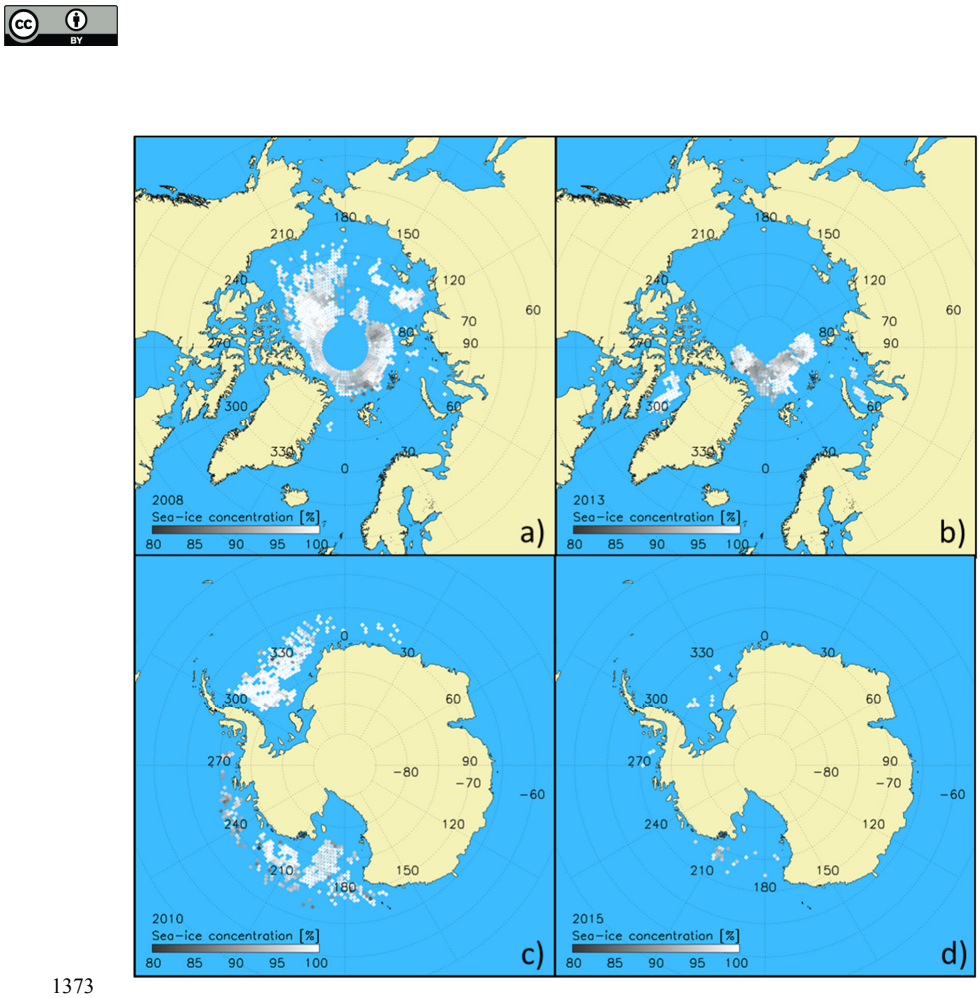

Figure 4. Illustration of the typical distribution of near-100% SIC reference data by means of the co-located OSI-450 sea-ice concentration in **(a,b)** the Arctic and **(c,d)** the Antarctic for a year with good (left) and poor (right) data coverage.

https://doi.org/10.5194/tc-2019-120
Preprint. Discussion started: 17 June 2019

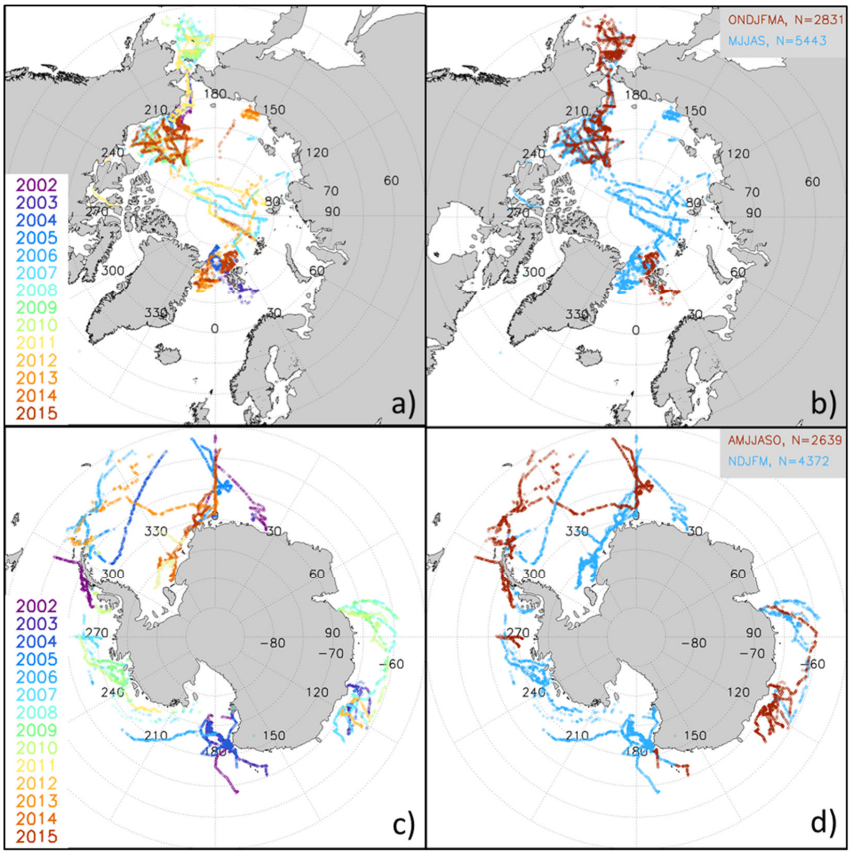

Figure 5. Spatiotemporal distribution of the ship tracks in **(a,b)** the Arctic and **(c,d)** the Antarctic from which ship-based visual observations of the sea-ice cover were used. Maps on the left illustrate the years, maps on the right distinguish between winter (red) and summer (cyan) months.

https://doi.org/10.5194/tc-2019-120
Preprint. Discussion started: 17 June 2019

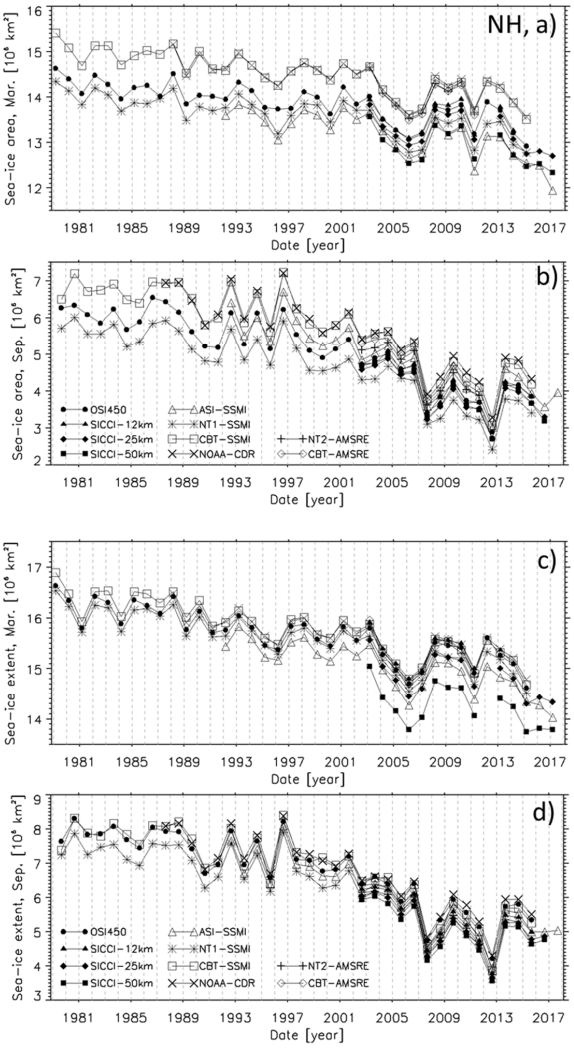

Figure 6. Arctic sea-ice area **(a,b)** and extent **(c,d)** computed for **(a,c)** March and **(b,d)** September from the sea-ice concentration data sets used. See Table 2 for start and end month of the respective time series.

https://doi.org/10.5194/tc-2019-120
Preprint. Discussion started: 17 June 2019

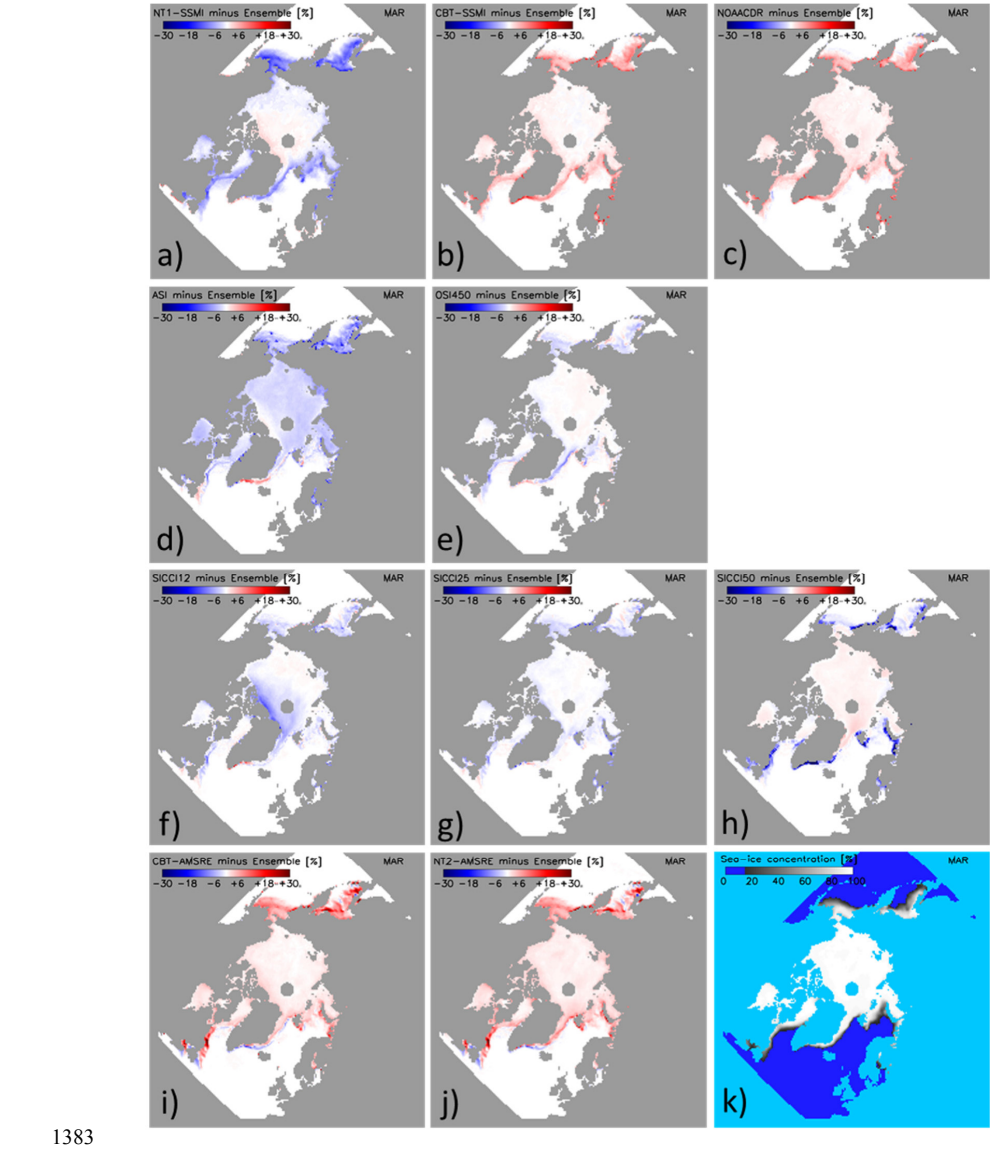

Figure 7. (a) to **(j)** Maps of the difference between the multi-annual average monthly SIC of the individual algorithms and the 10-algorithm ensemble mean multi-annual average monthly SIC **(k)** for the Arctic for March 2003-2011. Differences are only computed for sea-ice concentration of both data sets > 15%.

https://doi.org/10.5194/tc-2019-120
Preprint. Discussion started: 17 June 2019

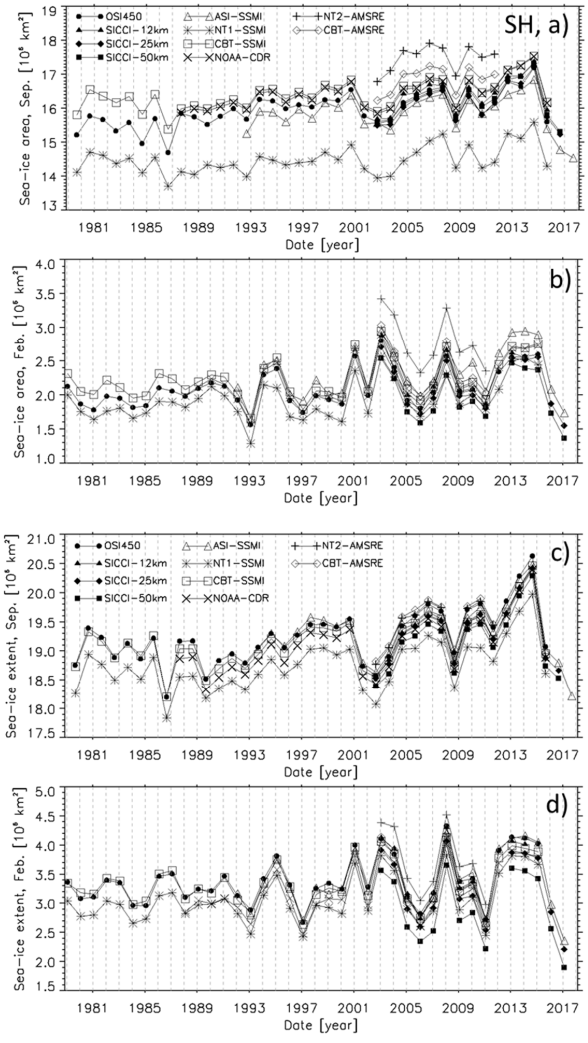

Figure 8. As Fig. 6 but for the Antarctic.

https://doi.org/10.5194/tc-2019-120
Preprint. Discussion started: 17 June 2019

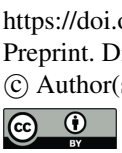

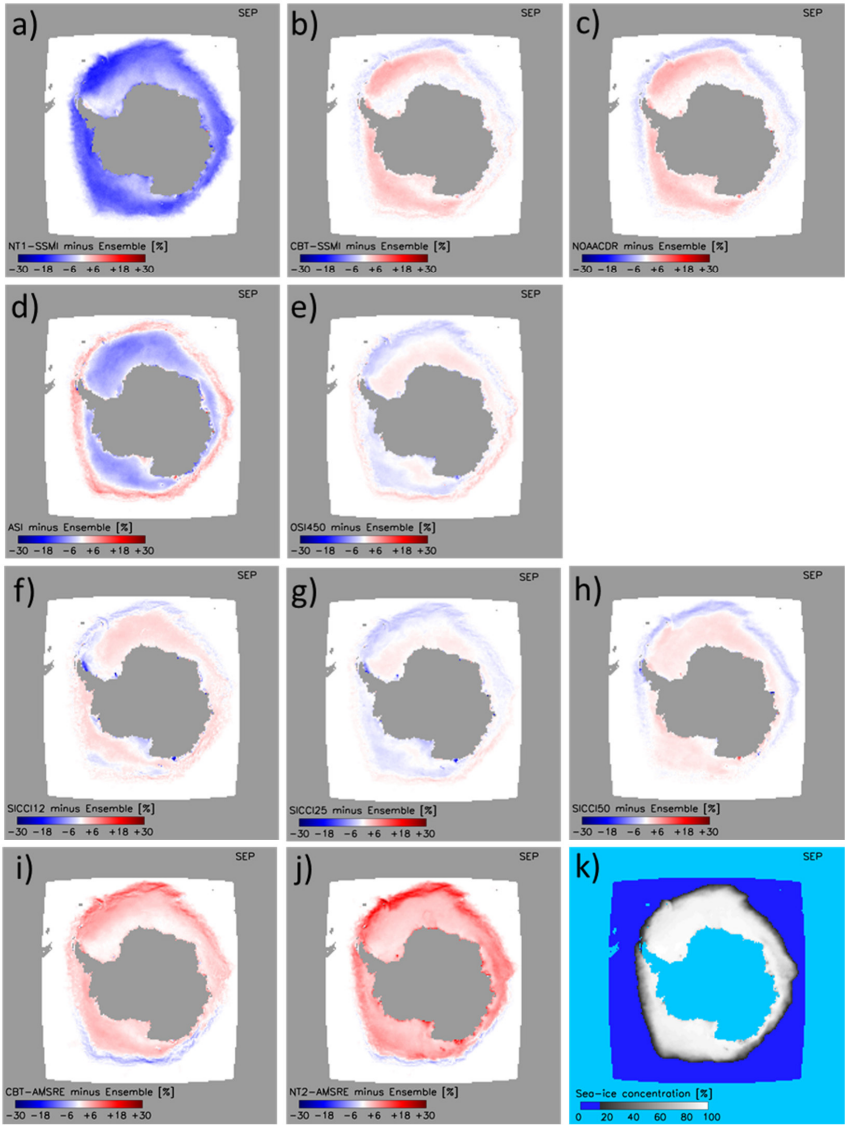

1389

1390 **Figure 9. (a)** to **(j)** Maps of the difference between the multi-annual average monthly SIC of the individual algorithms and the 10-algorithm
1391 ensemble mean multi-annual average monthly SIC **(k)** for the Antarctic for September 2002-2011. Differences are only computed for sea-
1392 ice concentration of both data sets > 15%.

https://doi.org/10.5194/tc-2019-120
Preprint. Discussion started: 17 June 2019

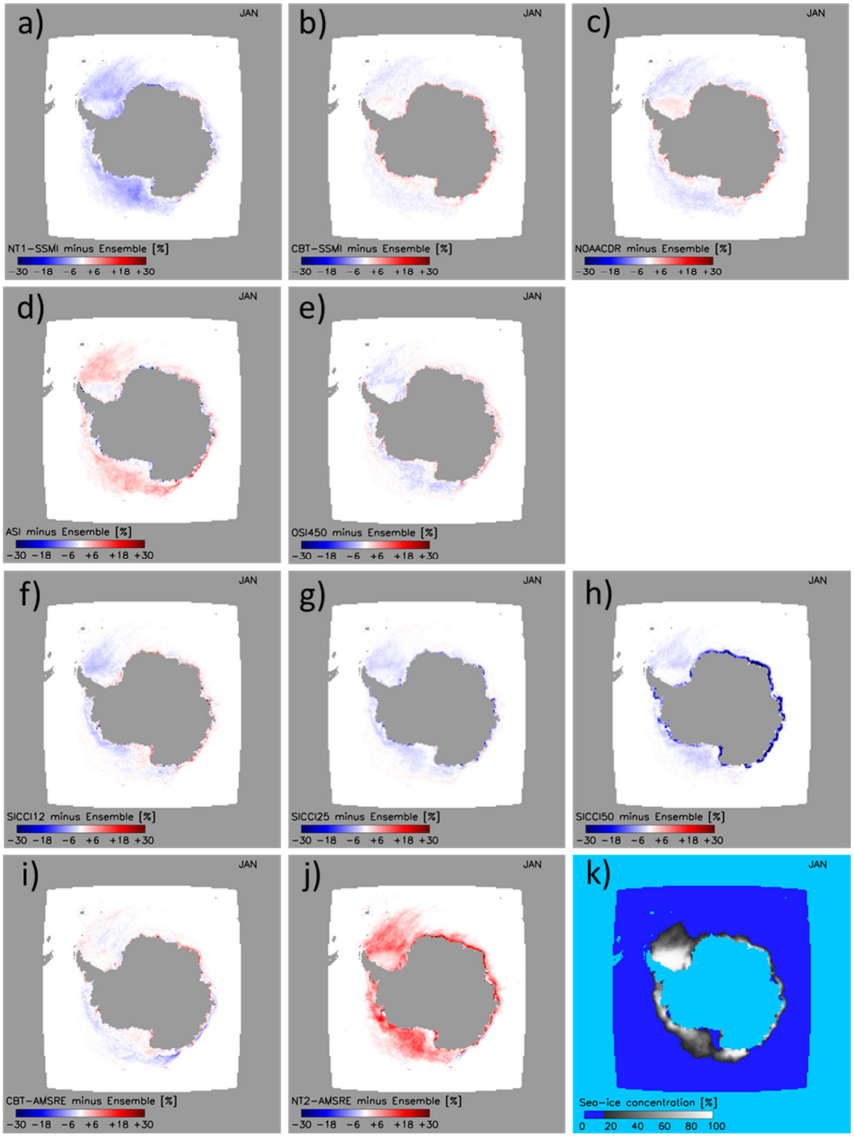

Figure 10. As Fig. 9 but for January 2003-2011.

https://doi.org/10.5194/tc-2019-120
Preprint. Discussion started: 17 June 2019

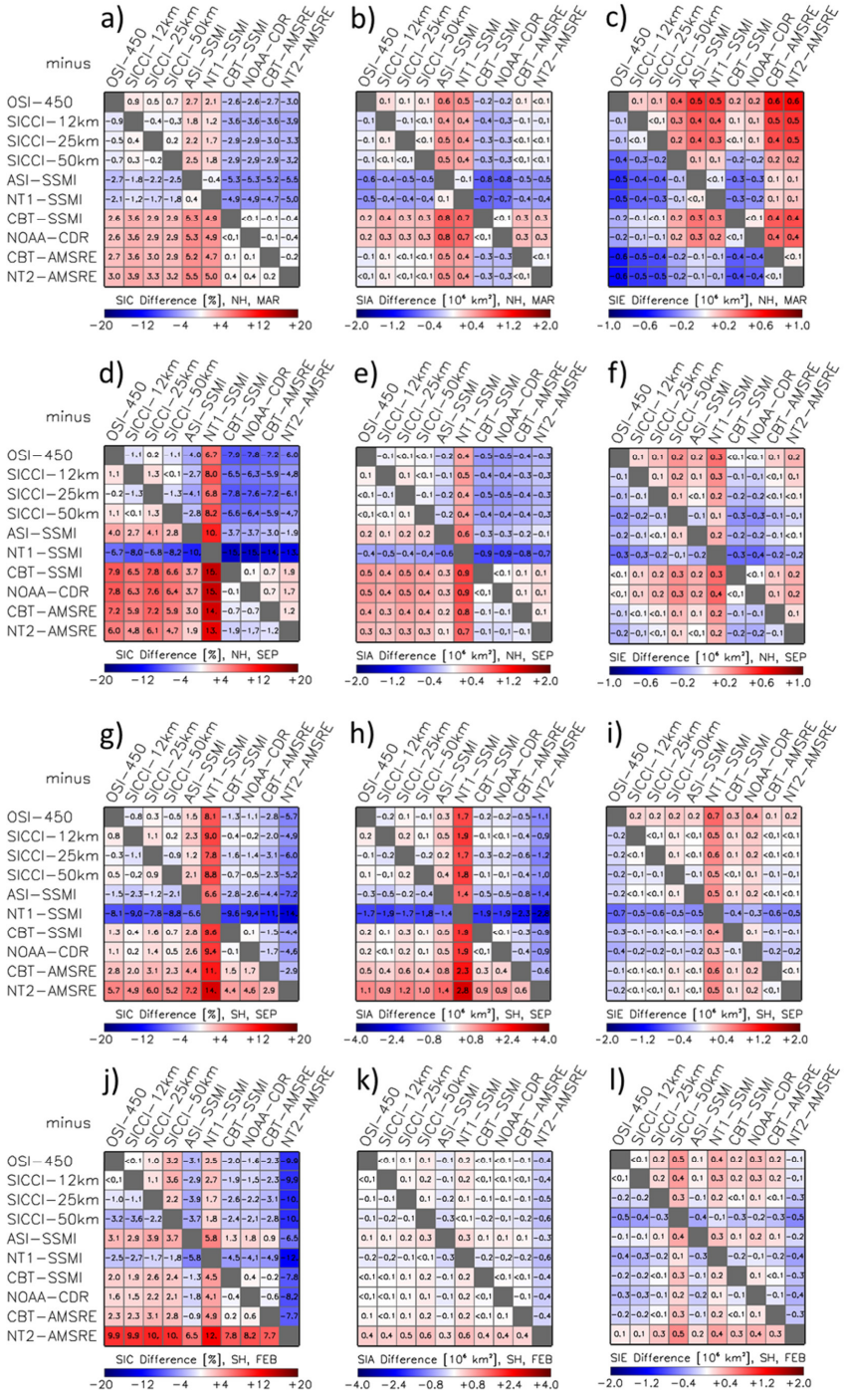

Figure 11. Differences (row minus column) between all ten products of, from left to right, the average sea-ice concentration, average SIA, and average SIE for the Arctic **(a)** through **(f)** and the Antarctic **(g)** through **(l)**. The averages are computed from monthly mean values of the respective months (MARch, SEPtember, FEBruary) of the AMSR-E period 06/2002 to 09/2011. All data are on EASE 2.0 grid with 50 km grid resolution. The landmask of the SICCI-50km product is applied to all products. For matrices of all remaining months we refer to Fig. G1 through Fig. G6 in Appendix G.

https://doi.org/10.5194/tc-2019-120
Preprint. Discussion started: 17 June 2019

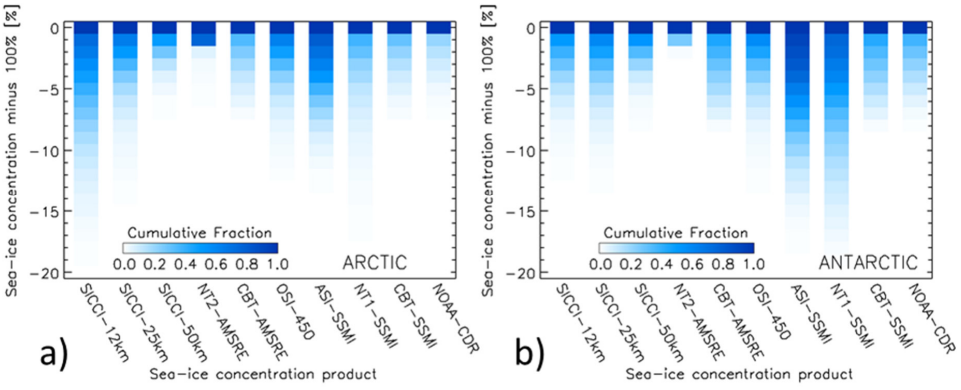

1402

1403 **Figure 12.** Cumulative distribution of the SIC difference to 100% at the near-100% reference SIC locations for all ten algorithms based on
1404 data for years 2007 through 2011 for **(a)** the Arctic, and **(b)** the Antarctic.

1405

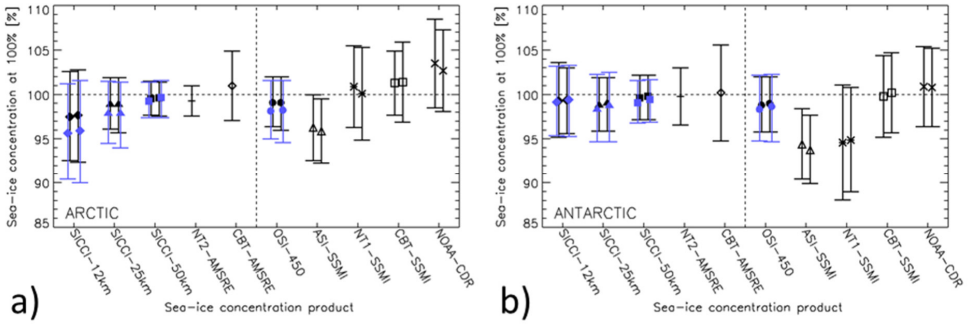

1406

1407 **Figure 13.** Summary of the results of the inter-comparison to the near-100% reference SIC (RRDP2) for **(a)** the Arctic and **(b)** the Antarctic.
1408 Shown for each sea-ice concentration product in black is the center of the Gaussian fit of the sea-ice concentration ≤ 99% at the respective
1409 RRDP2 locations (see Fig. 3). Bars denote ± one standard deviation of the Gaussian fit. For symbol pairs (all products but CBT-AMSRE
1410 and NT2-AMSRE) the left symbol denotes results for years 2007-2011, the right one for years 2007-2015. Blue symbols denote the mean
1411 non-truncated sea-ice concentration at the near-100% reference SIC for OSI-450 and SICCI products; blue bars denote the respective sea-
1412 ice concentration standard deviation.

https://doi.org/10.5194/tc-2019-120
Preprint. Discussion started: 17 June 2019

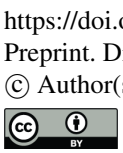

The Cryosphere
Discussions
Open Access
EGU

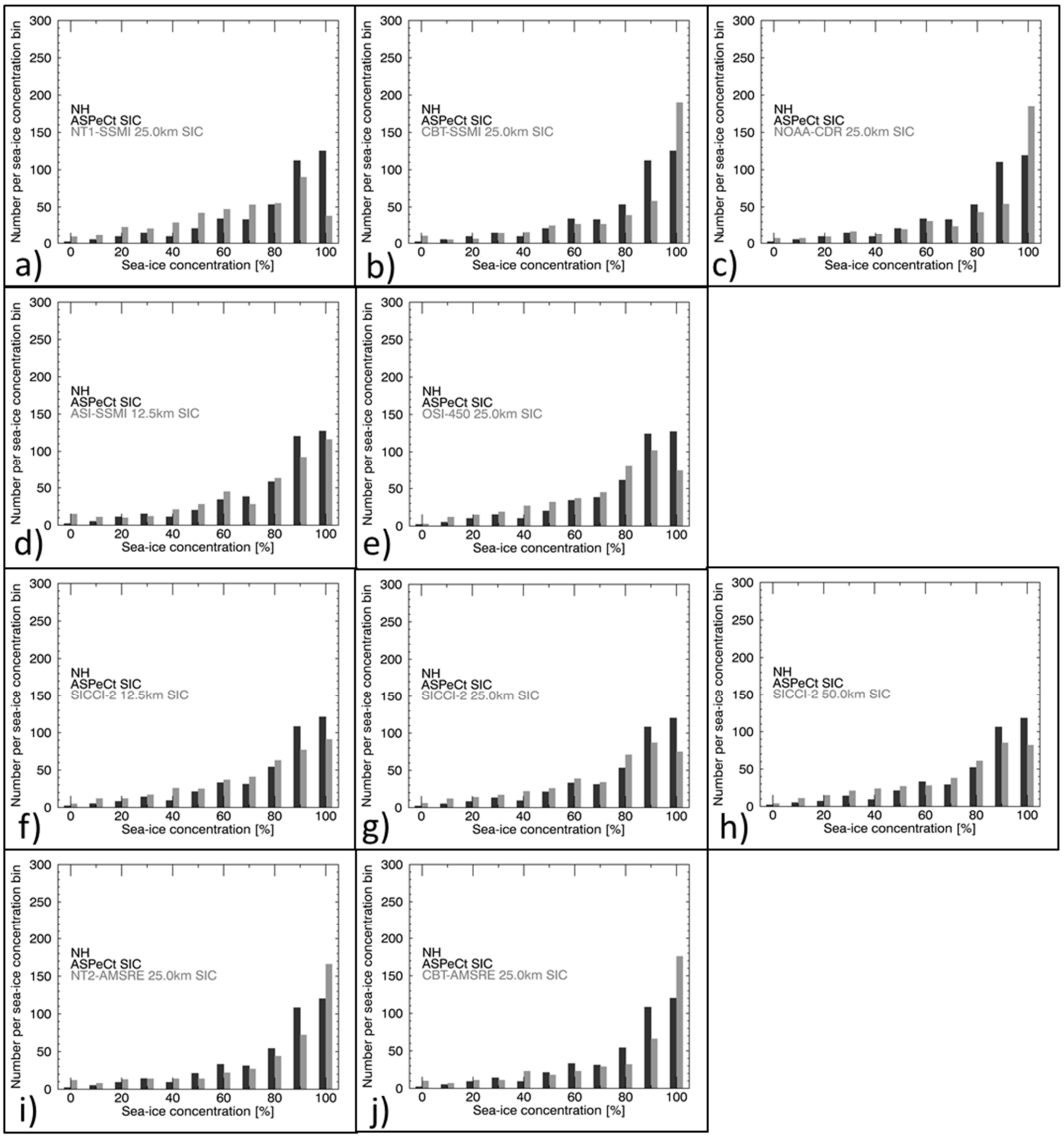

1413

1414 **Figure 14.** Histograms of co-located daily average SIC from visual ship-based observations (ASPeCt, note that we use ASPeCt also in the
1415 Arctic for simplicity even though these are observations under ASSIST/IceWatch) and from the ten satellite SIC products for the Arctic,
1416 using all data of years 2002-2011; bin-size is 10% except at 0% and 100% where bin-size is 5%.

https://doi.org/10.5194/tc-2019-120
Preprint. Discussion started: 17 June 2019

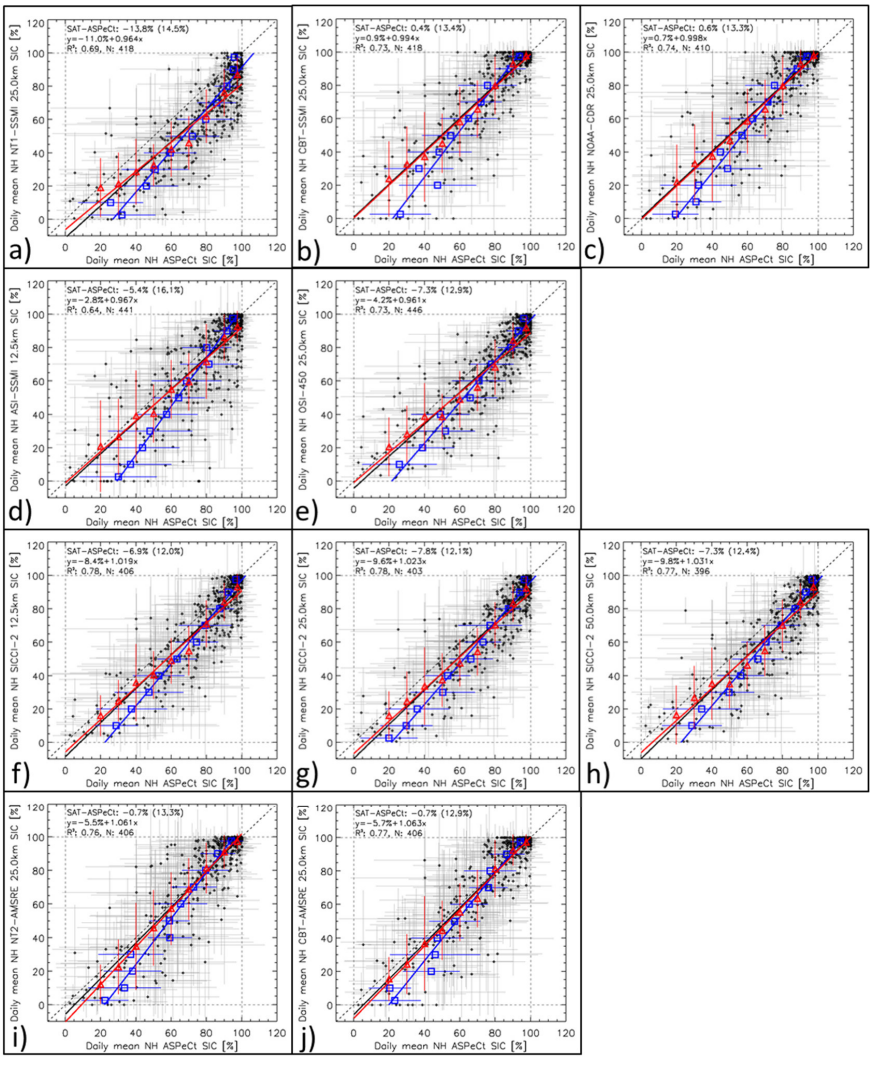

Figure 15. Scatterplots of co-located daily average SIC from visual ship-based observations (ASPeCt, x-axis, note that these are ASSIST/IceWatch for the Arctic, see caption of Fig. 13) and the ten satellite SIC algorithm products (SAT, y-axes) for the Arctic for years 2002-2011. Red symbols denote the average satellite SIC binned into 10% ASPeCt SIC intervals (except 0 … 5% and 95% … 100%, where 5% bins are used). Blue symbols denote the average ASPeCt SIC binned into 10% satellite SIC intervals, respectively. Error bars denote one standard deviation of the average. Dotted lines denote the 1-to-1 fit. Solid lines denote the linear regression of the respective value pairs. The mean difference and the standard deviation, the linear regression equation, the number of valid data pairs (N), and the squared linear correlation coefficient (R^2) is given in the top left or every image for the daily SIC values.

https://doi.org/10.5194/tc-2019-120
Preprint. Discussion started: 17 June 2019

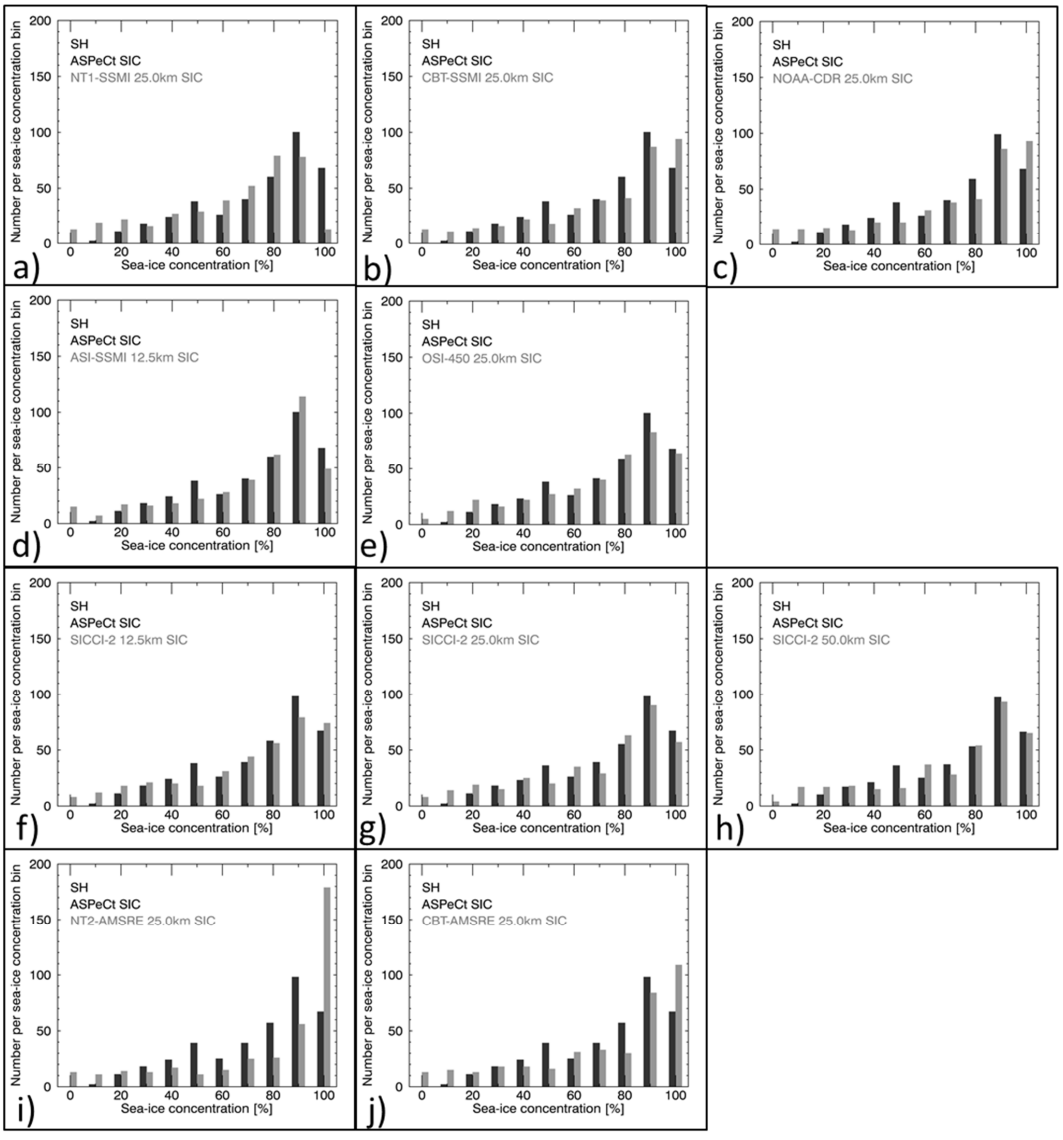

1425

1426 **Figure 16.** As Fig. 14 but for the Antarctic.

https://doi.org/10.5194/tc-2019-120
Preprint. Discussion started: 17 June 2019

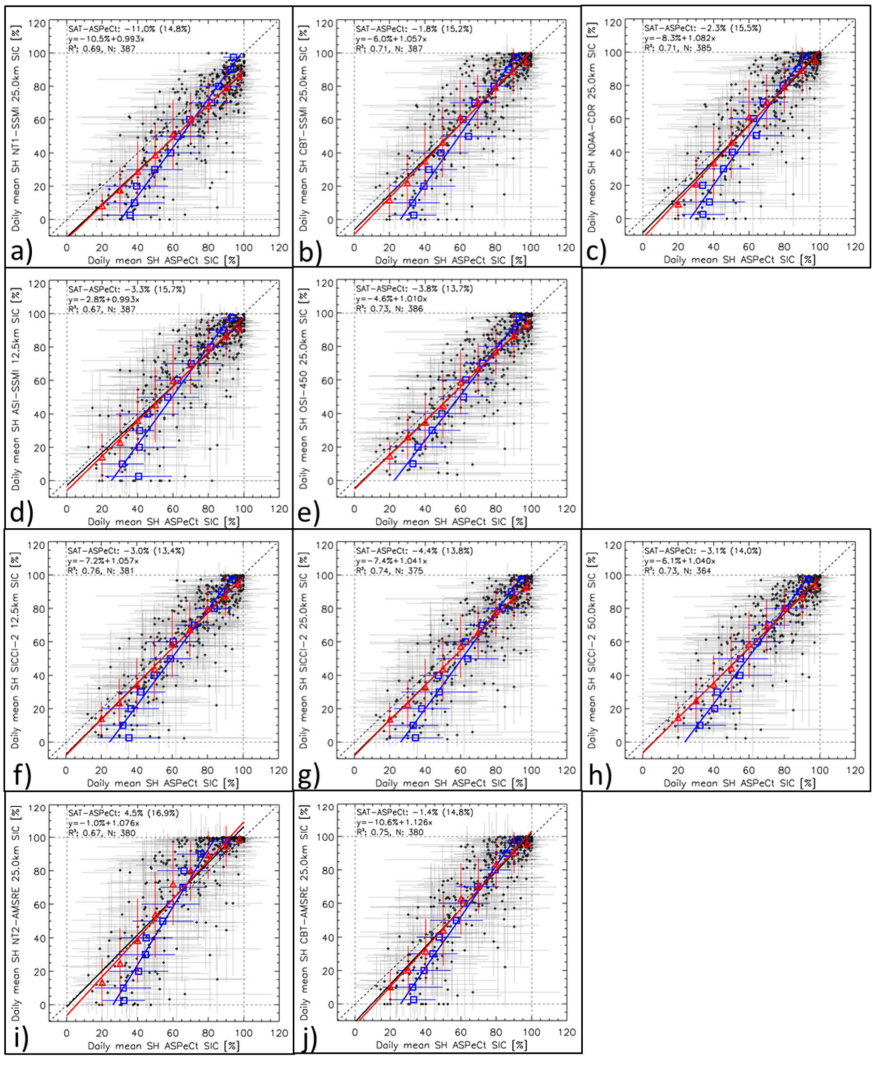

Figure 17. As Fig. 15 but for the Antarctic.

https://doi.org/10.5194/tc-2019-120
Preprint. Discussion started: 17 June 2019

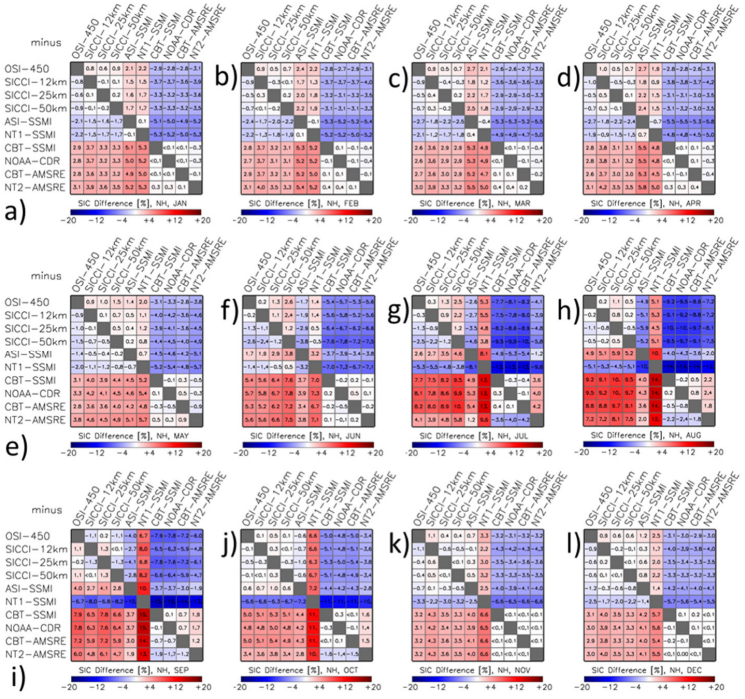

Figure G1. Differences between all ten products of the average sea-ice concentration for the Arctic. The averages are computed from monthly mean values of the respective months of the AMSR-E period 06/2002 to 09/2011. All data are on EASE 2.0 grid with 50 km grid resolution. The land-mask of the SICCI-50km product is applied to all products.

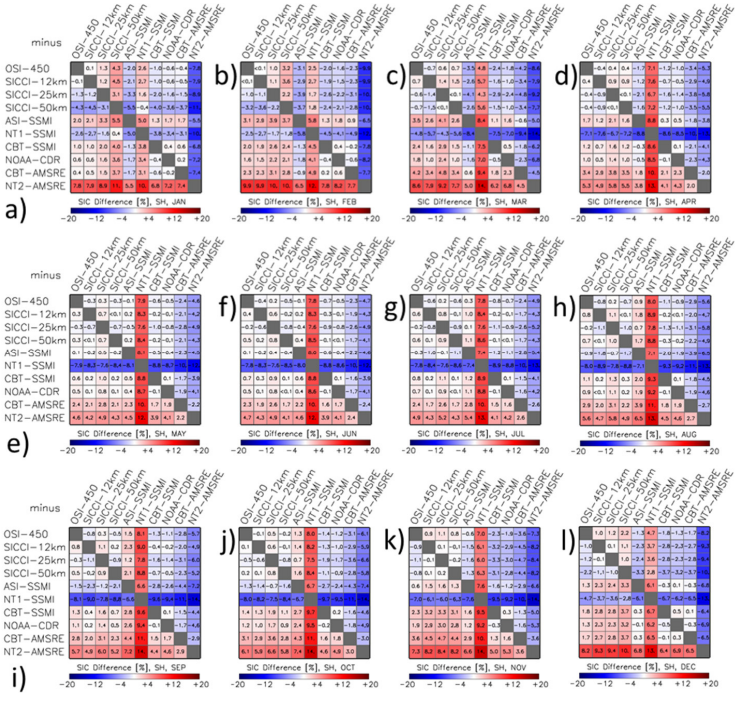

Figure G2. As Fig. G1 but for the Antarctic.

https://doi.org/10.5194/tc-2019-120
Preprint. Discussion started: 17 June 2019

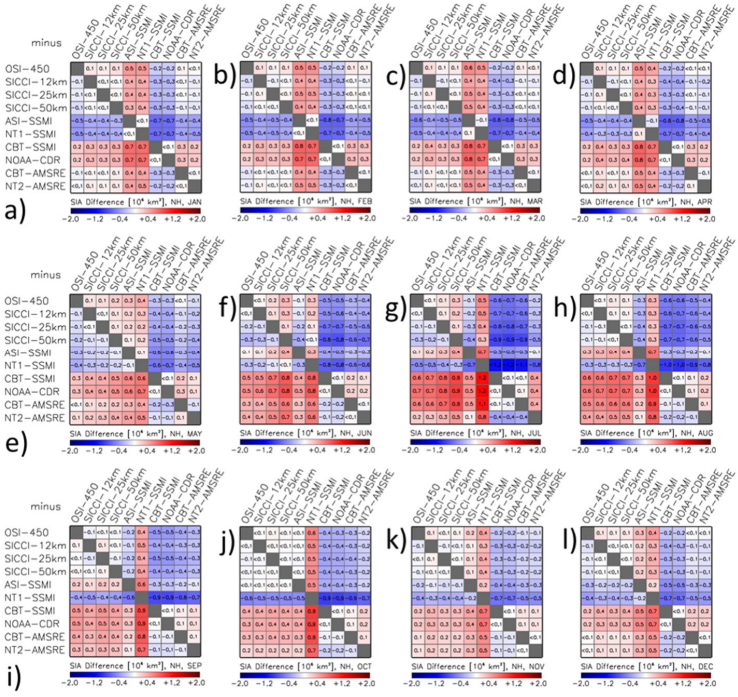

1435

1436 **Figure G3.** Differences between all ten products of the average sea-ice area (SIA) for the Arctic. The differences are computed from monthly
1437 mean SIA of the respective months of the AMSR-E period 06/2002 to 09/2011. All data are on EASE 2.0 grid with 50 km grid resolution.
1438 The land-mask of the SICCI-50km product is applied to all products.

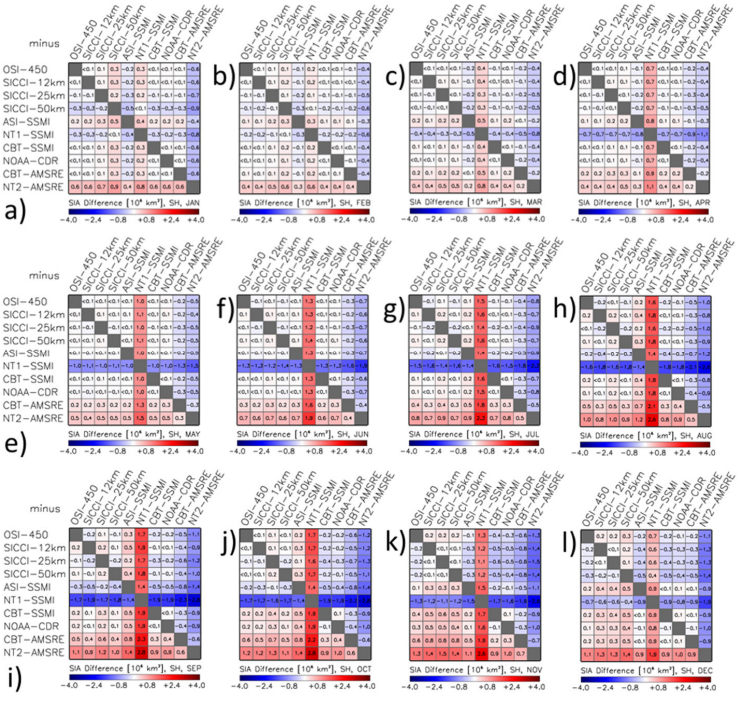

1439

1440 **Figure G4.** As Fig. G3 but for the Antarctic. Note the larger range of the SIA differences compared to the Arctic.

https://doi.org/10.5194/tc-2019-120
Preprint. Discussion started: 17 June 2019

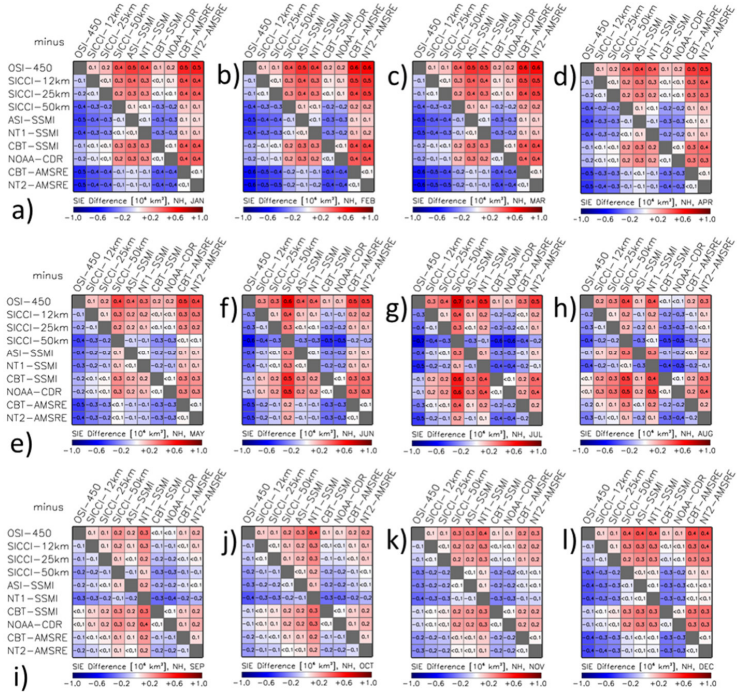

Figure G5. Differences between all ten products of the average sea-ice extent (SIE) for the Arctic. The differences are computed from monthly mean SIE of the respective months of the AMSR-E period 06/2002 to 09/2011. All data are on EASE 2.0 grid with 50 km grid resolution. The land-mask of the SICCI-50km product is applied to all products.

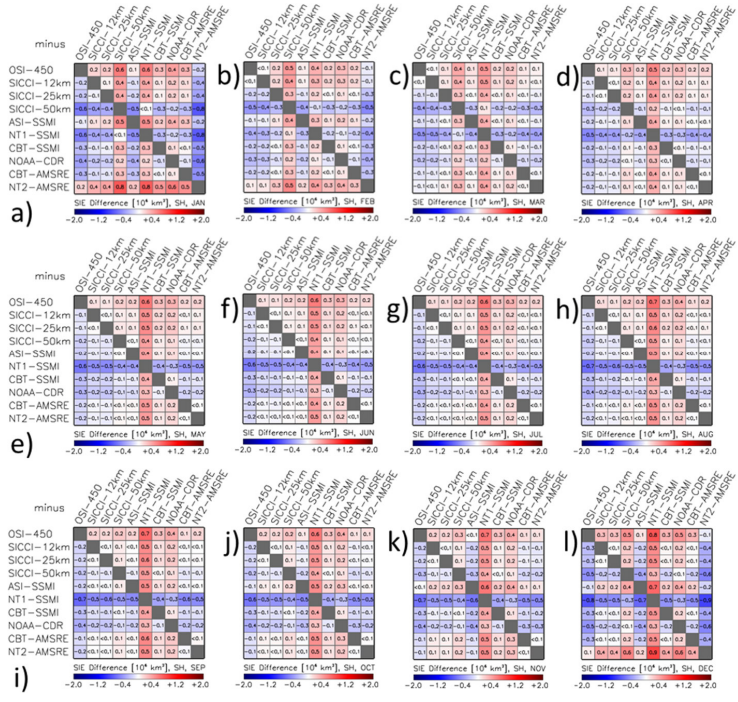

Figure G6. As Fig. G5 but for the Antarctic. Note the larger range of the SIE differences compared to the Arctic.

https://doi.org/10.5194/tc-2019-120
Preprint. Discussion started: 17 June 2019

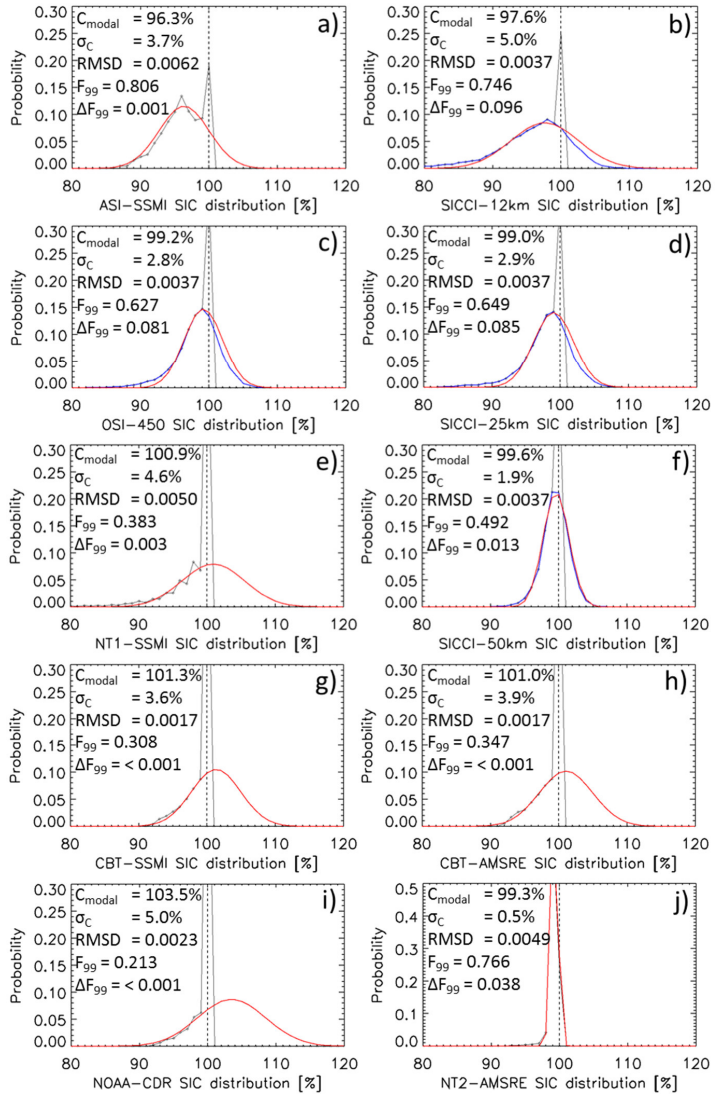

Figure H1. Sea-ice concentration distribution at RRDP2 near-100% reference sea-ice concentration locations in the Arctic during winter for 2007-2011. Black symbols and lines show values cut off at 100%; blue lines denote the original distribution (for OSI-450, SICCI-12km, SICCI-25km and SICCI-50km); red lines denote the distribution resulting from the Gaussian fit to values of the distribution ≤ 99%. In each image the modal sea-ice concentration (= center of the Gaussian fit: C_{modal}), the standard deviation of the fit σ_C and fit parameters with respect to the fraction of the distribution ≤ 99% (F_{99}, ΔF_{99}, see text in Sect. 2.1.4 for more explanation) and the root-mean-squared difference (RMSD) between original and fitted probability are given.

https://doi.org/10.5194/tc-2019-120
Preprint. Discussion started: 17 June 2019

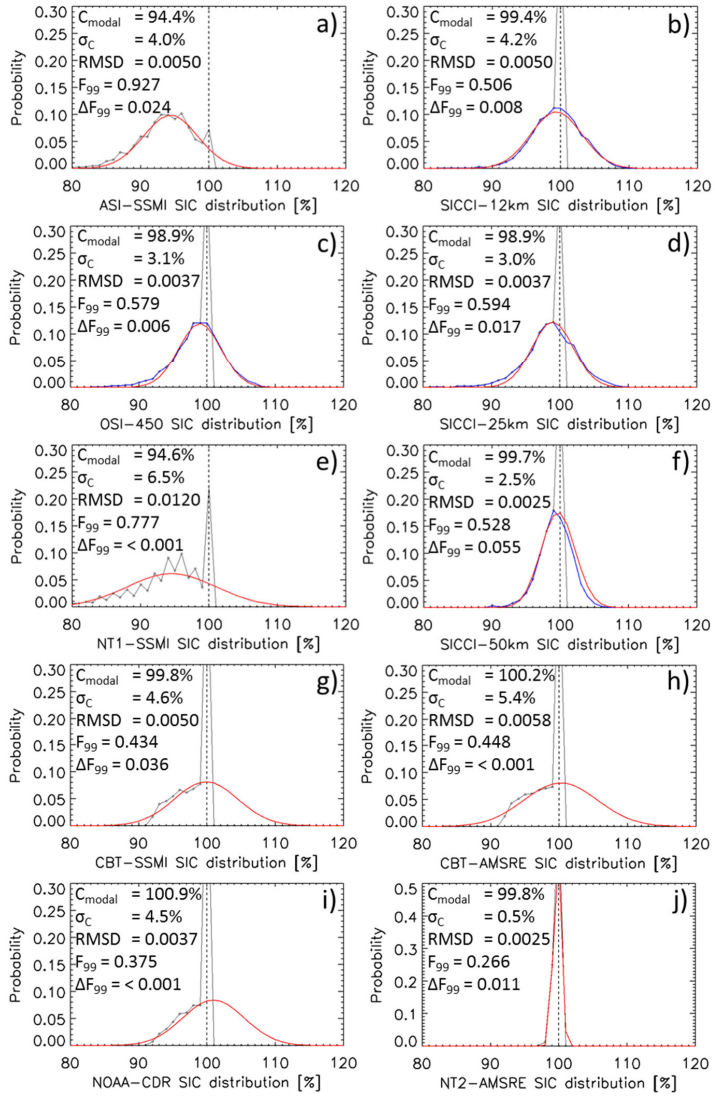

Figure H2. As Fig. H1 but for the Antarctic.